

AD-A074 950

SCIENCE APPLICATIONS INC BERKELEY CALIF
TRANSIENT ANALYSIS OF MULTICONDUCTOR TRANSMISSION LINE NETWORKS--ETC(U)
FEB 79 S K CHANG, F M TESCHE, D V GIRI

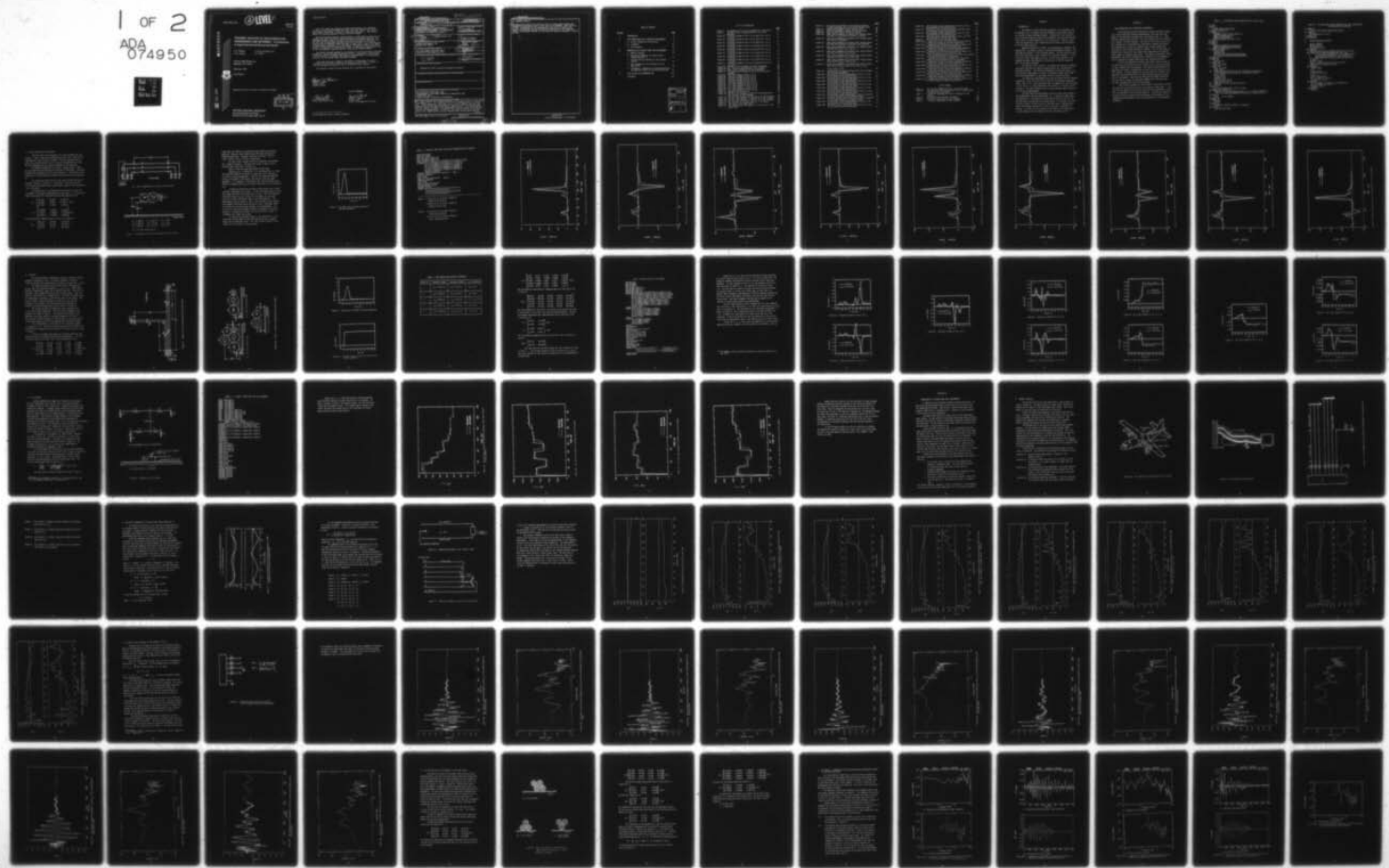
F29601-78-C-0002

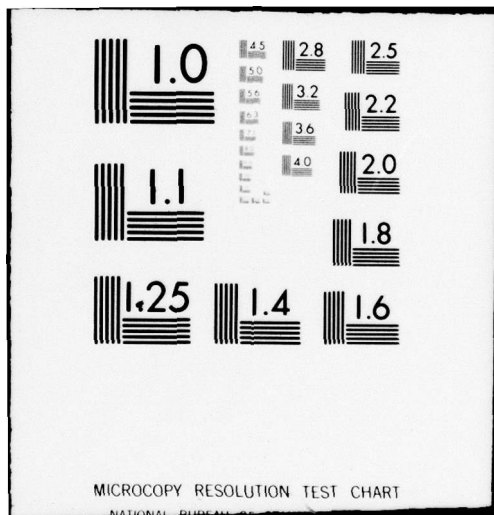
NL

AFWL-TR-78-152

UNCLASSIFIED

1 OF 2
ADA
074950





AFWL-TR-78-152

(2) LEVEL III

AFWL-TR-
78-152

A D E 200369

AD A 074950

TRANSIENT ANALYSIS OF MULTICONDUCTOR
TRANSMISSION LINE NETWORKS: A Comparison
of Experimental and Numerical Results

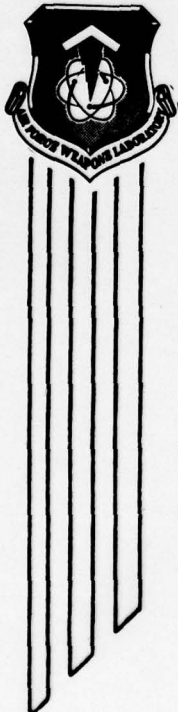
S. K. Chang
F. M. Tesche

T. K. Liu (LuTech, Inc.)
D. V. Giri

Science Applications, Inc.
Berkeley, CA 94701

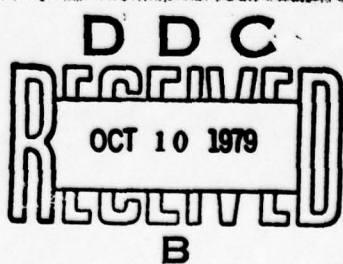
February 1979

Final Report



Approved for public release; distribution unlimited

DDC FILE COPY



AIR FORCE WEAPONS LABORATORY
Air Force Systems Command
Kirtland Air Force Base, NM 87117

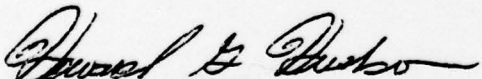
This final report was prepared by Science Applications, Inc., Berkeley, California, under Contract F29601-78-C-0002, Job Order 37630127 with the Air Force Weapons Laboratory, Kirtland Air Force Base, New Mexico. Capt Howard G. Hudson (ELT) was the Laboratory Project Officer-in-Charge.

When US Government drawings, specifications, or other data are used for any purpose other than a definitely related Government procurement operation, the Government thereby incurs no responsibility nor any obligation whatsoever, and the fact that the Government may have formulated, furnished, or in any way supplied the said drawings, specifications, or other data, is not to be regarded by implication or otherwise, as in any manner licensing the holder or any other person or corporation, or conveying any rights or permission to manufacture, use, or sell any patented invention that may in any way be related thereto.

This report has been authored by a contractor of the United States Government. Accordingly, the United States Government retains a nonexclusive, royalty-free license to publish or reproduce the material contained herein, or allow others to do so, for the United States Government purposes.

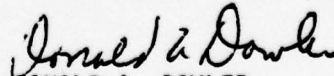
This report has been reviewed by the Office of Information (OI) and is releasable to the National Technical Information Service (NTIS). At NTIS, it will be available to the general public, including foreign nations.

This technical report has been reviewed and is approved for publication.


HOWARD G. HUDSON
Captain, USAF
Project Officer

FOR THE COMMANDER


J. PHILIP CASTILLO
Chief, Technology Branch


DONALD A. DOWLER
Colonel, USAF
Chief, Electromagnetics Division

UNCLASSIFIED

(18) AFWL, SBIET

SECURITY CLASSIFICATION OF THIS PAGE (When Data Entered)

(19) REPORT DOCUMENTATION PAGE		READ INSTRUCTIONS BEFORE COMPLETING FORM
1. REPORT NUMBER AFWL-TR-78-152	2. GOVT ACCESSION NO. AD-E200 369	3. RECIPIENT'S CATALOG NUMBER
4. TITLE (and Subtitle) TRANSIENT ANALYSIS OF MULTICONDUCTOR TRANSMISSION LINE NETWORKS: A Comparison of Experimental and Numerical Results.		5. TYPE OF REPORT & PERIOD COVERED Final Report
6. AUTHOR(s) S. K. Chang, F. M. Tesche, D. V. Giri		7. CONTRACT OR GRANT NUMBER(s) F29601-78-C-0002
8. PERFORMING ORGANIZATION NAME AND ADDRESS Science Applications, Inc. Berkeley, CA 94701		9. PROGRAM ELEMENT, PROJECT, TASK AREA & WORK UNIT NUMBERS 64711F 37630127
10. CONTROLLING OFFICE NAME AND ADDRESS Air Force Weapons Laboratory (ELT) Kirtland Air Force Base, NM 87117		11. REPORT DATE February 1979
12. MONITORING AGENCY NAME & ADDRESS (if different from Controlling Office) (12) 108		13. NUMBER OF PAGES 106
14. DISTRIBUTION STATEMENT (of this Report)		15. SECURITY CLASS. (of this report) Unclassified
16. DISTRIBUTION STATEMENT (of the abstract entered in Block 20, if different from Report)		15a. DECLASSIFICATION/DOWNGRADING SCHEDULE
17. SUPPLEMENTARY NOTES		
18. KEY WORDS (Continue on reverse side if necessary and identify by block number) Multiconductor Transmission Lines Electromagnetic Pulse (EMP) Coupling to Transmission Lines TACAMO Power Cable Laboratory Model Transmission Line Networks		
19. ABSTRACT (Continue on reverse side if necessary and identify by block number) This report computes the transient responses of some multiconductor transmission-line networks, e.g., (a) a three-wire line, (b) a T-network, and (c) an H-network. These computations, which make use of the QV7T computer code were then compared with the available experimentally measured data. Very good agreement was seen between the numerical and experimental results for both pulse and step function driving waveforms. In addition, the transient response of the power cable in the TACAMO aircraft was also computed under certain approximations.		
(over) A		

UNCLASSIFIED

SECURITY CLASSIFICATION OF THIS PAGE(When Data Entered)

20. ABSTRACT (Cont'd)

The power cable consists of seven wires for the 3-phase power system, and measurements were made earlier on this cable in the ATHAMAS I (HPD) facility at AFWL. Considering all the approximations that had to be made in the numerical computations and the difficulties encountered in the TACAMO-EMP testing, the agreement between the calculated and measured responses is seen to be fair.

UNCLASSIFIED

SECURITY CLASSIFICATION OF THIS PAGE(When Data Entered)

TABLE OF CONTENTS

<u>Section</u>		<u>Page</u>
I	INTRODUCTION	5
II	DATA COMPARISONS WITH LABORATORY MEASUREMENTS	6
	A. 3-Wire Transmission Line Section	9
	B. T-network	23
	C. The H-network	37
III	COMPARISON WITH TACAMO POWER CABLE MEASUREMENT	46
	A. Network Topology	47
	B. Equivalent Impedance at Pressure Break Toward Engine No. 1	52
	C. The Open Circuit Voltages for the Thevenin Circuit	66
	D. The Transmission Line Parameters of the Power Cable	83
	E. The Results - Comparison of the Calculated and the Measured Current at the Distribution Box	87
IV	CONCLUSIONS AND RECOMMENDATIONS	103
	REFERENCES	104

ACCESSION for		
NTIS	White Section <input checked="" type="checkbox"/>	
DDC	Buff Section <input type="checkbox"/>	
UNANNOUNCED <input type="checkbox"/>		
JUSTIFICATION _____		
BY _____		
DISTRIBUTION/AVAILABILITY CODES		
Dist. AVAIL. and/or SPECIAL		
A		

LIST OF ILLUSTRATIONS

	<u>Page</u>
Figure 1. The geometry of the 3-wire transmission line section	10
Figure 2. The open circuit voltage waveform of the pulse generator	12
Figure 3a. Transient voltage of wire 1 at J_2 when wire 1 at J_1 is driven	14
Figure 3b. Transient voltage of wire 2 at J_2 when wire 1 at J_1 is driven	15
Figure 3c. Transient voltage of wire 3 at J_2 when wire 1 at J_1 is driven	16
Figure 4a. Transient voltage of wire 1 at J_2 when wire 2 at J_1 is driven	17
Figure 4b. Transient voltage of wire 2 at J_2 when wire 2 at J_1 is driven	18
Figure 4c. Transient voltage of wire 3 at J_2 when wire 2 at J_1 is driven	19
Figure 5a. Transient voltage of wire 1 at J_2 when wire 3 at J_1 is driven	20
Figure 5b. Transient voltage of wire 2 at J_2 when wire 3 at J_1 is driven	21
Figure 5c. Transient voltage of wire 3 at J_2 when wire 3 at J_1 is driven	22
Figure 6a. Geometry of the T-network with 50Ω terminations	24
Figures 6b,c,d. The wire configurations of the T-network	25
Figure 7a. Open circuit voltage of the pulse generator	26
Figure 7b. The open circuit voltage of the unit-step function generator	26
Figure 8a. Transient voltage of wire 1 at J_3	31
Figure 8b. Transient voltage on wire 2 at J_3	31
Figure 8c. Transient voltage on wire 3 at J_3	32
Figure 8d. Transient voltage on wire 4 at J_4	33
Figure 8e. Transient voltage on wire 5 at J_4	33
Figure 9a. Unit step response on wire 1 at J_3	34
Figure 9b. Unit step response on wire 2 at J_4	34
Figure 9c. Unit step response on wire 3 at J_4	35
Figure 9d. Unit step response on wire 4 at J_4	36
Figure 9e. Unit step response on wire 5 at J_4	36
Figure 10. Geometry of the H-network	38
Figure 11a. The unit step response at junction J_1 (voltage across the resistor) of the H-network	41
Figure 11b. The unit step response at junction J_4 of the H-network	42
Figure 11c. The unit step response at junction J_5 of the H-network	43
Figure 11d. The unit step response at junction J_6 of the H-network	44
Figure 12. The location of the power cable to be tested	48
Figure 13. The layout of the power cable	49
Figure 14. The transmission-line network for the analysis of the power cable	50

	<u>Page</u>
Figure 15. The phase and amplitude of the measured impedance of 100Ω terminated coax, with the calibration curve	53
Figure 16. Impedance measurement using a coaxial cable	55
Figure 17. Power cable geometry outside the pressure break	55
Figure 18. Measured 100Ω load at the end of the coax	57
Figure 19. Power cable impedance at pressure seal looking toward the wing (for A_1 -Ground, B_1 -Ground, C_1 -Ground)	58
Figure 20. Power cable impedance at pressure seal looking toward the wing (for D_1 -Ground)	59
Figure 21. Power cable impedance at pressure seal looking toward the wing (for A_2 -Ground, B_2 -Ground, and C_2 -Ground)	60
Figure 22. Power cable impedance at pressure seal looking toward the wing (for A_1-B_1 , A_1-C_1 , B_1-C_1)	61
Figure 23. Power cable impedance at pressure seal looking toward the wing (for A_2-B_2 , A_2-C_2 , B_2-C_2)	62
Figure 24. Power cable impedance at pressure seal looking toward the wing (for A_1-D_1 , B_1-D_1 , and C_1-D_1)	63
Figure 25. Power cable impedance at pressure seal looking toward the wing (for D_1-A_2 , D_1-B_2 , D_1-C_2)	64
Figure 26. Power cable impedance at pressure seal looking toward the wing (for A_1-A_2 , A_1-B_2 , A_1-C_2 , B_1-B_2 , B_1-C_2 , C_1-A_2 , C_1-B_2 , C_1-C_2)	65
Figure 27. Configuration for obtaining the open-circuit voltages from current measurement	67
Figure 28a. The transient current measurement on wire A_1 of the 4-wire bundle at the pressure break	69
Figure 28b. The short circuit current spectrum on wire A_1 of the 4-wire bundle at the pressure break	70
Figure 29a. The transient current measurement on wire B_1 of the 4-wire bundle at the pressure break	71
Figure 29b. The short circuit current spectrum on wire B_1 of the 4-wire bundle at the pressure break	72
Figure 30a. The transient current measurement on wire C_1 of the 4-wire bundle at the pressure break	73
Figure 30b. The short circuit current spectrum on wire C_1 of the 4-wire bundle at the pressure break	74
Figure 31a. The transient current measurement on wire D_1 (neutral) of the 4-wire bundle at the pressure break	75
Figure 31b. The short circuit current spectrum on wire D_1 (neutral) of the 4-wire bundle at the pressure break	76
Figure 32a. The transient current measurement on wire A_2 of the 3-wire bundle at the pressure break	77
Figure 32b. The short circuit current spectrum on wire A_2 of the 3-wire bundle at the pressure break	78

	<u>Page</u>
Figure 33a. The transient current measurement on wire B_2 of the 3-wire bundle at the pressure break	79
Figure 33b. The short circuit current spectrum on wire B_2 of the 3-wire bundle at the pressure break	80
Figure 34a. The transient current measurement on wire C_2 of the 3-wire bundle at the pressure break	81
Figure 34b. The short circuit current spectrum on wire C_2 of the 3-wire bundle at the pressure break	82
Figure 35. The cross section of the power cable	84
Figure 36a,b. Comparison of the wire current spectrum on phase A_1 of the 4-wire bundle at the distribution box	88
Figure 36c,d. Comparison of transient wire current on phase A_1 of the 4-wire bundle at the distribution box	89
Figure 37a,b. Comparison of the wire current spectrum on phase B_1 of the 4-wire bundle at the distribution box	90
Figure 37c,d. Comparison of transient wire current on phase B_1 of the 4-wire bundle at the distribution box	91
Figure 38a. Wire current spectrum on phase C_1 of the 4-wire bundle at the distribution box (not measured)	92
Figure 38b. Transient wire current on phase C_1 of the 4-wire bundle at the distribution box (not measured)	93
Figure 39a,b. Comparison of the wire current spectrum on phase A_2 of the 3-wire bundle at the distribution box	94
Figure 39c,d. Comparison of transient wire current on phase A_2 of the 3-wire bundle at the distribution box	95
Figure 40a,b. Comparison of the wire current spectrum on phase B_2 of the 3-wire bundle at the distribution box	96
Figure 40c,d. Comparison of transient wire current on phase B_2 of the 3-wire bundle at the distribution box	97
Figure 41a,b. Comparison of the wire current spectrum on phase C_2 of the 3-wire bundle at the distribution box	98
Figure 41c,d. Comparison of transient wire current on phase C_2 of the 3-wire bundle at the distribution box	99

LIST OF TABLES

Table 1a.	The original UPDATE correction set for QV7T code	7
Table 1b.	The additional UPDATE correction set for interpolating the pulsed driving waveform	8
Table 2.	Listing of input data for 3-wire transmission line section	13
Table 3.	Wire radius and dielectric constants	27
Table 4.	Listing of input data for the T-network	29
Table 5.	Listing of input data for the H-network	39

SECTION I

INTRODUCTION

The analysis of multiconductor transmission line networks plays an important role in studying the electromagnetic pulse (EMP) response of aircraft or other aerospace systems. Transmission lines may easily pick up the EMP transient fields which penetrate into the system through slits, holes, or other apertures in its exterior skin. Many of these lines are connected to vital electronics which control the functioning of the in-flight vehicles.

Recently Tesche and Liu [Ref. 1] have developed a computer code, denoted QV7T, to analyze a general lossless multiconductor network. The code does the analysis in the frequency domain. The Fast Fourier Transform (FFT) algorithm is used to obtain the transient responses. In contrast with direct time domain analysis, the QV7T code solves all the propagation modes simultaneously, by making use of the BLT equations [Ref. 2] and matrix methods.

The purpose of this report is to compare the transient responses calculated from the QV7T code with measured data for selected multiconductor networks. The transient measurements include two types, i.e., the laboratory measurement on several experimental models and the EMP simulation measurements of the cables inside an actual aircraft.

The laboratory measurements have been provided by Mission Research Corporation, using test facilities at the Air Force Weapons Laboratory (AFWL) [Ref. 3, 4]. Three different types of networks will be considered in this report: a 3-wire transmission line section, a T-network, and an H-network. The pulse responses and unit step responses were included in the laboratory measurements.

The EMP simulation measurement involves a power cable tested in the TACAMO Add-On Testing program [Ref. 5]. A seven wire power cable from engine No. 1 runs parallel to the edge of the wing and picks up the EMP energy from outside the pressure break. This energy is carried into the interior of the aircraft by the power cable. Measured data enable the Thévenin equivalent circuit to be used to represent the sources. The short circuit currents of the cable at the distribution box were measured and are compared with the calculated results.

SECTION II

DATA COMPARISONS WITH LABORATORY MEASUREMENTS

From discussions with the personnel of Mission Research Corporation, we have obtained laboratory measurements from some simplified models of multiconductor transmission line networks [Ref. 3]. Three different networks were provided: the 3-wire transmission line section, the T-network, and the H-network. The wires of the 3-wire section and the T-network were insulated with polyethylene, neoprene and rubber. The H-network was a single wire network (over a ground plane) and consisted of wires without dielectric cladding. For all the cases considered here, the wires of the network were supported with styrofoam blocks above an aluminum ground plane. Time domain reflectometry (TDR) measurements were used to determine the transmission line parameters, such as the per-unit-length capacitance, and inductance matrices.

The driving waveforms for these cases were a pulse excitation for the 3-wire line section and the T-network, and a unit-step function for the T-network and the H-network. The pulsed driving waveform was digitized and linearly interpolated for use in the FFT routines in the QV7T program. The QV7T program has also been modified to employ the numerical driving waveform data of the excitation function for each wire of the network. Table 1a shows the original UPDATE correction set, and Table 1b shows the additional UPDATE set of the QV7T code for the interpolation of the driving waveform.

The transient response for each network configuration has been obtained both by calculation and by the laboratory measurement. The case by case comparison of the calculated and the experimental results will be considered in the following sections. Through the comparisons we shall be able to establish the confidence of the accuracy of the computational techniques, as well as the adequacy of the measurement procedures.

TABLE 1a. THE ORIGINAL UPDATE CORRECTION SET FOR QV7T CODE

```

*D JUN8
*D MAIN.3
  1 TAPE8,TAPE9,TAPE10,TAPE21
*D TYMDRIV.9,TYMDRIV.10
*I TYMDRIV.13
  DIMENSION TT(20),VTT(20),COEF(2,20)
  NAMELIST/WVFORM/ISTEP,TO
  NAMELIST/FFTDR/TMAX,M
  NAMELIST/WVMATCH/NTT,SCAL,TT,VTT
*D DTUBE.14
*D DTUBE.17
*I DTUBE.18
  NAMELIST/LINEPRM/XK,SL,SLEN,IFLAG
  NAMELIST/SOURCES/XLPOS,VSRC,CSRC
*D TYMDRIV.61,TYMDRIV.63
  ALPHA1=4.0E6
  ALPHA2=4.76E8
  TM=ALOG(ALPHA1/ALPHA2)/(ALPHA1-ALPHA2)
  A1=1.0/(EXP(-ALPHA1*TM)-EXP(-ALPHA2*TM))
*D DJUNC.105
*I DJUNC.103
  ZL(KR,KC)=0.0
*I TYMDRIV.161
  WRITE (2) NLOAD
*I TYMDRIV.195
  WRITE (2) NL,NN
  PRINT 100,NL
100  FORMAT(1H0,10X,*PRINT OUT OF LOAD QUANTITIES FOR LOAD*13//,
116X,*TIME(NS)*,10X,*VOLTAGE(V)*,10X,*CURRENT (AMPS)*/)
  DO 101 I=1,NN
  VV=REAL(VT(I))
  VI=REAL(IT(I))
  WRITE (2) XT(I),VV,VI
  PRINT 102,XT(I),VV,VI
102  FORMAT(1H ,8X,F12.3,9X,E13.3,9X,E13.3)
101  CONTINUE
*TYMDRIV.131
  WRITE (2) NT,NN1,(VT(I),XT(I),I=1,NN1)
*D TYMDRIV.202,TYMDRIV.203
22   FORMAT(*1 DRIVING WAVEFORM FOR TUBE *13* IS A DOUBLE EXPONENTIAL
1 WITH THE FOLLOWING PARAMETERS*/10X,*A1=E12.3*ALPHA1=*E12.3/ 1
*D DJUNC.89
C..  JZL=1 .. ZL IS A MATRIX
*D JNSCM.156
*I JNSCM.150
  NPP=NWW
*D MODAL.23
C    DIAGONISTIC PRINT OUT OCCURS IF IDBUG.GE.3
*D DTUBE.21
C    LOOP OVER EACH TUBE

```

TABLE 1b. THE ADDITIONAL UPDATE CORRECTION SET FOR INTERPOLATING
THE PULSED DRIVING WAVEFORM

```

*I TYMDRIV.74
C      ISTEP = 3 FOR ACTURAL WAVEFORM EXCITATION
*I TYMDRIV.76
      IF(ISTEP.EQ.3) Go To 301
*I TYMDRIV.125
      301 CONTINUE
C
C      ACTUAL WAVEFORM EXCITATION
C
      READ (5,WVMATCH)
      DO 306 I=1,NTT
      VTT(I)=VTT(I)*SCAL
306 CONTINUE
      PRINT 304,NT,NTT,(III1,TT(III1),VTT(III1),III1=1,NTT)
304 FORMAT(1H1,5X,*DRIVING WAVEFORM FOR TUBE *,13,
1      * IS AN ACTUAL WAVEFORM WITH*,I3,* SAMPLE POINTS *
2      *AS FOLLOWS*/5X,*POINT NO.*,3X,*TIME(NS)*,5X,
3      *AMPLITUDE(VOLTS)*/20(8X,I3,6X,F8.2,5X,E13.5()))
      NTT1=NTT-1
      DO 302 I=1,NTT1
      COEF(1,I)-(VTT(I+1)-VTT(I))/(TT(I+1)-TT(I))
      COEF(2,I)=VTT(I)-COEF(1,I)*TT(I)
302 CONTINUE
      TTTMAX=TT(NTT)
      I1=1
      DO 303 I=1,NN1
      T=DT*FLOAT(I-1)*1.E9
      III1=I1
      DO 305 III2=III1,NTT1
      IF(T.GT.TT(I1+1)) I1=I1+1
      IF(I1.GE.NTT) I1=I1-1
305 CONTINUE
      IF(T.LE.TTTMAX) VT(I)=COEF(1,I1)*T+COEF(2,I1)
      IF(T.GT.TTTMAX) VT(I)=0.0
      VT(NN1+I)=-VT(I)
303 CONTINUE
      GO TO 13

```

A. 3-wire Transmission Line Section

The first case to be discussed is a 3-wire transmission line section. Figure 1 shows the configuration of this line. Each wire is terminated by a 50Ω resistor to ground. The pulse generator has an effective resistance of 25Ω , due to the parallel combination of the 50Ω load impedance and the internal impedance of the generator.

The network topology for this case is rather simple. There are one branch and two junctions at both ends of the branch. The pulse generator was connected to one wire at junction J_1 . The results to be studied will be the transient voltages across the resistors at junction J_2 .

The three wires have different radii and different dielectric coatings, as shown in Figure 1b. The centers of the wires are all 4.16 cm above the ground plane, and the total length of the transmission line is 20 meters.

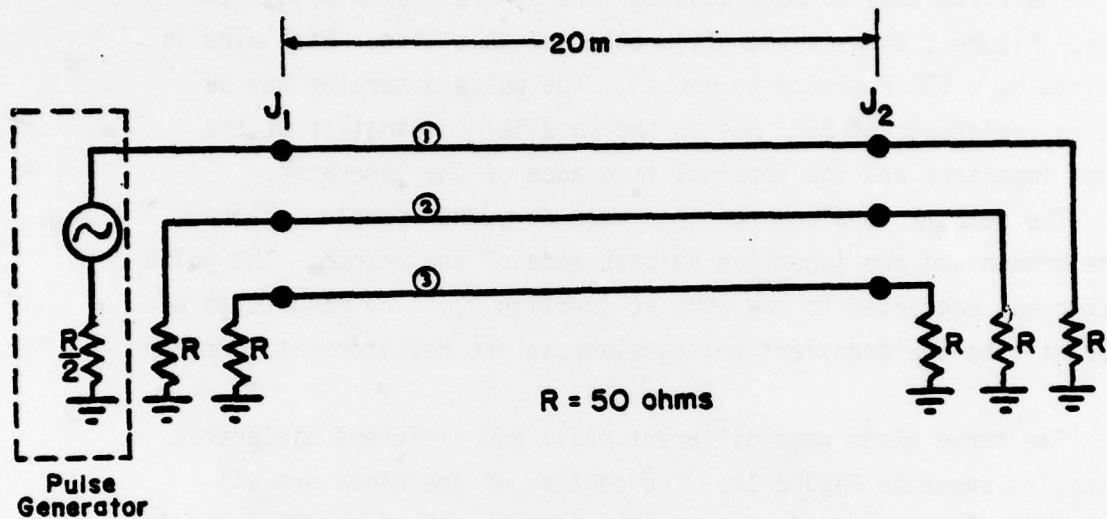
The transmission line parameters were obtained by using the time domain reflectometry measurement technique [Ref. 3]. The per-unit-length capacitance and inductance matrices were measured to be

$$[C] = \begin{bmatrix} 46.4807 & -20.9093 & -20.5534 \\ -20.9093 & 33.8339 & -4.1526 \\ -20.5534 & -4.1526 & 31.0993 \end{bmatrix} \text{ pF/m}$$

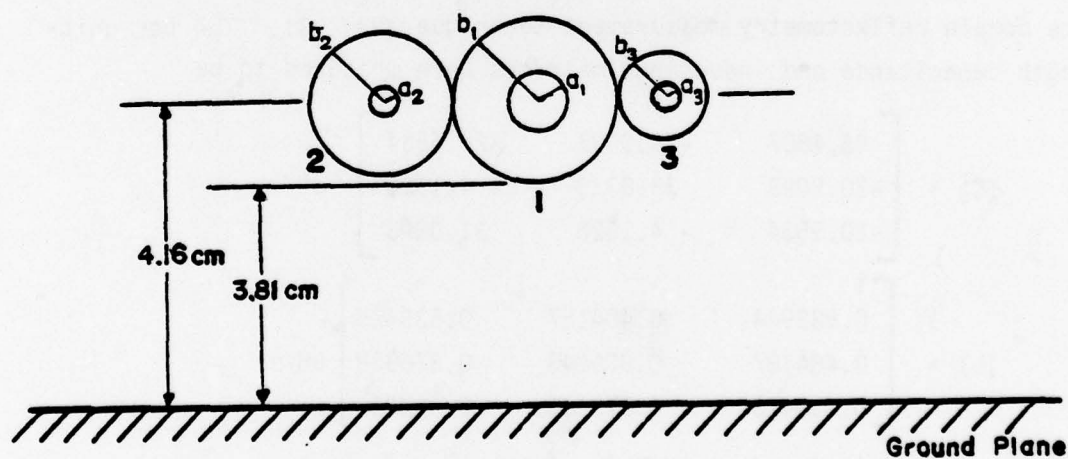
$$[L] = \begin{bmatrix} 0.883944 & 0.484157 & 0.535475 \\ 0.484157 & 0.939843 & 0.378936 \\ 0.535475 & 0.378936 & 0.992230 \end{bmatrix} \mu\text{H/m}$$

The characteristic impedance matrix of the line is given by

$$[Z_0] = \begin{bmatrix} 232.419 & 148.382 & 159.830 \\ 148.382 & 237.879 & 121.279 \\ 159.830 & 121.279 & 258.320 \end{bmatrix} \Omega$$



(a) 3-wire transmission line section with 50Ω load



(b) The wire configurations

Figure 1. The geometry of the 3-wire transmission line section

Since there are three wires coated with three different dielectric materials, there are three separate quasi-TEM modes traveling at different velocities. The modal velocities are 2.829×10^8 m/s, 2.009×10^8 m/s, 2.178×10^8 m/s, respectively.

The open circuit voltage of the pulse generator was measured and is shown in Figure 2. The pulse has a peak of about 6 volts. The half-power pulse width is about 2 ns.

Table 2 lists the input data cards for QV7T code.

Figures 3a, b, c, Figures 4a, b, c, and Figures 5a, b, c show the transient responses at junction J_2 when one wire at junction J_1 is driven by the pulse generator. Both the calculated and measured results are plotted in the figures, and they all show very good agreement. It is apparent in the figures that there are three transmission line modes traveling at different velocities on the transmission line.

It should be noted that the results shown here do not include secondary reflections at the loads. It took the fastest mode 70 ns and the slowest mode 100 ns to travel from J_1 to J_2 . The first secondary reflection pulse at J_2 has to travel 3×20 meters and it occurs about 210 ns after the turn-on time of the pulse generator. The measurements were not taken for such a long duration of the response. The secondary reflection pulses are usually low in magnitude, hence the sensitivity and noise cause problems in the measurement. The calculations were not performed to obtain the secondary reflections because it is necessary to reduce the time resolution in order to accommodate the larger time window.

For most of the responses shown in the comparisons, it was found that the amplitudes of the calculated pulses are in general larger than the measured values. This could be attributable to the transmission line losses in the experiment.

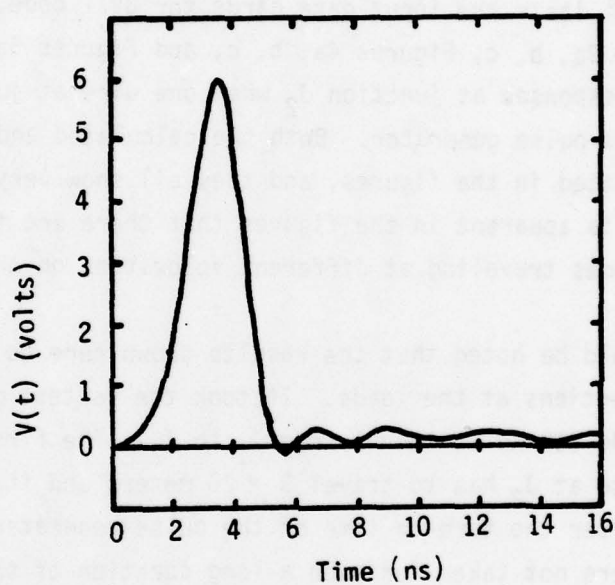


Figure 2. The open circuit voltage waveform of the pulse generator

TABLE 2. LISTING OF INPUT DATA FOR 3-WIRE TRANSMISSION LINE SECTION

```

$TOPO NB=1,NJ=2$
$BRNH IB=1,NWW=3$
$JNC JN=1,NBJJ=1,IBB(1)=1$
$JNC JN=2,NBJJ=1,IBB(1)=1
$LDPTS NLOAD=3,LLOAD(1)=1,1,1,JLOAD(1)=2,2,2,LLNO(1)=1,2,3$
$LINEPRM XK(1,1)=46.4807E-12,-20.9093E-12,-20.5534E-12,
           XK(1,2)=-20.9093E-12,33.8339E-12,-4.1526E-12,
           XL(1,1)=0/993944E-6,0.484157E-6,0.535475E-6,
           XL(1,2)=0.484157E-6,0.939843E-6,0.378936E-6,
           XL(1,3)=0.535475E-6,0.378936E-6,0.992230E-6,
           XLEN=20.0,IFLAG=0$
$SOURCES XLPOS=0.0,VSRC(1)=1.0,0.0,0.0      Note 1.
$CCNN JN=1,NOCC=1$
$LDCC JZL=2$
$LOAD Z(1)=25.0,50.0,50.0$      Note 2.
$CONN JN=2,NOCC=1$
$LDCC JZL=2$
LOAD Z(1)=50.0,50.0,50.0$
$FFTDR TMAX=400.,M=10$
$WVFORM ISTEP=3$
$WVMATCH NTT=13,TT(1)=0.0,2.4,3.5,4.4,5.6,6.8,7.8,
           9.0,11.0,12.4,14.4,16.0,18.0,
           VTT(1)=0.0,3.0,6.0,3.0,-0.1,0.3,0.05,0.25,
           0.1,0.2,0.0,0.18,0.0,SCAL=1.0

```

Note 1. If wire 2 at J_1 is driven, change to

$VSRC(1)=0.0,1.0,0.0$$

If wire 3 at J_1 is driven, change to

$VSRC(1)=0.0,0.0,1.0$$

Note 2. If wire 2 at J_1 is driven, change to

$Z(1)=50.0,25.0,50.0$$

If wire 3 at J_1 is driven, change to

$Z(1) = 50.0,50.0,25.0$$

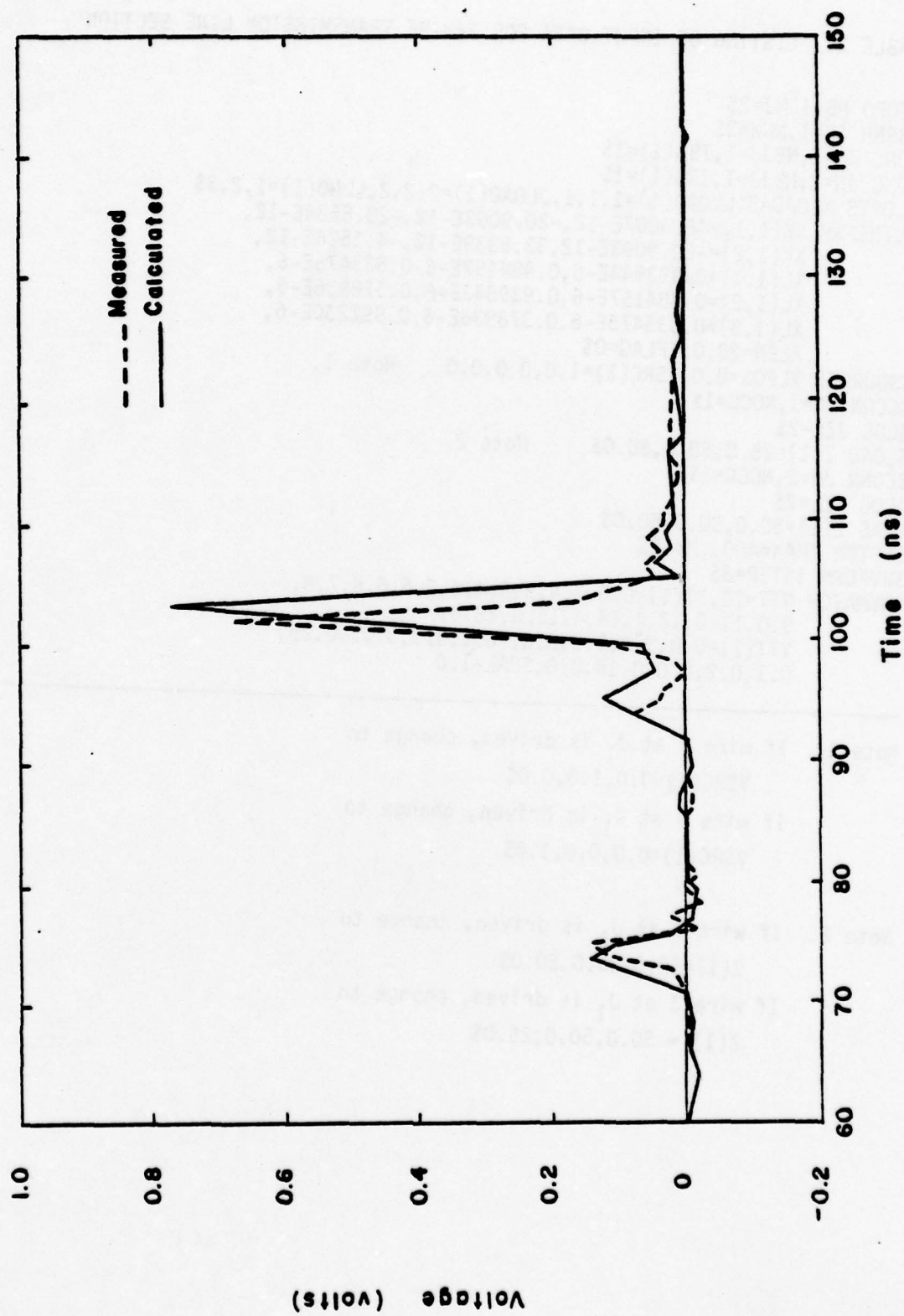


Figure 3a. Transient voltage of wire 1 at J_2 when wire 1 at J_1 is driven.

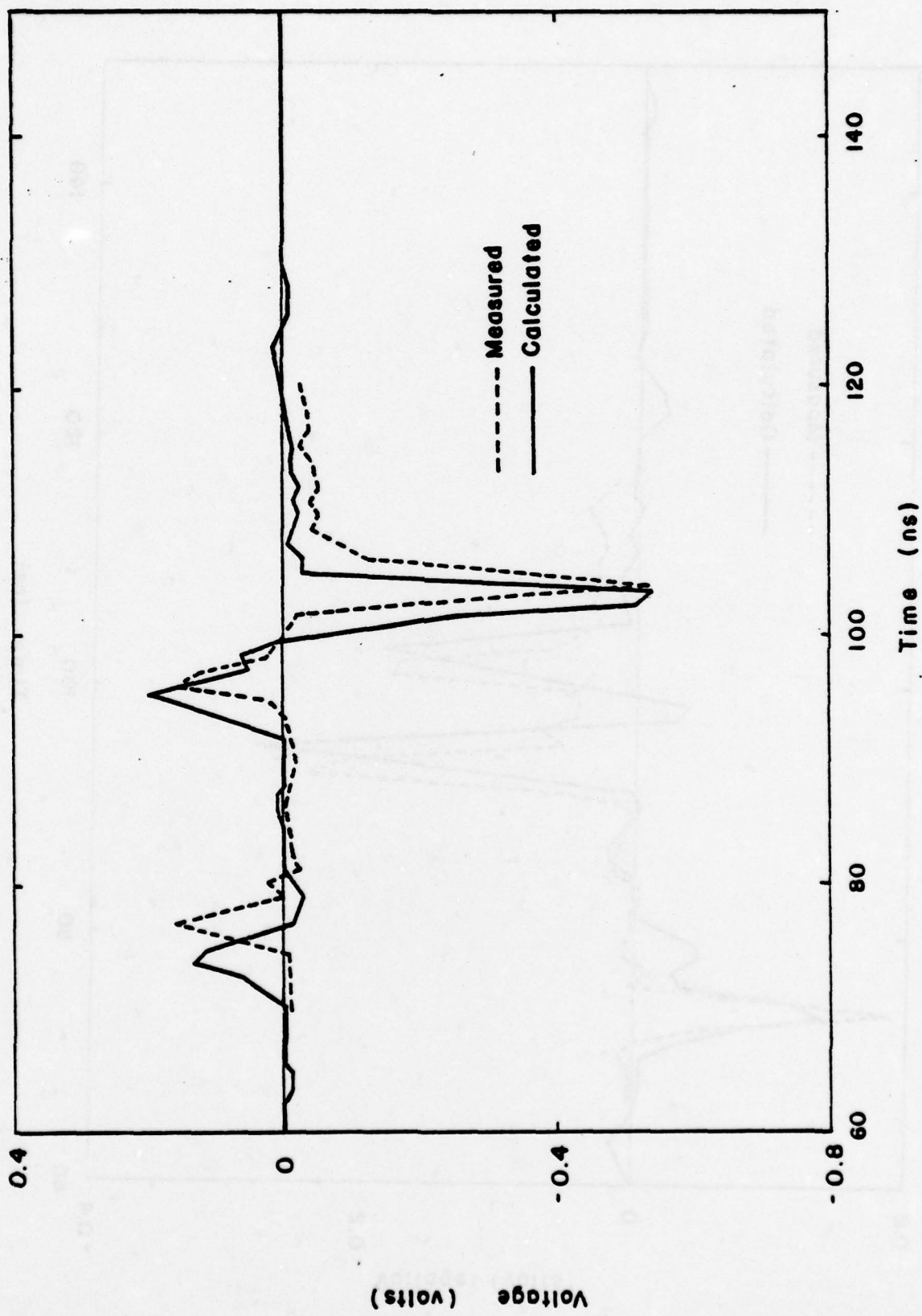


Figure 3b. Transient voltage of wire 2 at J_2 when wire 1 at J_1 is driven.

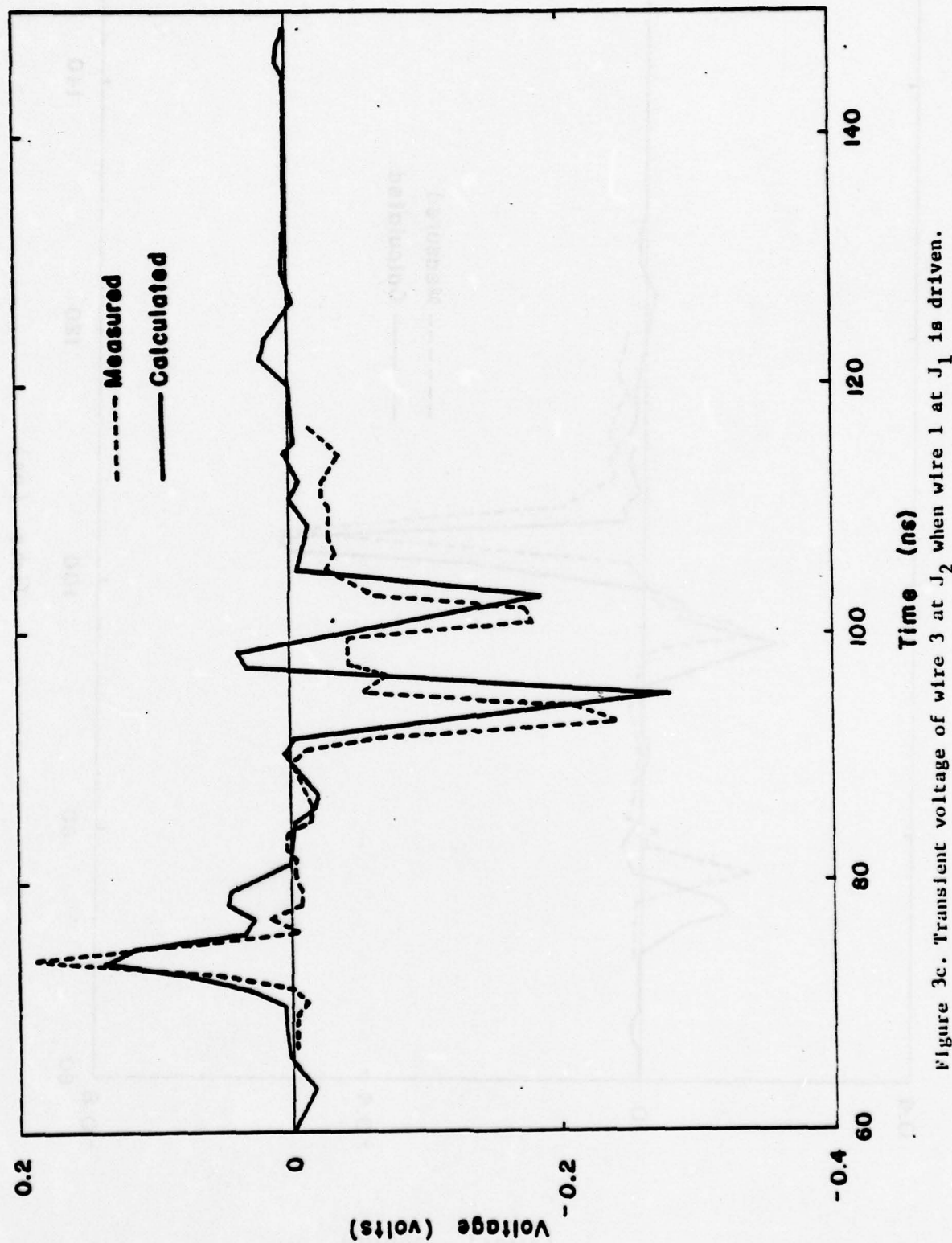


Figure 3c. Transient voltage of wire 3 at J_2 when wire 1 at J_1 is driven.

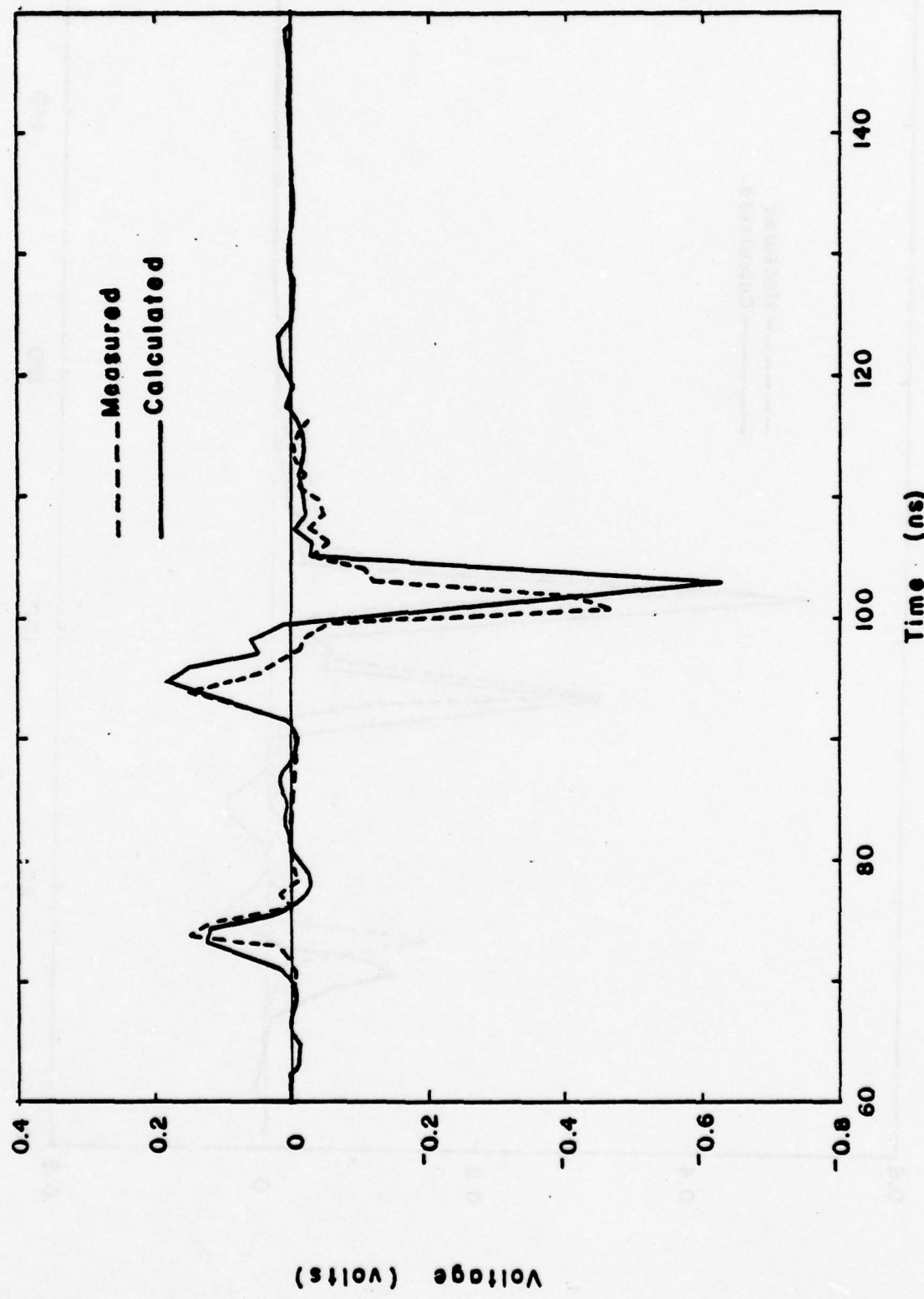


Figure 4a. Transient voltage of wire 1 at J_2 when wire 2 at J_1 is driven.

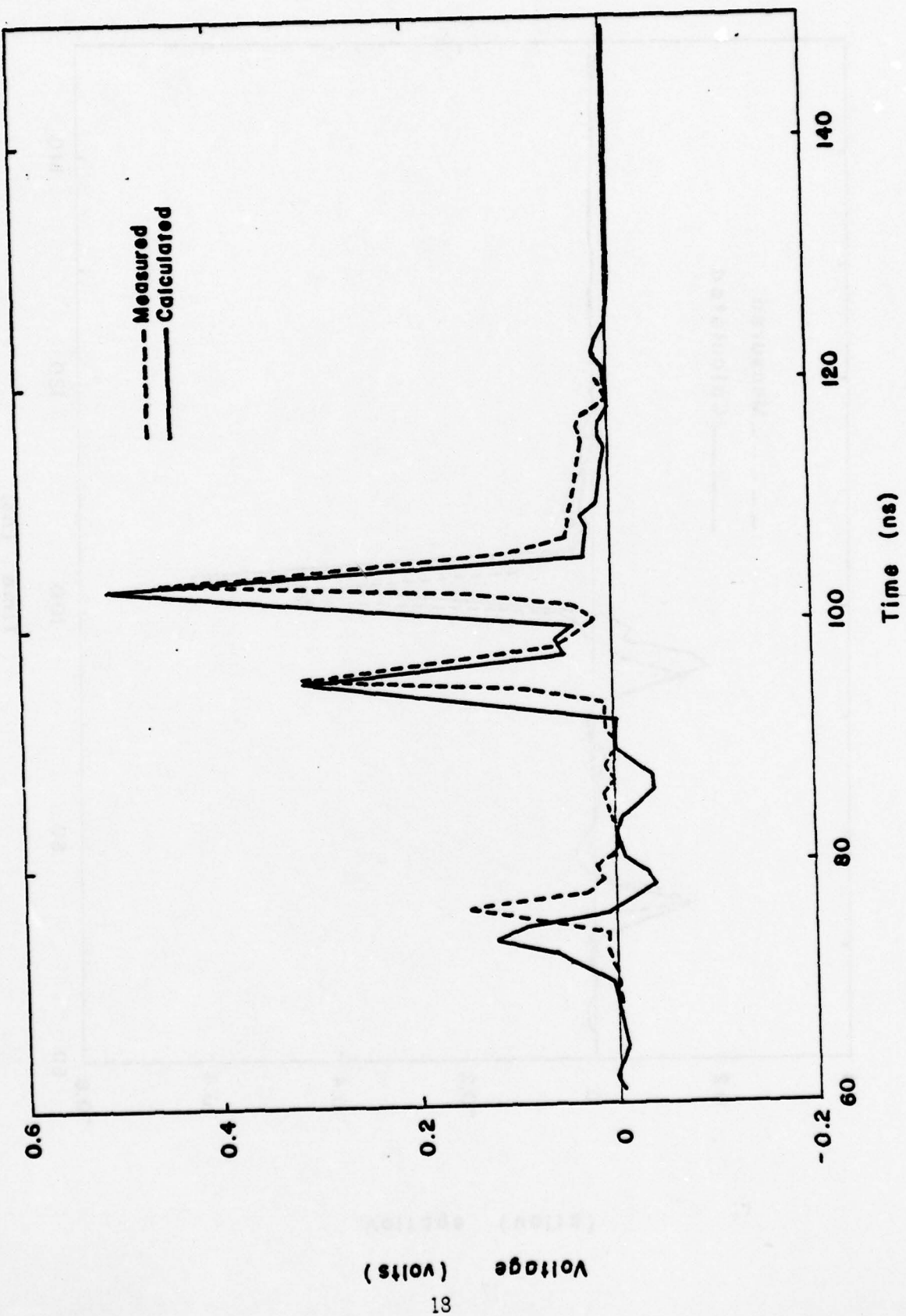


Figure 4b. Transient voltage of wire 2 at J_2 when wire 2 at J_1 is driven.

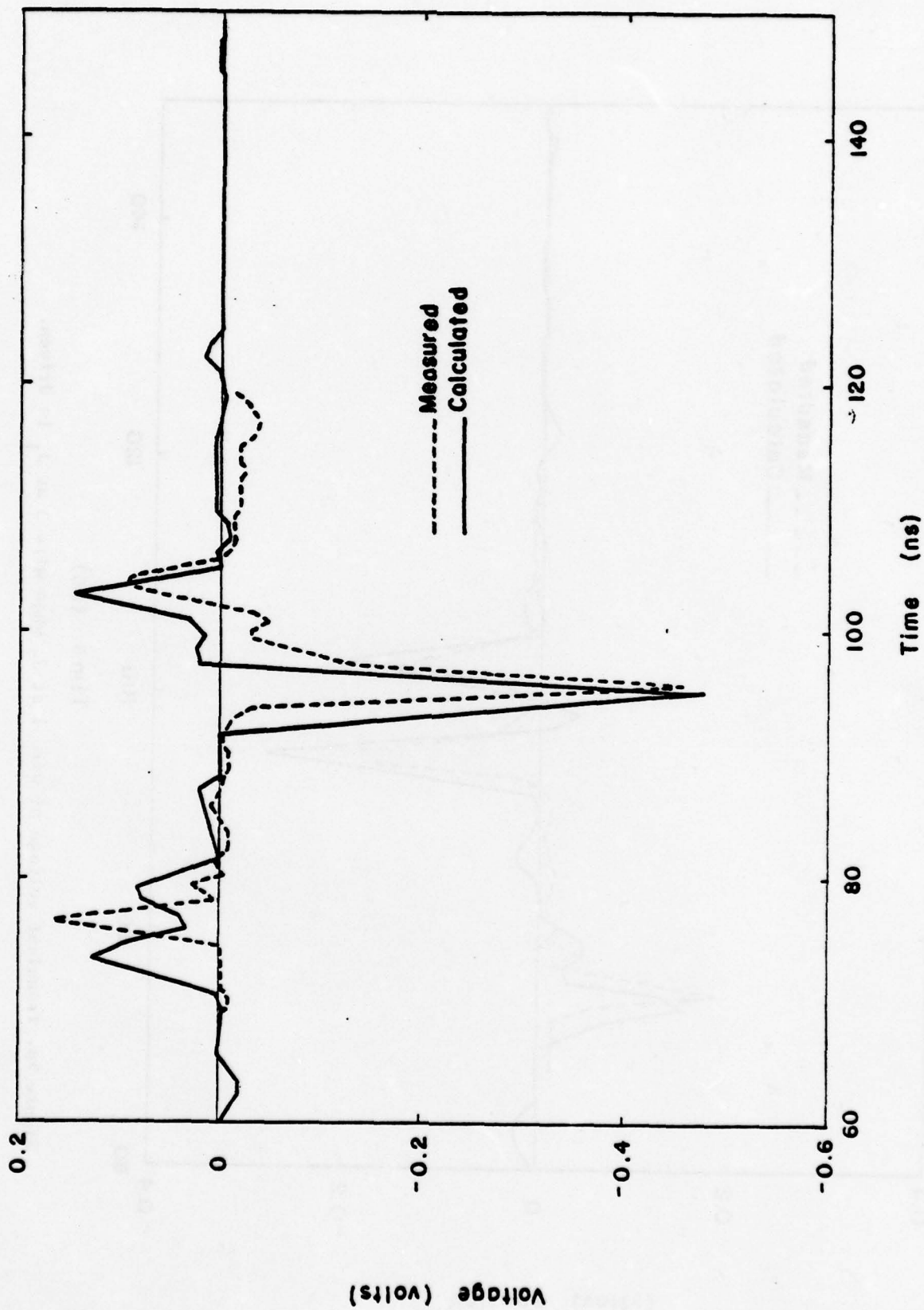


Figure 4c. Transient voltage of wire 3 at J_2 when wire 2 at J_1 is driven.

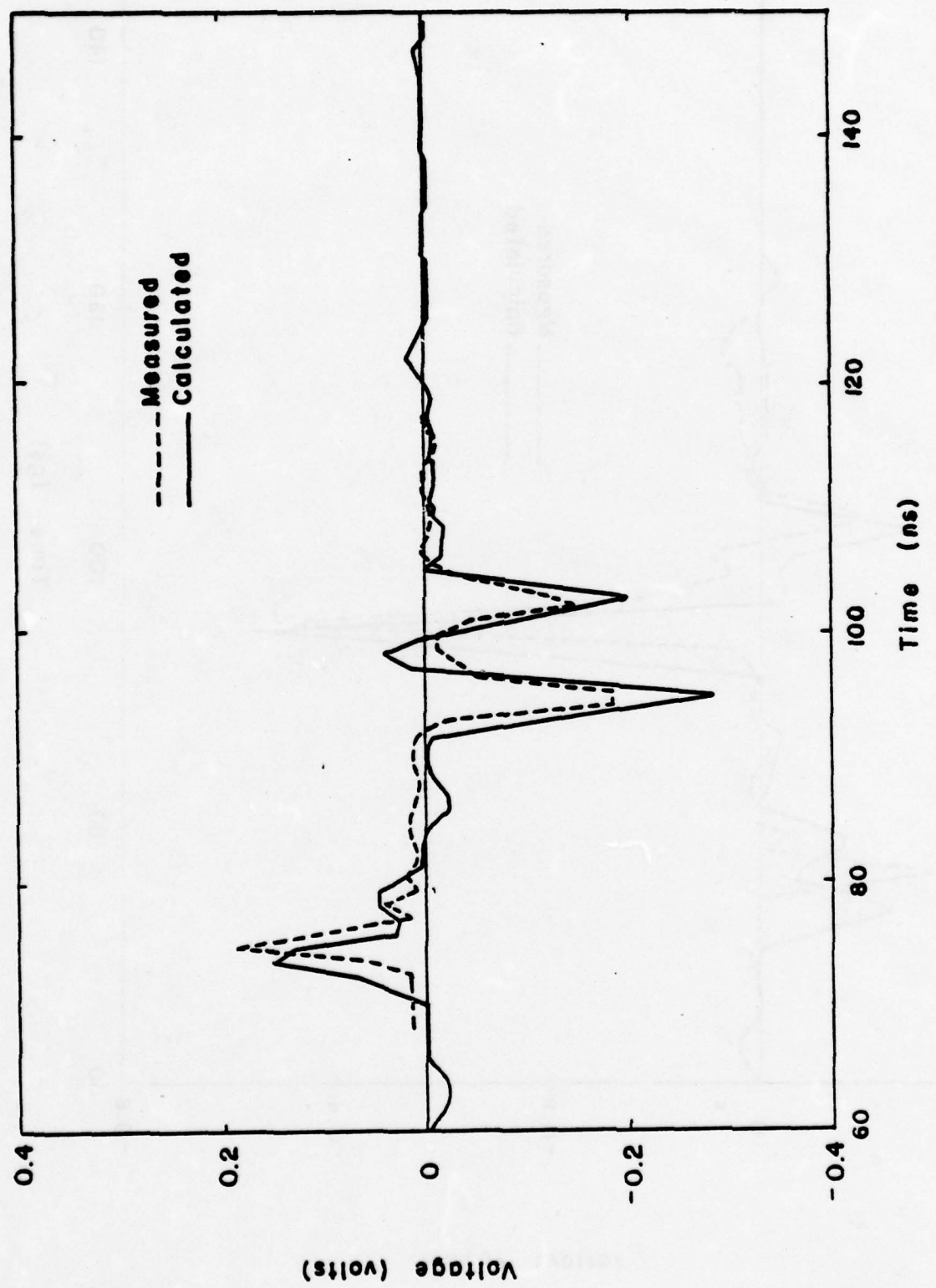


Figure 5a. Transient voltage of wire 1 at J_1 and wire 3 at J_2 when wire 3 at J_2 is driven.

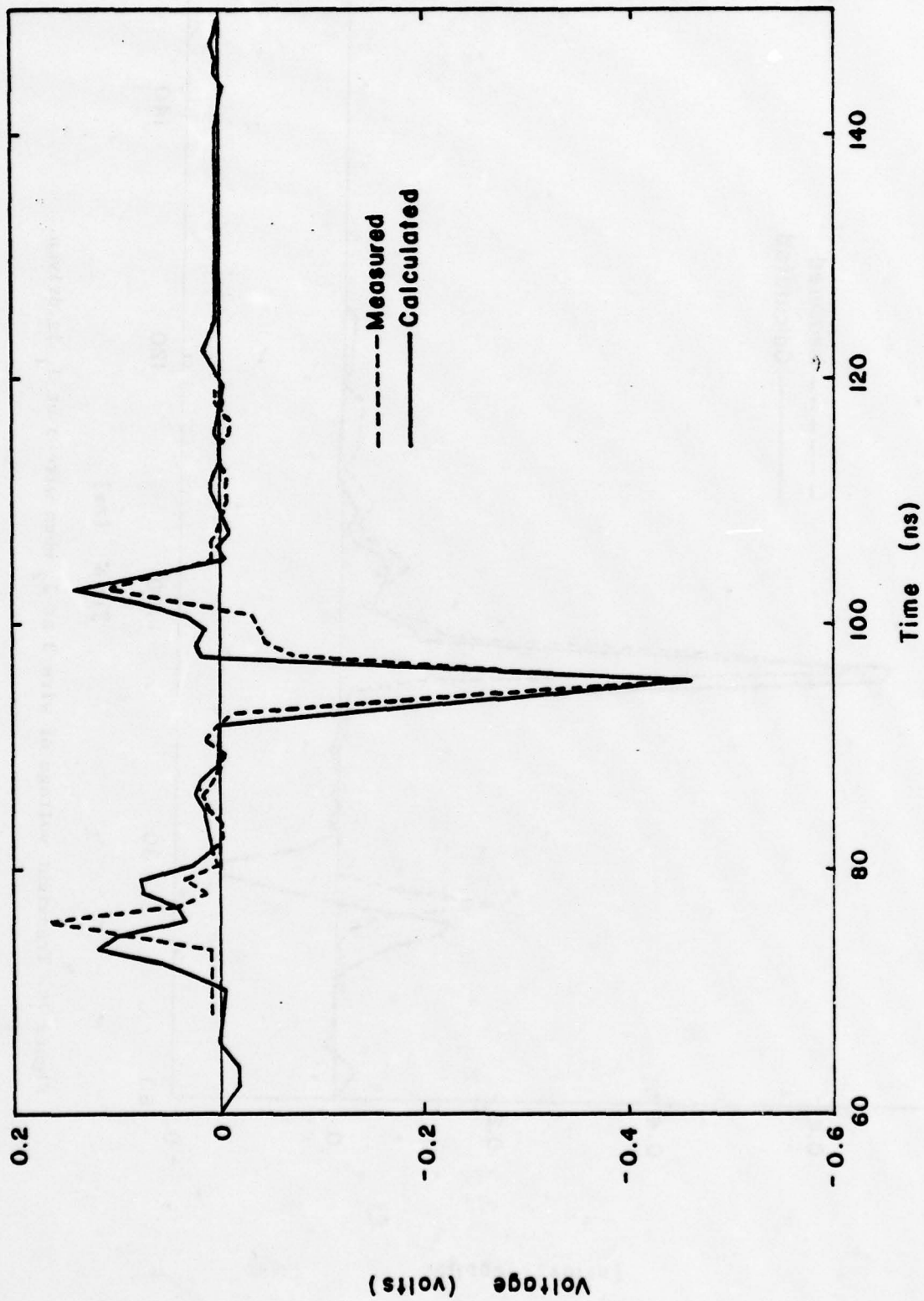


Figure 5b. Transient voltage of wire 2 at J_2 when wire 3 at J_1 is driven.

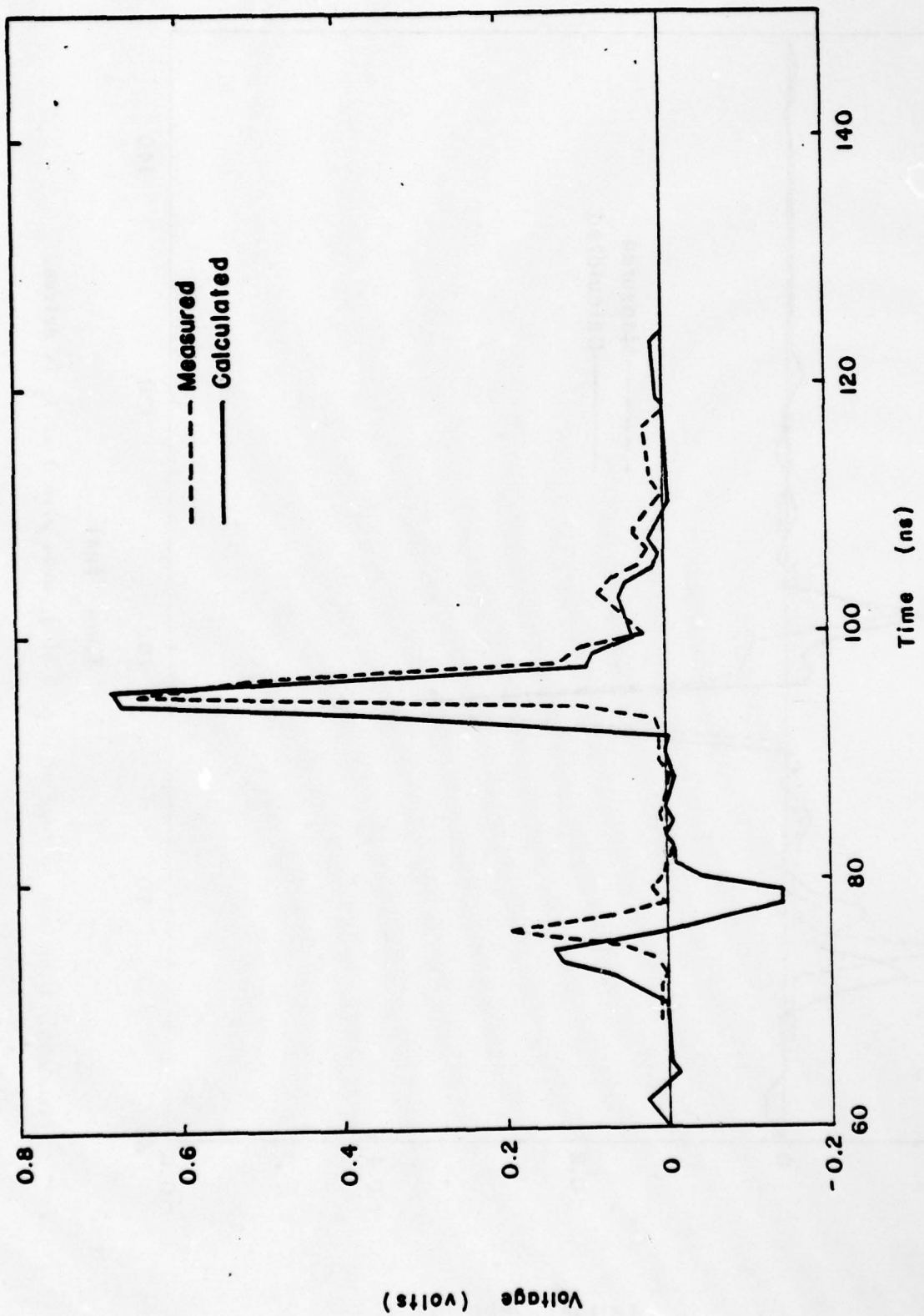


Figure 5c. Transient voltage of wire 3 at J_2 when wire 3 at J_1 is driven.

B. T-network

The T-network being investigated involves a junction of multi-conductor transmission lines. The network geometry is shown in Figure 6a and the wire configurations are shown in Figures 6b, c, and d.

The network topology involves three branches denoted by B_1 , B_2 , B_3 , and, four junctions denoted by J_1 , J_2 , J_3 , J_4 . These three branches, respectively, have five, three and two wires. The wires at junction J_1 were loaded with 50Ω resistors to the ground. Wire 1 at junction 1 was driven by a voltage source. The wires of branch 2 were all terminated at junction J_3 with 50Ω resistors to the ground. The wires of branch 3 were terminated at junction J_4 also with 50Ω resistors to the ground. The three branches are connected at junction J_2 with the branching of wires as shown in Figure 6a.

The voltage sources considered are a pulse generator and a unit-step function generator. The open circuit voltages of the generator are shown in Figure 7. The internal resistances of the generators are 50Ω as shown in the network geometry of Figure 6. The transient voltage responses of the resistors at junctions J_3 and J_4 have been measured and will be compared with calculated results.

The configurations of the wires of all branches are shown in Figures 6b, c, d. The radius of the conductors and insulators and the dielectric constants of the insulators of various wires are listed in Table 3.

The per-unit-length capacitance and inductance matrices were obtained from the time domain reflectometry measurements. Thus, the [C] and [L] matrices for the 5-wire line were measured to be,

$$[C] = \begin{bmatrix} 52.555 & -16.125 & -17.761 & -8.895 & -5.632 \\ -16.125 & 42.145 & -2.319 & -15.357 & -14.264 \\ -17.761 & -2.319 & 35.779 & -3.145 & -6.841 \\ -8.895 & -15.357 & -3.145 & 41.771 & -9.705 \\ -5.6325 & -14.264 & -6.841 & -9.705 & 25.355 \end{bmatrix} \text{ pF/m}$$

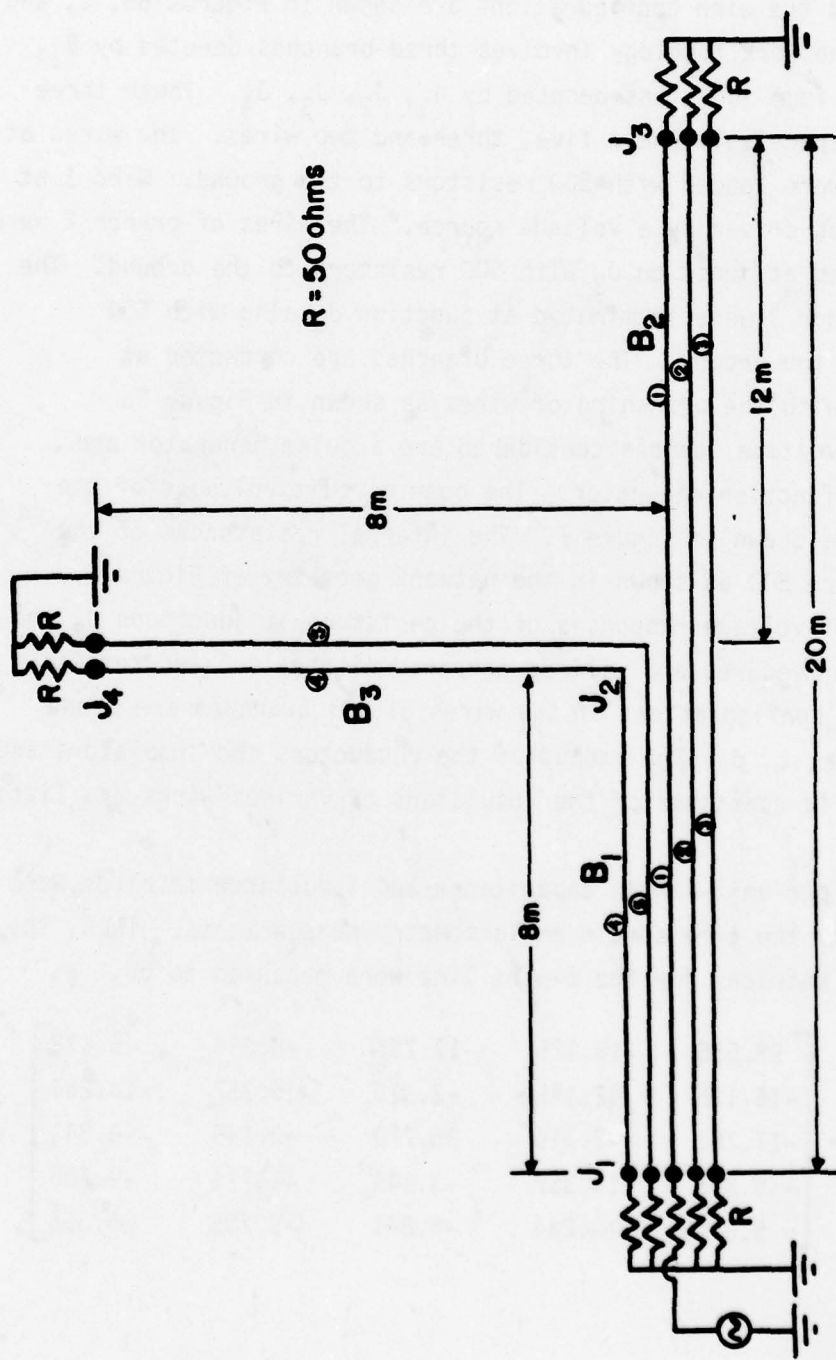
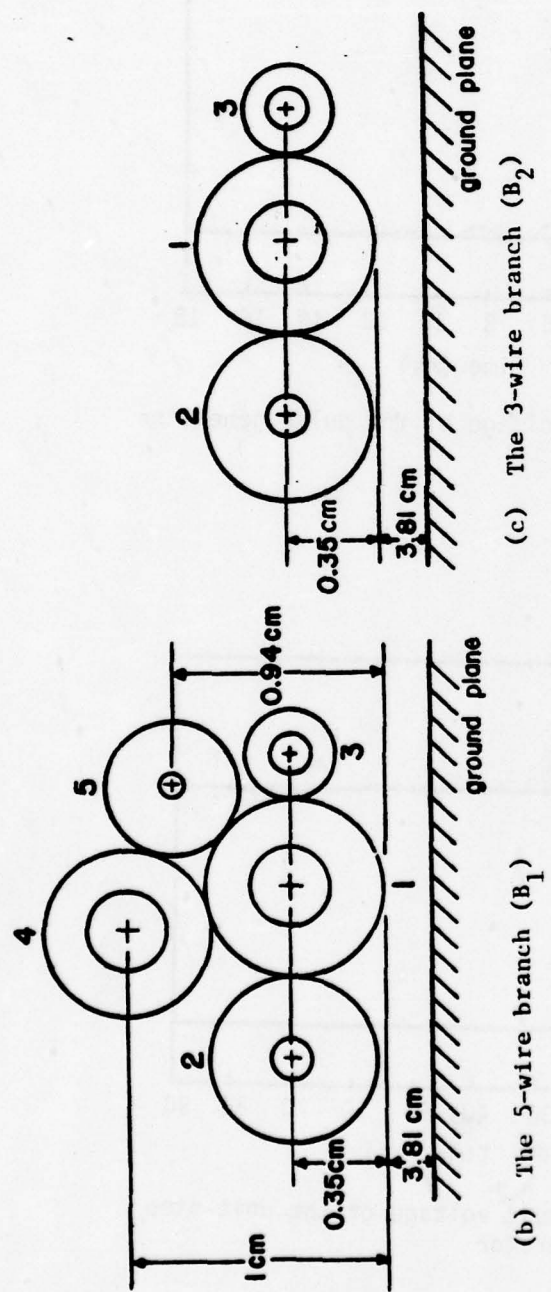
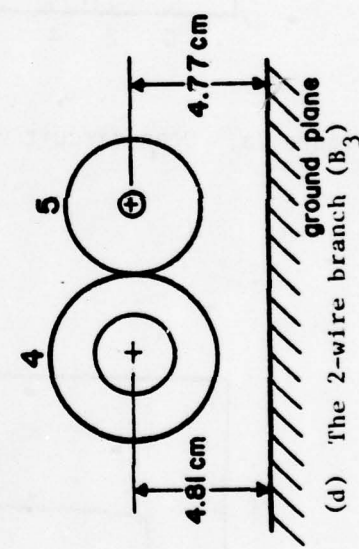


Figure 6a. Geometry of the T-network with 50Ω terminations



(c) The 3-wire branch (B_2)



(d) The 2-wire branch (B_3)

Figures 6b, c and d. The wire configurations of the T-network

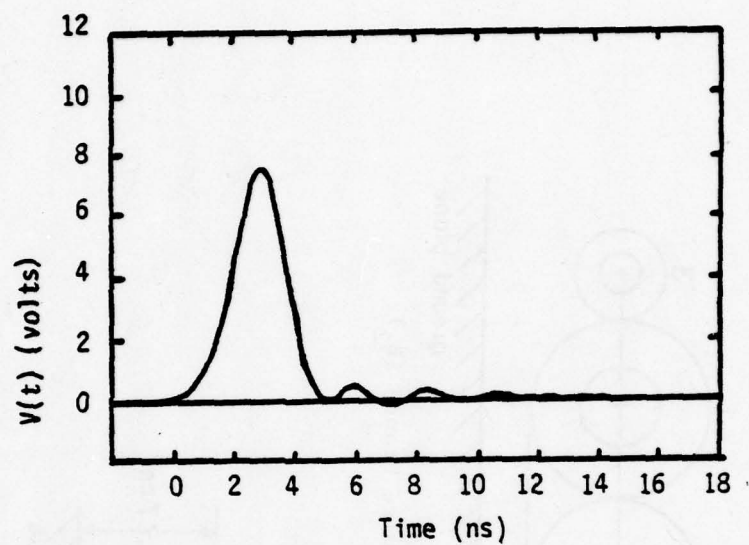


Figure 7a. Open circuit voltage of the pulse generator

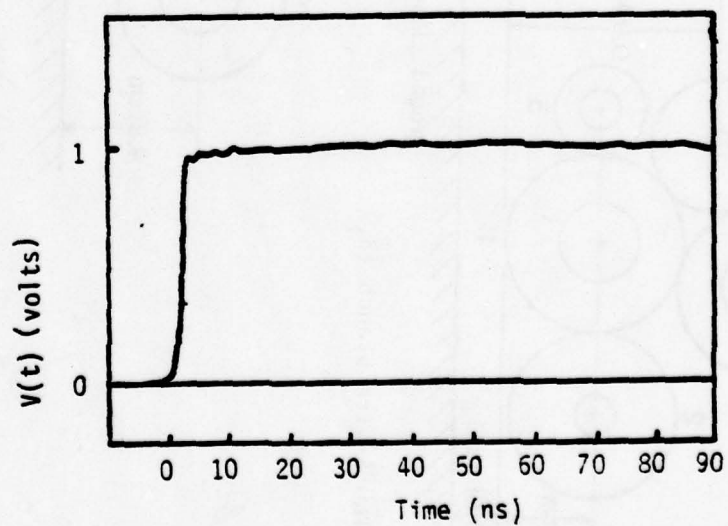


Figure 7b. The open circuit voltage of the unit-step function generator

TABLE 3. WIRE RADIUS AND DIELECTRIC CONSTANTS

Wire no.	Conductor radius	Insulator radius	ϵ_r of insulator
1	$a_1 = 0.108 \text{ cm}$	$b_1 = 0.35 \text{ cm}$	$\epsilon_1 = 2.25$
2	$a_2 = 0.062 \text{ cm}$	$b_2 = 0.33 \text{ cm}$	$\epsilon_2 = 4.10$
3	$a_3 = 0.062 \text{ cm}$	$b_3 = 0.15 \text{ cm}$	$2.7 < \epsilon_3 < 3.0$
4	$a_4 = 0.111 \text{ cm}$	$b_4 = 0.34 \text{ cm}$	$\epsilon_4 = 1.65$
5	$a_5 = 0.0125 \text{ cm}$	$b_5 = 0.25 \text{ cm}$	$\epsilon_5 = 1.41$

$$[L] = \begin{bmatrix} 0.902 & 0.4775 & 0.5399 & 0.48516 & 0.5133 \\ 0.4775 & 0.9513 & 0.38426 & 0.48609 & 0.4239 \\ 0.5399 & 0.38426 & 1.0067 & 0.4247 & 0.5343 \\ 0.48516 & 0.48609 & 0.4247 & 0.8507 & 0.5568 \\ 0.5133 & 0.4239 & 0.5343 & 0.5568 & 1.116 \end{bmatrix} \mu\text{H/m}$$

The corresponding characteristic impedance matrix of the 5-wire line is given by

$$[Z_0] = \begin{bmatrix} 223.073 & 138.964 & 150.885 & 138.278 & 145.372 \\ 138.964 & 229.164 & 115.579 & 140.970 & 125.528 \\ 150.885 & 115.579 & 247.950 & 123.761 & 149.056 \\ 138.278 & 140.970 & 123.761 & 225.051 & 155.647 \\ 145.372 & 125.528 & 149.056 & 155.647 & 295.409 \end{bmatrix} \Omega$$

The line parameters of the 3-wire line branch B_2 are exactly the same as those given in the 3-wire line section discussed before. The per-unit-length capacitance and inductance matrices of the 2-wire line in branch B_3 are

$$[C] = \begin{bmatrix} 26.746 & -14.684 \\ -14.684 & 20.052 \end{bmatrix} \text{ pF/m}$$

$$[L] = \begin{bmatrix} 0.8295 & 0.5334 \\ 0.5334 & 1.1012 \end{bmatrix} \mu\text{H/m}$$

The corresponding impedance matrix of the 2-wire line in branch B_3 is given by

$$[Z_0] = \begin{bmatrix} 227.59 & 156.939 \\ 156.939 & 302.948 \end{bmatrix} \Omega$$

The input data for the QVTT program for this T-network is shown in Table 4. The voltage responses at the load points at J_3 and J_4 have been computed for the purpose of comparing with the experimentally observed data.

TABLE 4. LISTING OF INPUT DATA FOR THE T-NETWORK

```

$TOPO NB=3,NJ=4$
$BRNH IB=1,NWW=5$
$BRNH IB=2,NWW=3$
$BRNH IB=3,NWW=2$
$JNC JN=1,NBJJ=1,IBB(1)=1S
$JNC JN=2,NBJJ=3,IBB(1)=1,2,3S
$JNC JN=3,NBJJ=1,IBB(1)=2S
$JNC JN=4,NBJJ=1,IBB(1)=3S
$LDPTS NLOAD=5,JLOAD(1)=3,3,3,4,4,LLOAD(1)=2,2,2,3,3,LLNO(1)=1,2,3,1,2S
$LINEPRM XK(1,1)=52.555E-12,-16.125E-12,-17.761E-12,-8.895E-12,-5.6325E-12,
    XK(1,2)=-16.125E-12,42.1453E-12,-2.319E-12,-15.357E-12,-1.4264E-12,
    XK(1,3)=-17.761E-12,-2.319E-12,35.779E-12,-3.145E-12,-6.8411E-12,
    XK(1,4)=-8.895E-12,-15.357E-12,-3.145E-12,41.771E-12,-9.705E-12,
    XK(1,5)=-5.6325E-12,-1.4264E-12,-6.8411E-12,-9.705E-12,25.355E-12,
    XL(1,1)=0.902E-6,0.4775E-6,0.5399E-6,0.48516E-6,0.51334E-6,
    XL(1,2)=0.4775E-6,0.9513E-6,0.38426E-6,0.48609E-6,0.4239E-6,
    XL(1,3)=0.5399E-6,0.38426E-6,1.0067E-6,0.4247E-6,0.5343E-6,
    XL(1,4)=0.48516E-6,0.48609E-6,0.4247E-6,0.8507E-6,0.5568E-6,
    XL(1,5)=0.51334E-6,0.4239E-6,0.5343E-6,0.5568E-6,1.116E-6,
    XLEN=8.0,IFLAG=0$  

$SOURCES XLPOS=0.0,VSRC(1)=1.0S
$LINEPRM XK(1,1)=46.4807E-12,-20.9093E-12,-20.5534E-12,
    XK(1,2)=-20.9093E-12,33.8339E-12,-4.1526E-12,
    XK(1,3)=-20.5534E-12,-4.1526E-12,31.0993E-12,
    XL(1,1)=0.883944E-6,0.484157E-6,0.535475E-6,
    XL(1,2)=0.484157E-6,0.939843E-6,0.378936E-6,
    XL(1,3)=0.535475E-6,0.378936E-6,0.992230E-6,
    XLEN=12.0,IFLAG=0$  

$SOURCESS
$LINEPRM XK(1,1)=26.746E-12,-14.684E-12,
    XK(1,2)=-14.684E-12,20.052E-12,
    XL(1,1)=0.8295E-6,0.5334E-6,
    XL(1,2)=0.5334E-6,1.1012E-6,
    XLEN=8.0,IFLAG=0$  

$SOURCESS
$CONN JN=1,NOCC=1$  

$LOC JZL=2$  

$LOAD Z(1)=50.0,50.0,50.0,50.0,50.0$  

$CONN JN=2,NOCC=5$  

$CNM JC(1)=1,0,0,0,0,1,0,0,0,0$  

$CNM JC(1)=0,1,0,0,0,0,1,0,0,0$  

$CNM JC(1)=0,0,1,0,0,0,0,1,0,0$  

$CNM JC(1)=0,0,0,1,0,0,0,0,1,0$  

$CNM JC(1)=0,0,0,0,1,0,0,0,0,1$  

$CONN JN=3,NOCC=1$  

$LOC JZL=2$  

$LOAD Z(1)=50.0,50.0,50.0$  

$CONN JN=4,NOCC=1$  

$LOC JZL=2$  

$LOAD Z(1)=50.0,50.0$  

$FFTDR TMAX=200.,M=9$  

$WVFORM ISTEP=3$  

$WVMATCH NTT=13,TT(1)=0.0,2.4,3.5,4.4,5.6,6.8,7.8,  

    9.0,11.0,12.4,14.4,16.0,18.0,  

    VTT(1)=0.0,3.0,6.0,3.0,-0.1,0.3,0.05,0.25,  

    0.1,0.2,0.0,0.18,0.0,SCAL=1.25$ } Note that for Unit-  

$WVFORM ISTEP=0$ } step response, change to:  

$WVFORM ISTEP=1$ } SWVFORM ISTEP=1$ and delete $WVMATCH...$  


```

Figures 8a, b, c, d, and e are the transient voltage responses of a pulse input driving on wire 1 at J_1 . For all the load points, the comparison between the measured and the calculated results show good agreement. For the response on wire 4 at J_4 , the measured curve has a very sharp peak at about 75 ns. The duration of the peak is about 1 ns. We were unable to obtain this peak from the calculation because the program limits us to the use of time steps no finer than 1 ns. We were later informed by the personnel of Mission Research Corporation* that their direct time domain calculation also did not show that particular peak. From their judgment, the peak may be caused by the coupling of nearby objects during the measurements.

The unit step responses of the T-network has also been compared. The excitation in the calculations is an ideal unit step function driving wire 1 at junction J_1 . The excitation of the laboratory measurement is shown in Figure 7b, and is observed to have a rise time of about 2 to 3 ns. Although this idealization will affect only the early time responses, it should be pointed out that the deviation of the calculations from the experimental data is not significant even at early times.

Figures 9a, b, c, d, and e show the comparison of calculated and measured transient responses on the load points at junctions J_3 and J_4 .

* A.K. Agrawal, Mission Research Corporation, personal communication, June 1978.

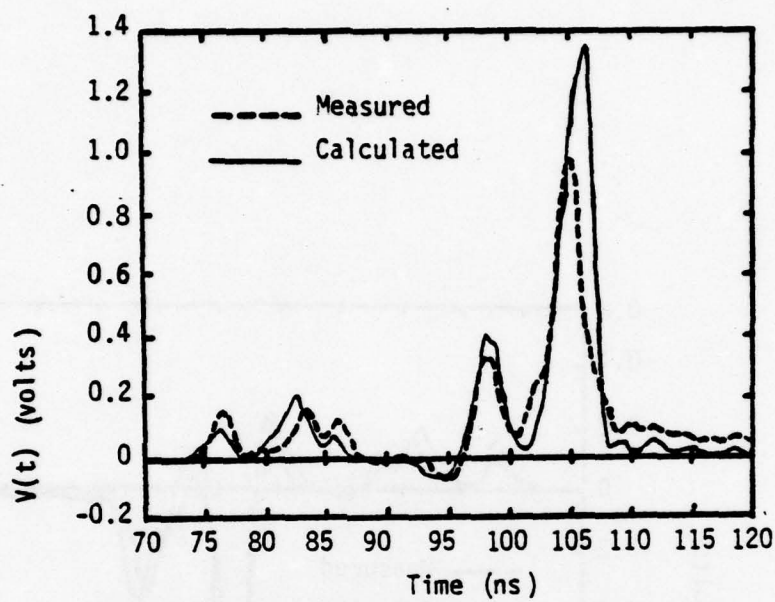


Figure 8a. Transient voltage on wire 1 at J_3

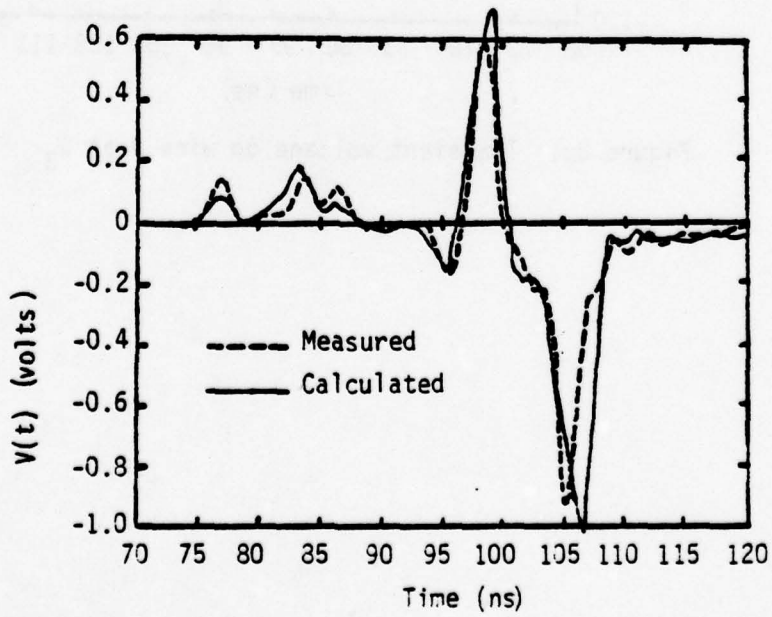


Figure 8b. Transient voltage on wire 2 at J_3

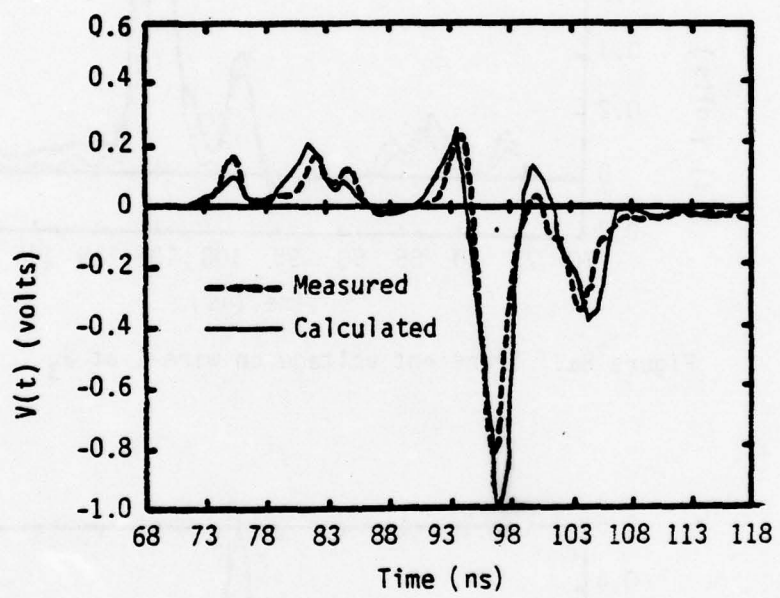


Figure 8c. Transient voltage on wire 3 at J_3

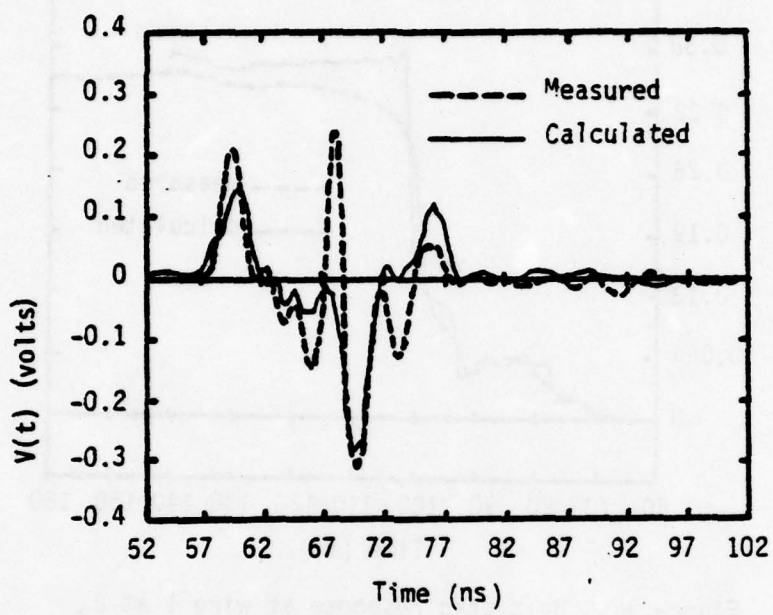


Figure 8d. Transient voltage on wire 4 at J_4

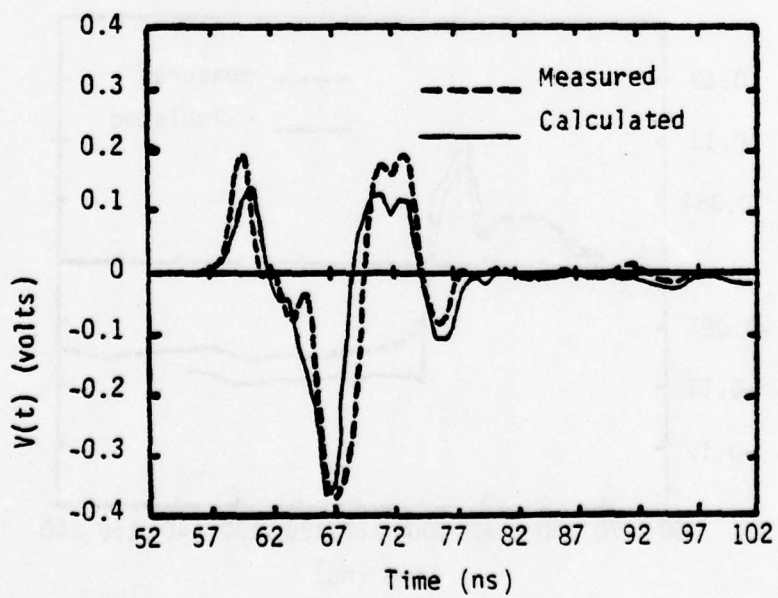


Figure 8e. Transient voltage on wire 5 at J_4

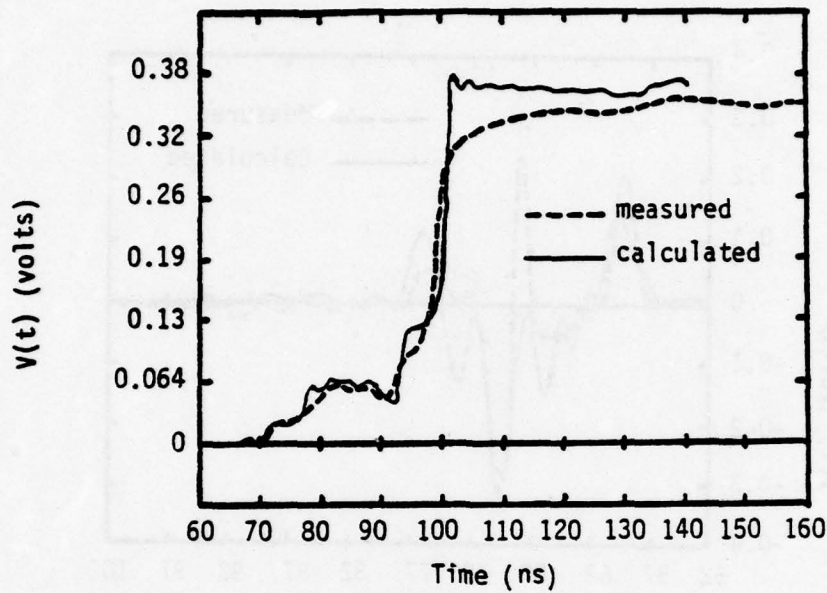


Figure 9a. Unit step response at wire 1 at J_3

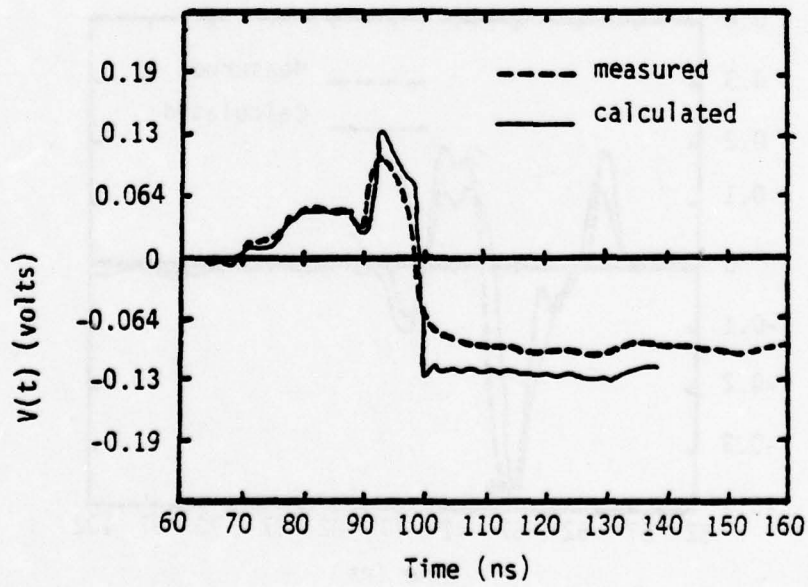


Figure 9b. Unit step response at wire 2 on J_4

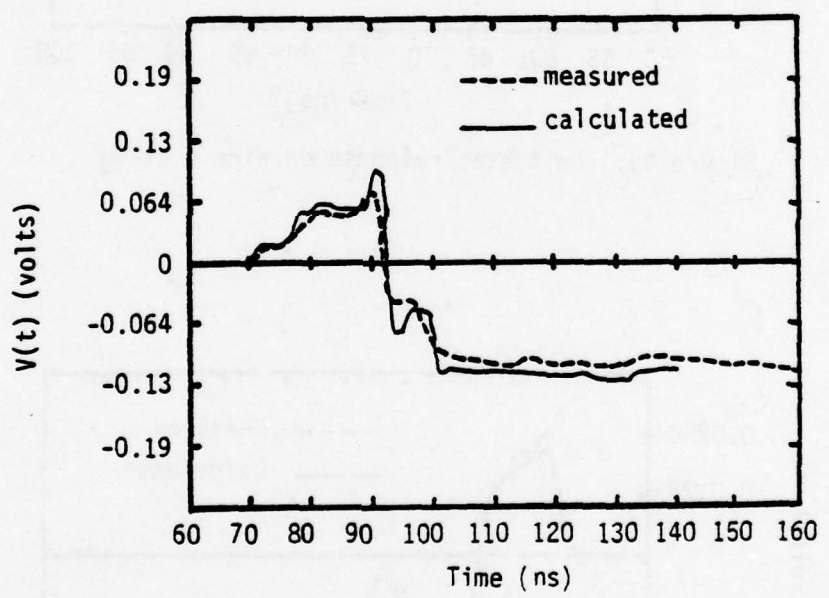


Figure 9c. Unit step response on wire 3 at J_3

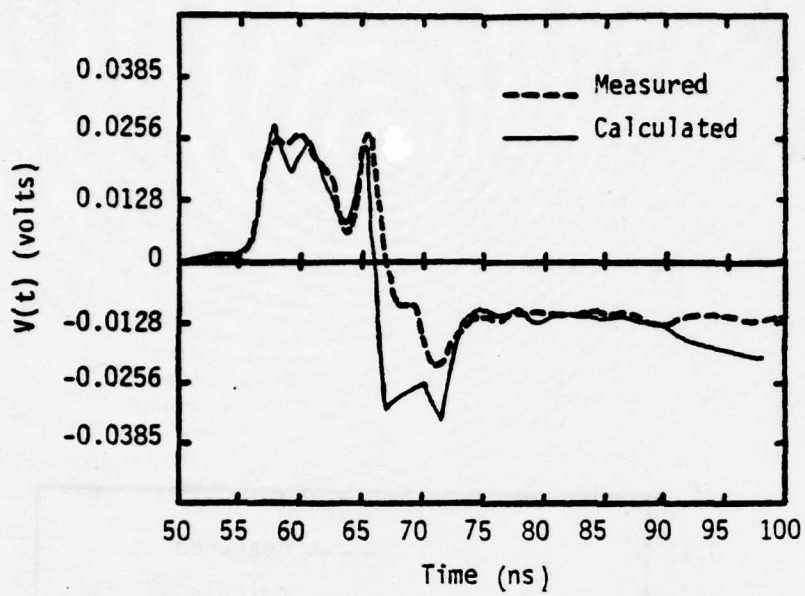


Figure 9d. Unit step response on wire 4 at J_4

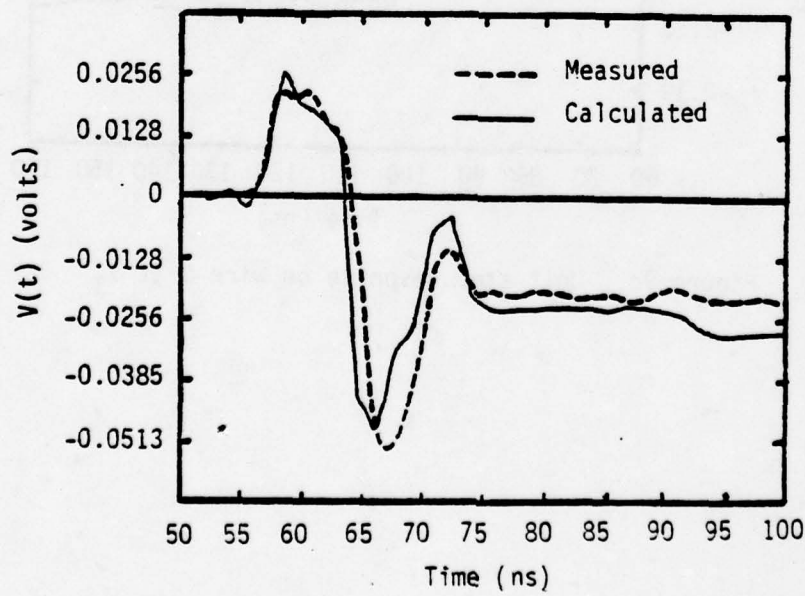


Figure 9e. Unit step response on wire 5 at J_4

C. The H-network

Having completed the comparison of numerical calculations with the experimental data for the 3-wire line section and the T-network, we now turn our attention to a somewhat more complicated transmission network. A diamond shaped network had originally been proposed; but owing to the complications in the laboratory setup, this was later changed to an H-shaped network, in consultation with AFWL personnel. The transient voltage responses in an H-network involving two transmission line junctions were experimentally measured and the results provided [Ref. 5] for the purpose of comparison with numerical results. The H-network as shown in Figure 10a consists of five single-wire transmission line sections of 1.524 m, 3.048 m and 4.572 m in length. The transit time of the signals in each section is about 5 ns, 10 ns, and 15 ns, respectively.

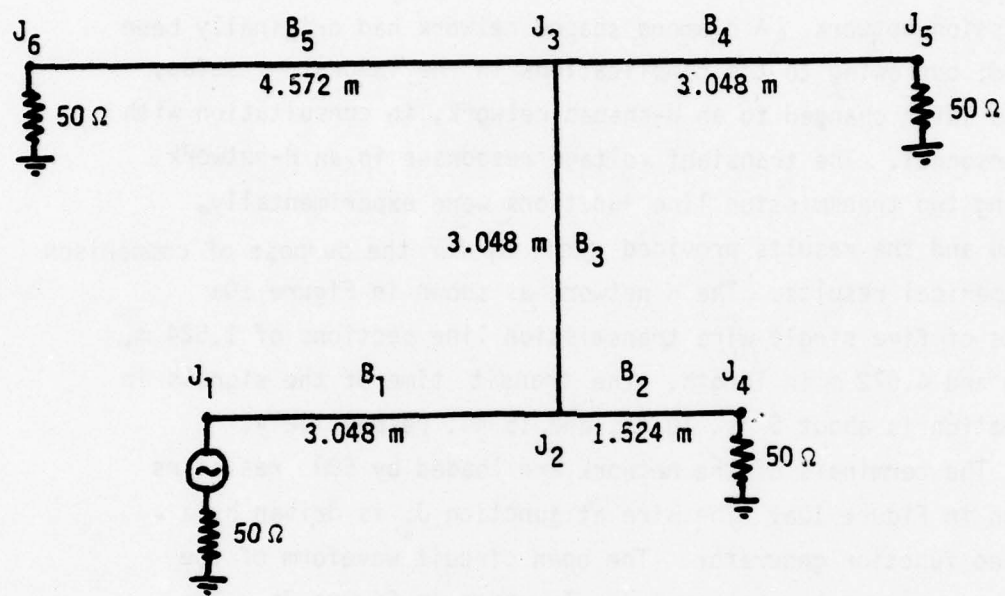
The terminals of the network are loaded by 50Ω resistors as shown in Figure 10a. The wire at junction J_1 is driven by a unit step function generator. The open circuit waveform of the function generator has been previously shown in Figure 7b. The voltages at junctions J_1 , J_4 , J_5 , and J_6 were experimentally observed and numerically computed as well.

All the transmission line sections have the same configurations and a typical cross section of the lines is shown in Figure 10b. The wires are supported over a ground plane by suitably placed styrofoam ($\epsilon_r \approx 1$) blocks. The ground plane is 0.915 m wide which will be approximated to be an infinite ground plane. The per-unit-length capacitance of the wire is*

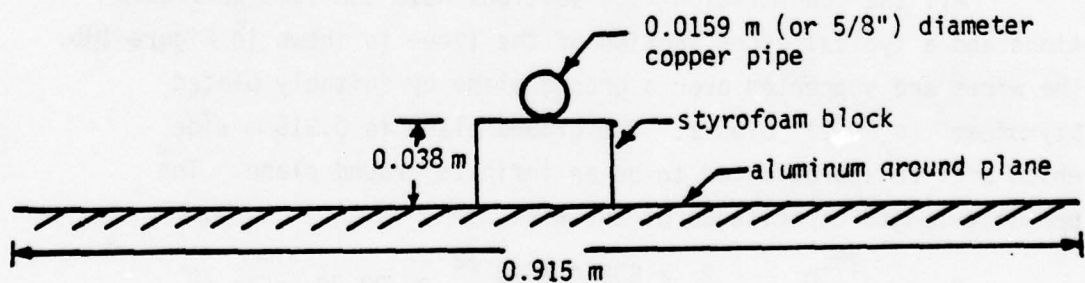
$$C = \frac{2\pi\epsilon_0}{\ln\left(\frac{2h}{a}\right)} = \frac{2 \times 8.854 \times 10^{-12}}{\ln\left(\frac{2 \times 4.605}{0.795}\right)} \approx 22.70 \text{ pF/m}$$

The input data for the QV7T program are shown in Table 5.

* EMP Interaction Handbook, Section 2.4.2, To be published by the Air Force Weapons Laboratory, Kirtland AFB, NM.



(a) The H-network with 50Ω terminations.



(b) Cross section -- any branch.

Figure 10. Geometry of the H-network

TABLE 5. LISTING OF INPUT DATA FOR THE H-NETWORKS

```

$TOPO NB=5,NJ=6$
$BRNH IB=1,NWW=1$
$BRNH IB=2,NWW=1$
$BRNH IB=3,NWW=1$
$BRNH IB=4,NWW=1$
$BRNH IB=5,NWW=1$
$JNC JN=1,NBJJ=1,IBB(1)=1$
$JNC JN=2,NBJJ=3,IBB(1)=1,2,3
$JNC JN=3,NBJJ=3,IBB(1)=3,4,5
$JNC JN=4,NBJJ=1,IBB(1)=2
$JNC JN=5,NBJJ=1,IBB(1)=4
$JNC JN=6,NBJJ=1,IBB(1)=5
$LDPTS NLOAD=4,JLØAD(1)=1,4,5,6,
          LLØAD(1)=1,2,4,5, LLNØ(1)=1,1,1,1
- $LINEPRM XK(1,1)=2.2697E-11, XLEN=3.048, IFLAG=1
$SOURCES XLPOS=0.0, VSRC(1)=1.0, CSRC(1)=0.0
- $LINEPRM XK(1,1)=2.2697E-11, XLEN=1.524, IFLAG=1
$SOURCES$
$LINEPRM XK(1,1)=2.2697E-11, XLEN=3.048, IFLAG=1
$SOURCES$
$LINEPRM XK(1,1)=2.2697E-11, XLEN=3.048, IFLAG=1
$SOURCES$
$LINEPRM XK(1,1)=2.2697E-11, XLEN=4.572, IFLAG=1
$SOURCES$
$CONN JN=1
$LDC JZL=1
$LOAD Z(1)=50.0
$CONN JN=2,NOCC=1
$CNM JC(1)=1,1,1
$CONN JN=3 NOCC=1
$CNM JC(1)=1,1,1
$CONN JN=4
$LDC JZL=1
$LOAD Z(1)=50.0
$CONN JN=5
$LDC JZL=1
$LOAD Z(1)=50.0
$CONN JN=6
$LDC JZL=1
$LOAD Z(1)=50.0
$FFTDR TMAX=400,M=9
$WVFORM ISTEP=1
$WVFORM ISTEP=0
$WVFORM ISTEP=0
$WVFORM ISTEP=0
$WVFORM ISTEP=0
TOPO NB=0

```

Figures 11a., b., c., d show the transient voltage responses across the 50Ω resistors at every termination of the network. As seen in Figures 11b and d, the measured signals are found to travel slower than the speed of light. The slowdown may be caused by the actual laboratory environment such as the styrofoam, the finite ground plane and other nearby objects.

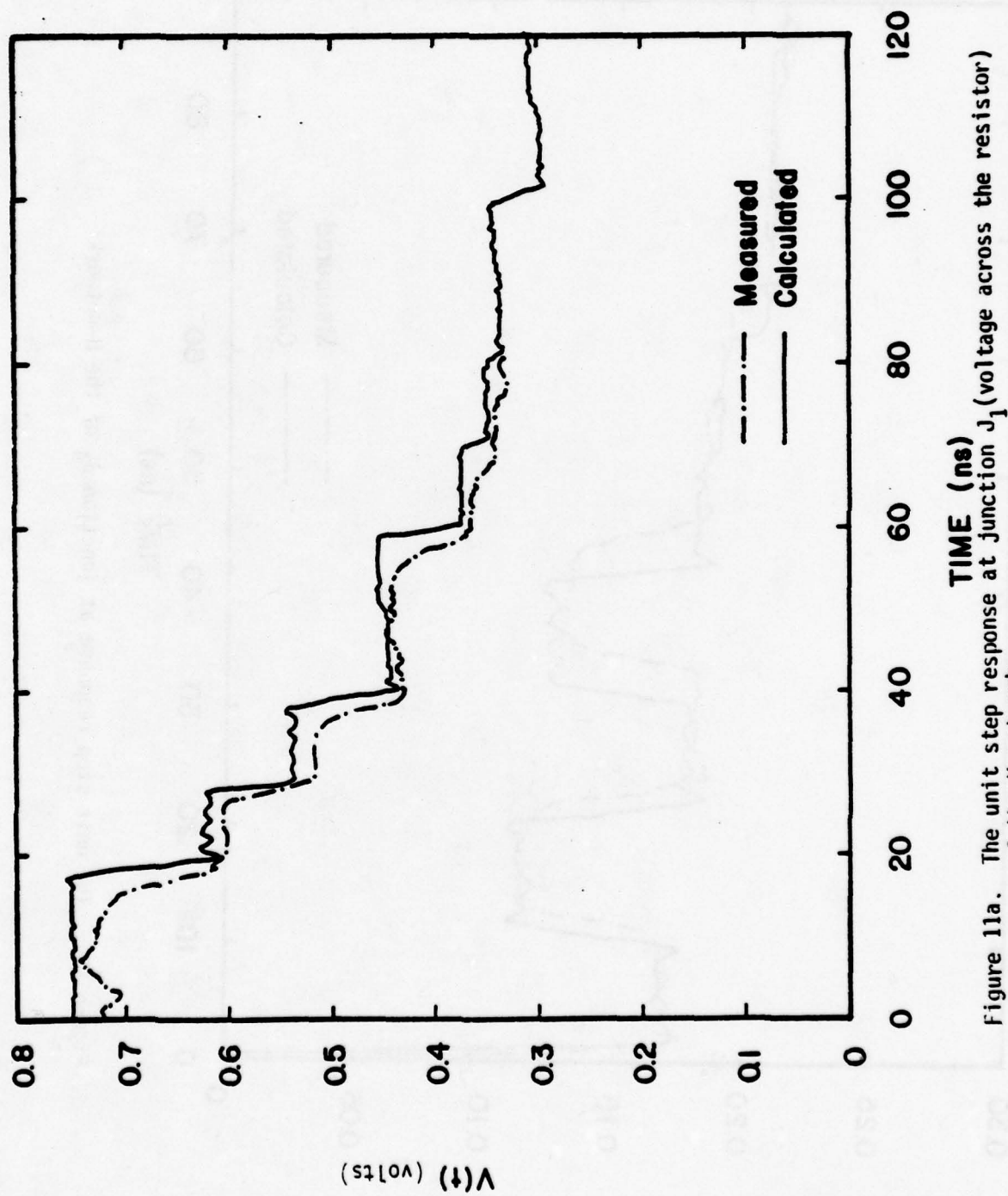


Figure 11a. The unit step response at junction J_1 (voltage across the resistor) of the II-network

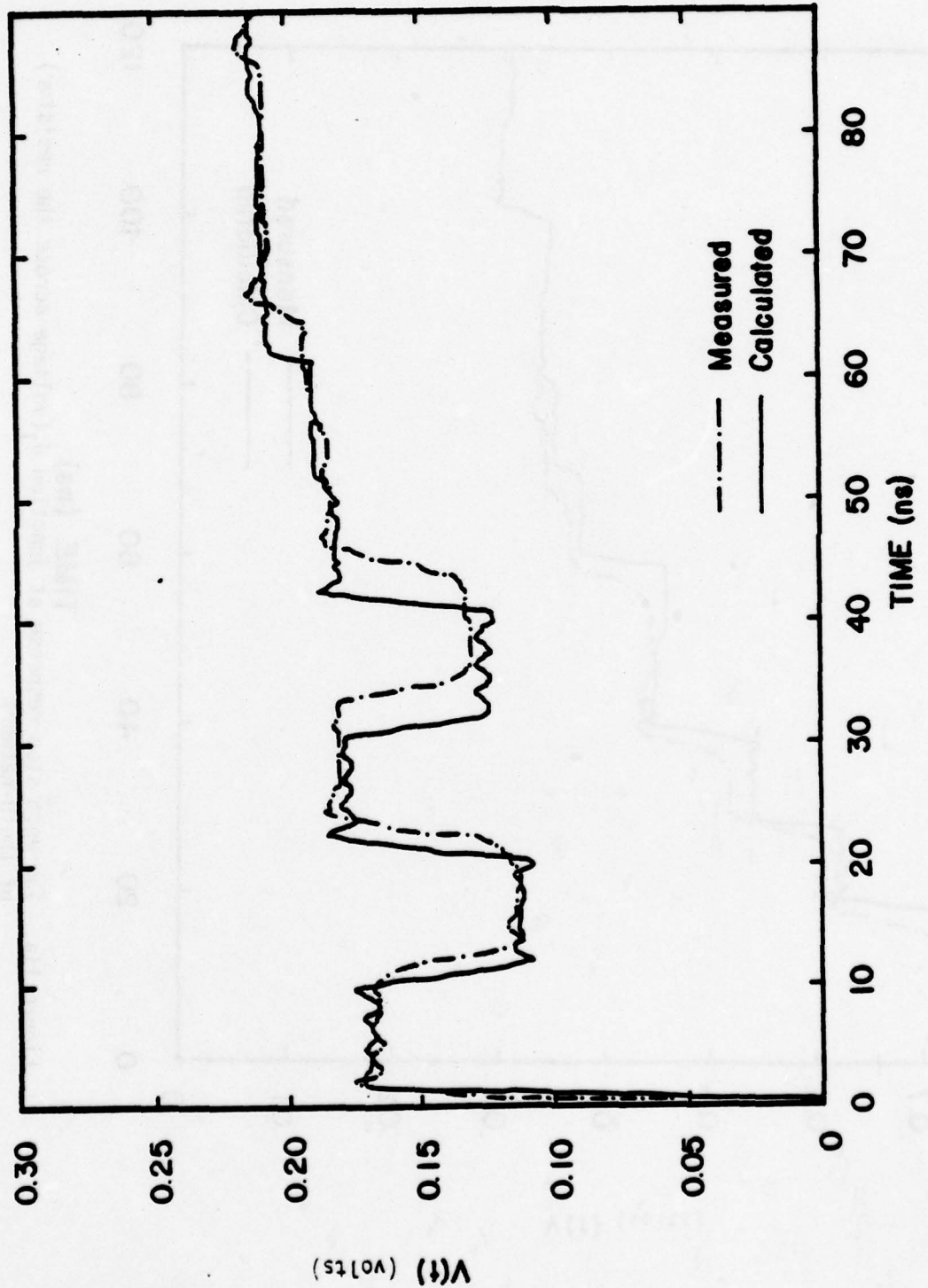


Figure 11b. The unit step response at junction J_4 of the H-network

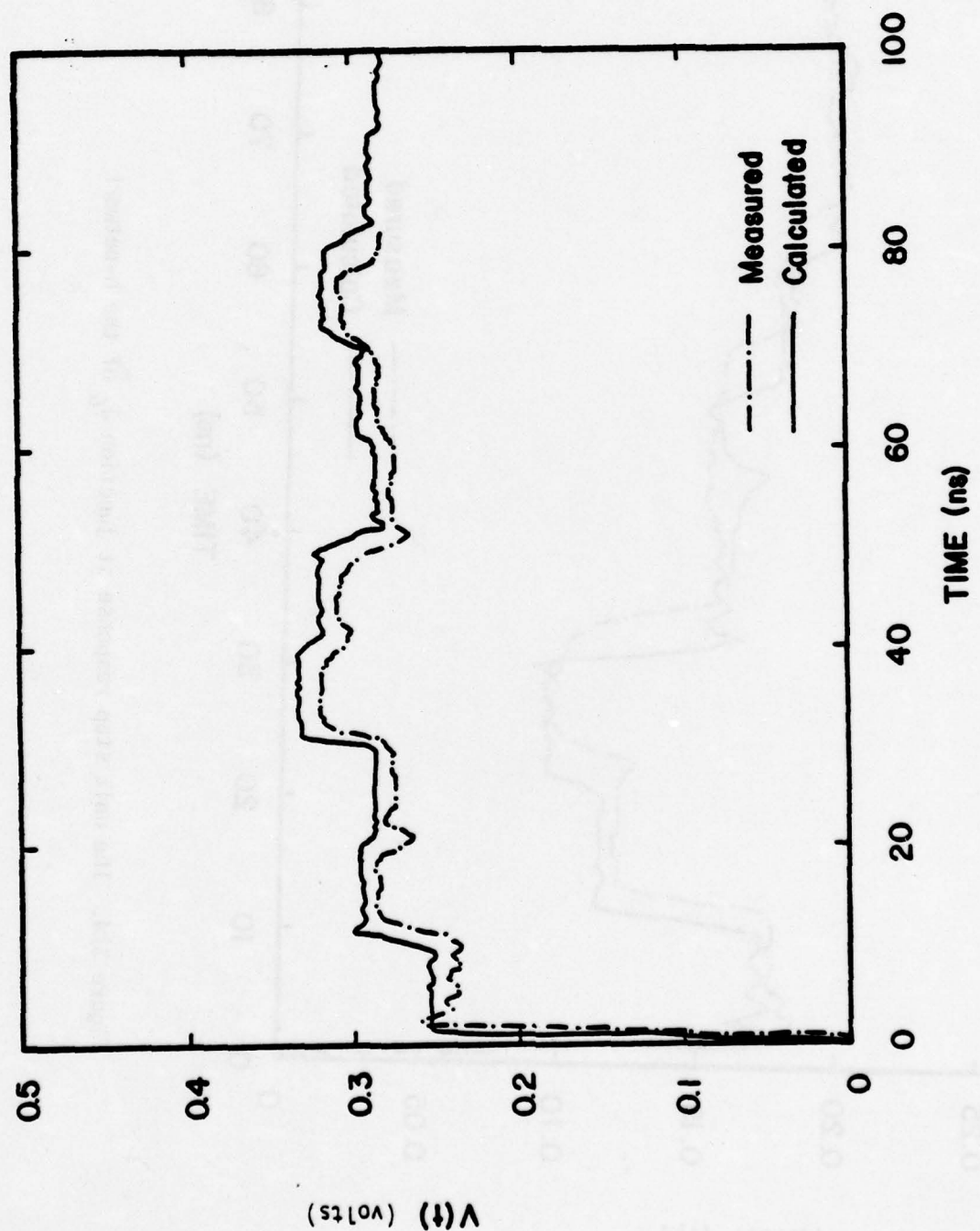


Figure 11c. The unit step response at junction J_5 of the H-network

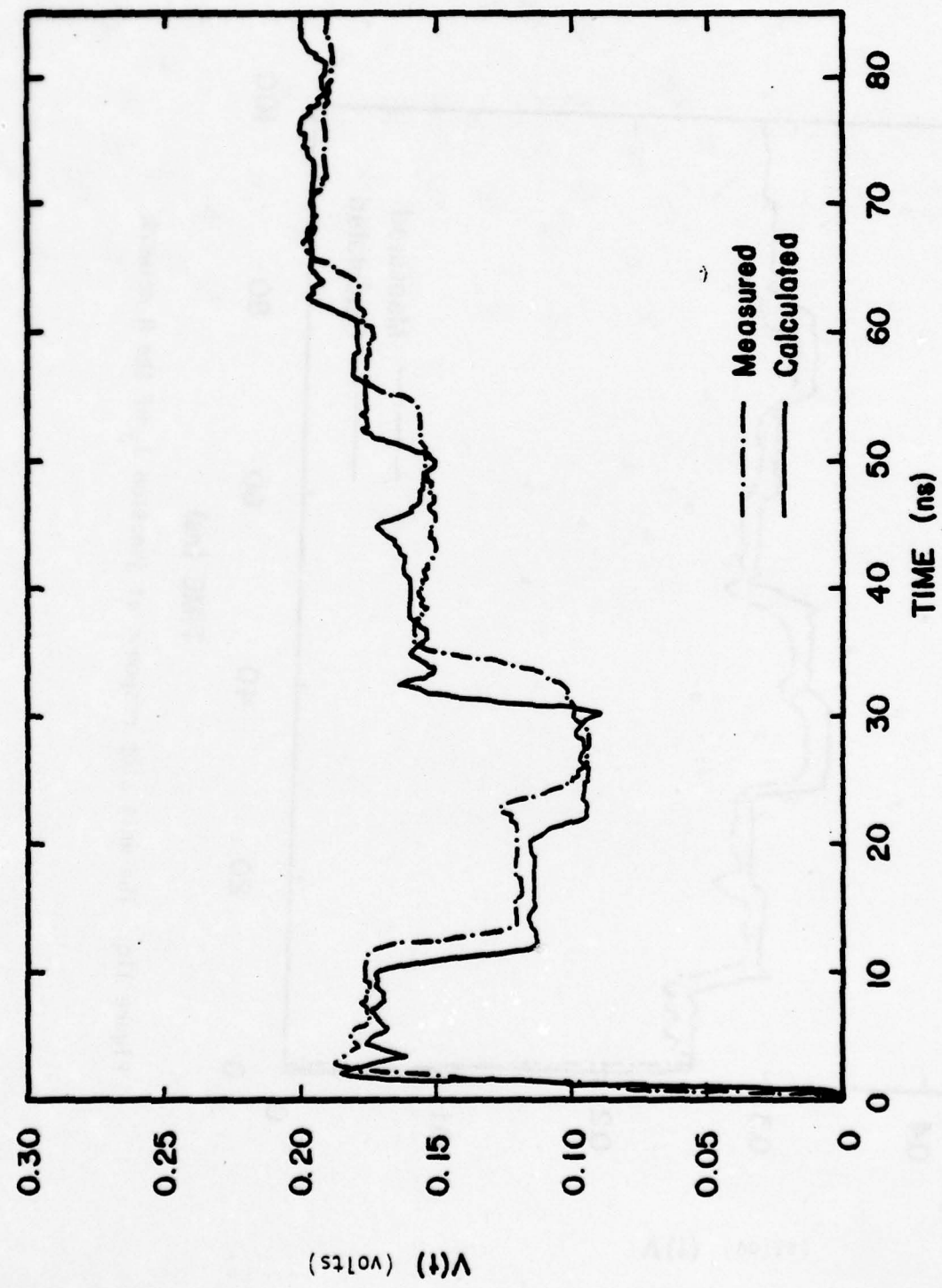


Figure 11d. The unit step response at junction J_6 of the H-network

Summarizing this section, we find that there is good agreement between the measured transient response on the laboratory models and the numerically evaluated responses which make use of the QV7T computer code. Since the measured driving waveform for the pulse input was digitized for use in the numerical computations, the agreement between the theory and experiment is seen to be somewhat better than for the step input, for which an idealized waveform was used in the calculation. However, it should be pointed out for the case of the step input the departure in calculated responses from the measured responses is not significant.

In the following section, we turn our attention to compute and compare the transient response on a power cable inside the TACAMO aircraft, with experimentally measured data in the ATHAMAS I (HPD) facility at AFWL.

SECTION III

COMPARISON WITH TACAMO POWER CABLE MEASUREMENT

In addition to the laboratory models discussed previously, we have also obtained adequate data on some cables in an aircraft from the TACAMO Add-On Testing. Specifically, the 60-90 kVA power cable assembly 13499 which is connected to No. 1 engine will be considered in this report for data comparisons.

The power cable consists of seven wires for the three phase power system. It runs parallel to the edge of the wing from the engine and enters the aircraft interior through two receptacles located at the pressure break. The two bundles of the cable inside the airplane body are terminated in the distribution box.

During the EMP simulation test, it is conjectured that the power cable picks up energy mainly from the portion of the cable along the edge of the wing. The excitation sources of the cable in the wing are distributed along the line, and hence difficult to determine. In order to simplify the measurement and analysis we shall use the Thévenin equivalent circuit to represent the outside section of the cable by input impedances and open circuit voltages. Neglecting the coupling of the energy into the power cable in the interior of the aircraft body from any other sources, we are able to establish a network model with the equivalent discrete sources at the pressure break.

Several major modifications on the QV7T computer code have been made to enable the calculation of the TACAMO power cable analysis. They are:

1. The original code is suitable only for networks with frequency independent loads. The program was modified to include the cases when some of the loads are frequency dependent.
2. Subroutines were added to generate the impedance of the equivalent circuit from the measured curves.
3. The code was modified to accept the numerical input waveform for each wire. The data were stored in a magnetic tape.

The network topology, impedance, sources, transmission line parameters, and the results of the data comparisons will be discussed separately.

A. Network Topology

The relative location of the power cable in the aircraft is shown in Figure 12. The cable consists of seven wires including one neutral and six others of the three phase power system. Thus, each phase has two wires that are electrically in parallel.

Figure 13 sketches the geometry of the cable inside the aircraft. The power cable actually includes two bundles, one with three wires and another with four wires (including the neutral). The neutral wire branches from the four-wire bundle and is grounded midway between the pressure break and the distribution box.

The terminations of the cable are very complicated impedance networks. For the purpose of comparing with the computer model, transmission lines with simple terminations are desired. Thus, the terminal at the distribution box is shorted and grounded to avoid the complications of the impedance inside the distribution box. The termination at the pressure break will be represented by the Thévenin equivalent circuit which includes the excitation sources. The impedance and driving waveforms of the equivalent circuit will be discussed in the following subsections.

The electrical configuration of the network becomes the one shown in Figure 14. The junctions and branches are defined as follows:

- Junction J_1 : At the pressure break where it connects to the Thévenin circuit.
- Junction J_2 : At the point where the neutral wire branches out from the bundle. It is about 2 meters in length from the pressure break.
- Junction J_3 : At the distribution box (grounded). The wires reaching this junction are connected to the original four wire branch. (Only three wires reach this junction because the neutral wire branches out.)
- Junction J_4 : At the distribution box (grounded). The wires reaching this junction come from the original three wire bundle.

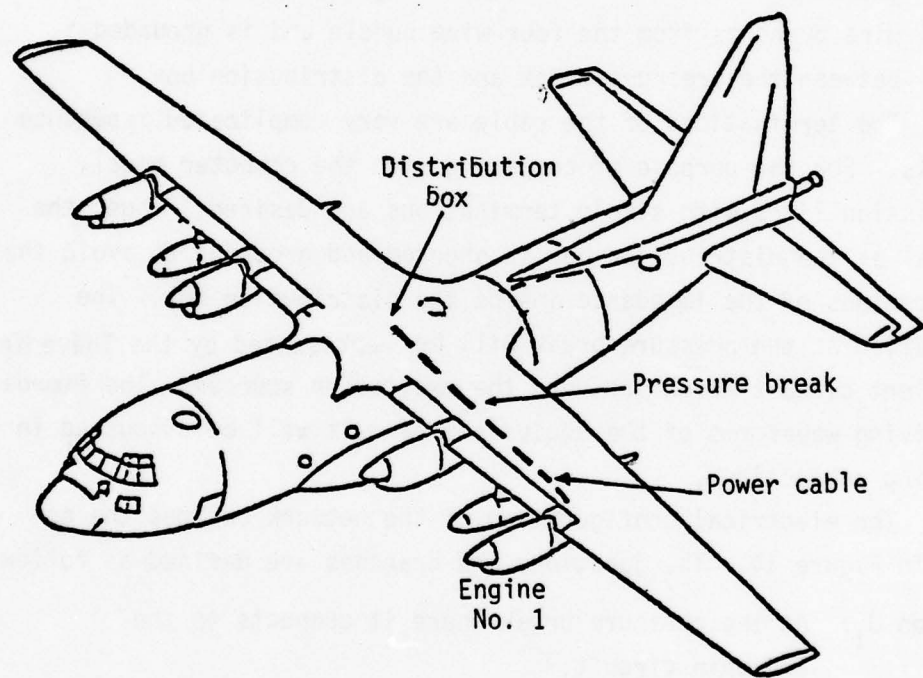


Figure 12. The location of the power cable to be tested

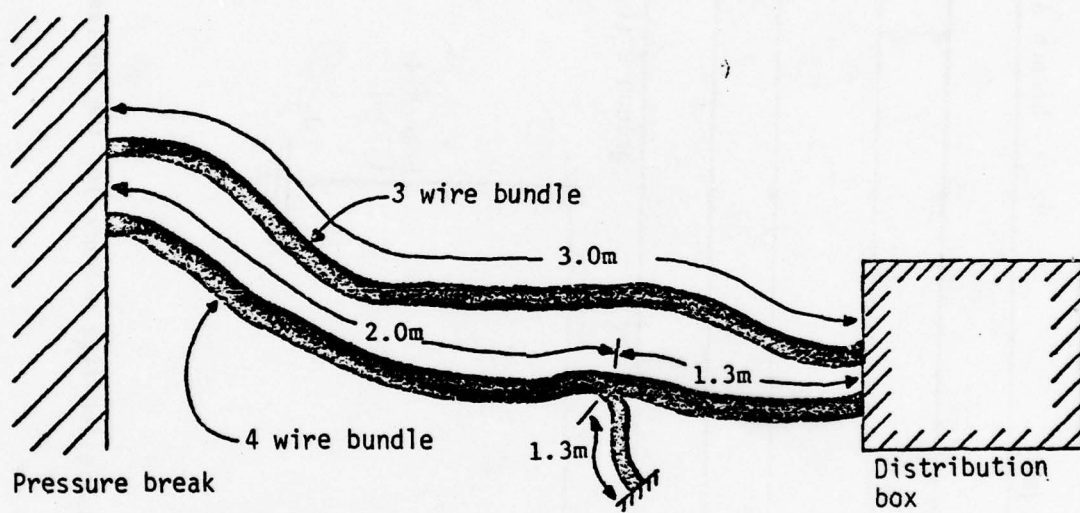


Figure 13. The layout of the power cable

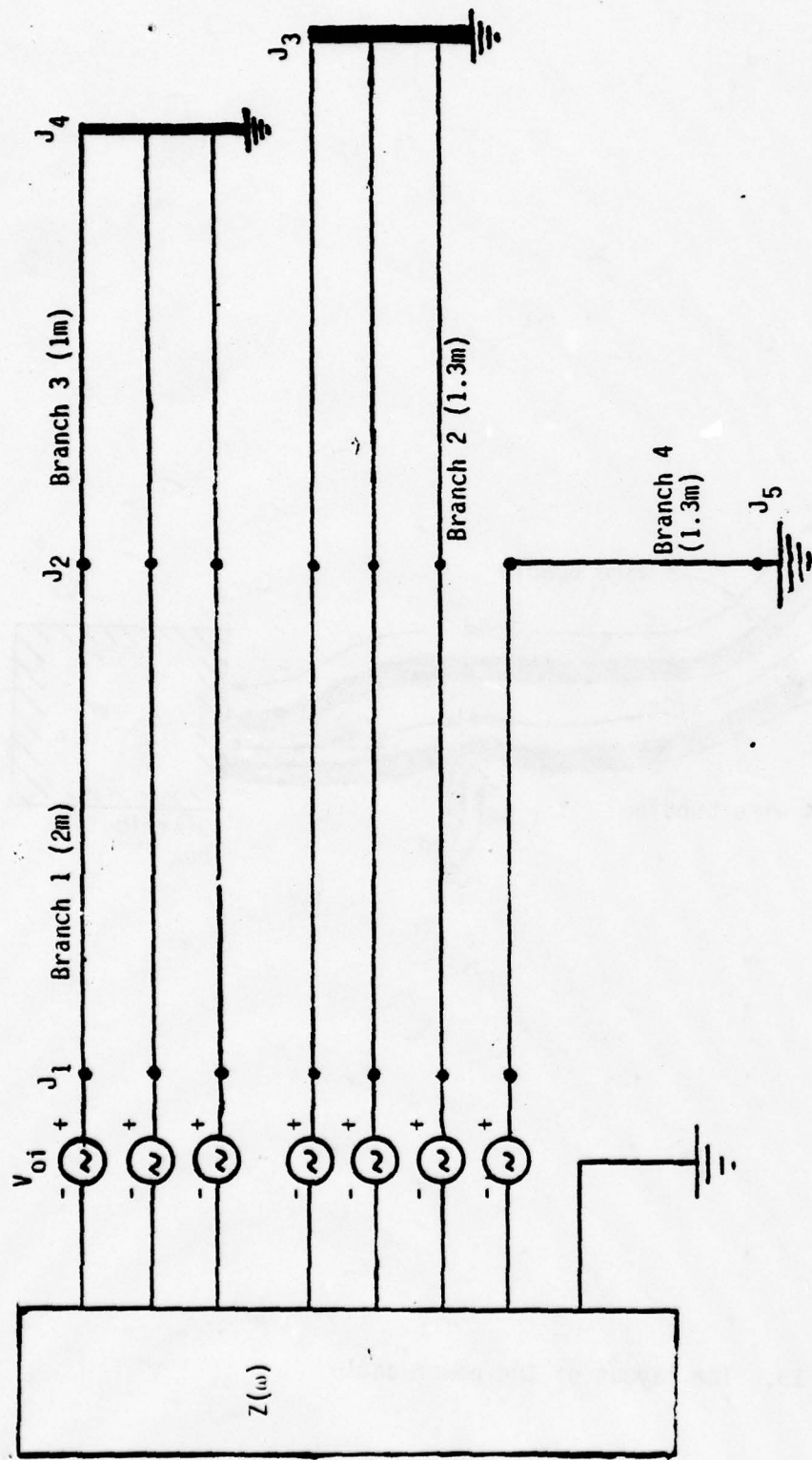


Figure 14. The transmission-line network for the analysis of the power cable.

Branch 1: This branch is 2 meters long and includes all the seven wires from J₁ to J₂.

Branch 2: This branch is 1.3 meters long and includes three wires from J₂ to J₃.

Branch 3: This branch is 1.0 meters long and includes three wires from J₂ to J₄.

Branch 4: This branch is 1.3 meters long and has only the neutral wire from J₂ to J₅ (ground).

B. Equivalent Impedance at Pressure Break Toward Engine No. 1.

The Thévenin equivalent circuit requires the measurement of the impedance matrix for the portion of the cable outside the pressure break. A network analyzer (HP8407A) with the calibrated impedance probe (HP1165A) was used to measure the impedance. The measurements were done in the frequency range of 1 - 110 MHz.

Since the impedance probe (HP1165A) could not reach the connectors at the pressure break during the impedance measurement, a coaxial cable was used to connect between the probe and the terminal. Thus, the measured impedance curves must account for the section of the coaxial cable using the Smith chart or transmission line analysis. The characteristic impedance of the coax is known to be 50Ω . Let the wavenumber and the length of the coaxial cable be β and l respectively. Assume that βl is proportional to the frequency f , we have

$$\beta l = Kf$$

where K (rad/MHz) is a constant independent of frequency. The value of K can be obtained from the curve of the 100Ω terminated coax as shown in Figure 15. Adjusting the curve to the calibration values given by the dashed lines in Figure 15, we found that

(1) at $f = 30.59$ MHz, $\beta l \approx \frac{\pi}{2}$

Hence, $K \approx (\frac{\pi}{2})/30.59 \approx 0.05135$ rad/MHz

(2) at $f = 62.80$ MHz, $\beta l \approx \pi$

Hence, $K \approx \pi/62.80 = 0.05003$ rad/MHz

(3) at $f = 90.90$ MHz, $\beta l \approx \frac{3\pi}{2}$

Hence, $K \approx (\frac{3\pi}{2})/90.90 = 0.05184$ rad/MHz

Taking the average value of the above cases, we have

$$\beta l \approx 0.05107 \times f$$

where f is the frequency in MHz.

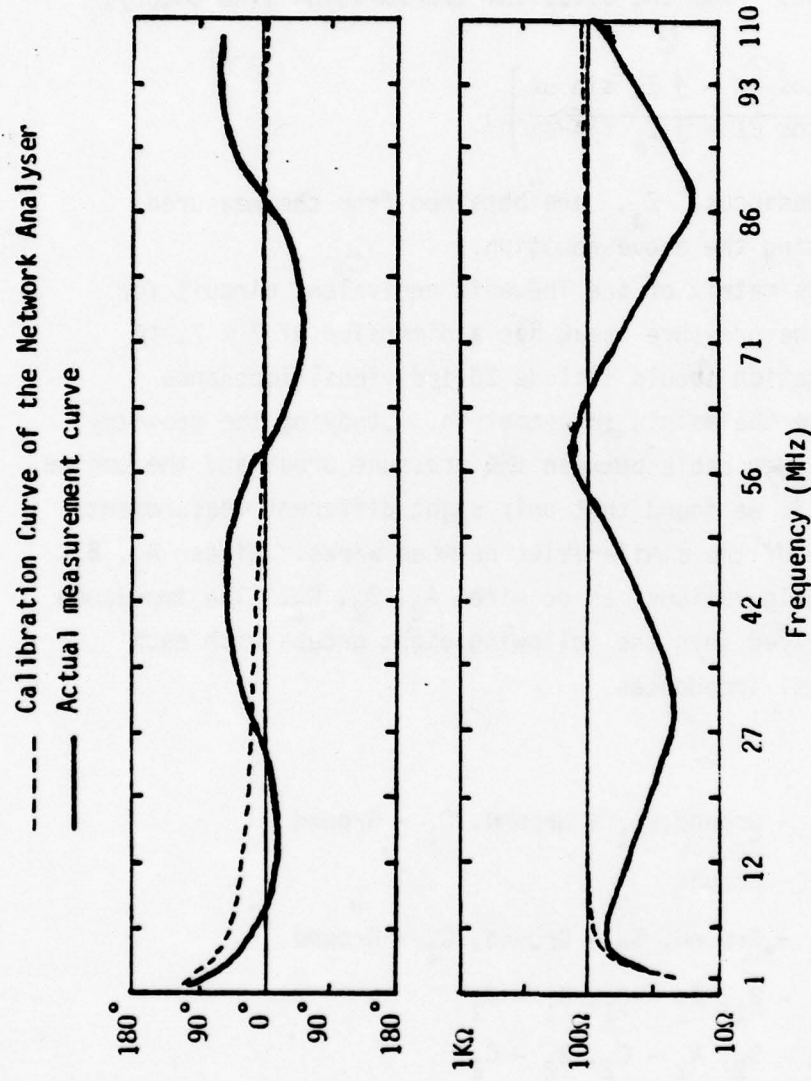


Figure 15. The phase and amplitude of the measured impedance of 100Ω terminated coax, with the calibration curve

All the impedance measurements should be adjusted according to the coax parameters. Figure 16 illustrates the setup of the measurement with coax. From the classical transmission line theory, we have

$$Z_a = Z_c \left[\frac{Z_m \cos \beta l - j Z_c \sin \beta l}{Z_c \cos \beta l - j Z_m \sin \beta l} \right]$$

Hence the actual impedances, Z_a , are obtained from the measured impedances, Z_m , using the above equation.

The impedance matrix of the Thévenin equivalent circuit for the power cable at the pressure break has a dimension of 7×7 . A complete characterization should include 28 individual impedance measurements, because the matrix is symmetric. Studying the geometry of the three-phase power cable between the pressure break and the engine as shown in Figure 17, we found that only eight different measurements are required because of the similarities between wires. Wires A_1, B_1, C_1 have similar configurations, as do wires A_2, B_2, C_2 . The impedance relations can be divided into the following eight groups with each group having identical impedances.

Group 1: A_1 - Ground, B_1 - Ground, C_1 - Ground

Group 2: D_1 - Ground

Group 3: A_2 - Ground, B_2 - Ground, C_2 - Ground

Group 4: $A_1 - B_1, A_1 - C_1, B_1 - C_1$

Group 5: $A_2 - B_2, A_2 - C_2, B_2 - C_2$

Group 6: $A_1 - D_1, B_1 - D_1, C_1 - D_1$

Group 7: $A_2 - D_1, B_2 - D_1, C_2 - D_1$

Group 8: $A_1 - A_2, A_1 - B_2, A_1 - C_2$

$B_1 - A_2, B_1 - B_2, B_1 - C_2$

$C_1 - A_2, C_1 - B_2, C_1 - C_2$.

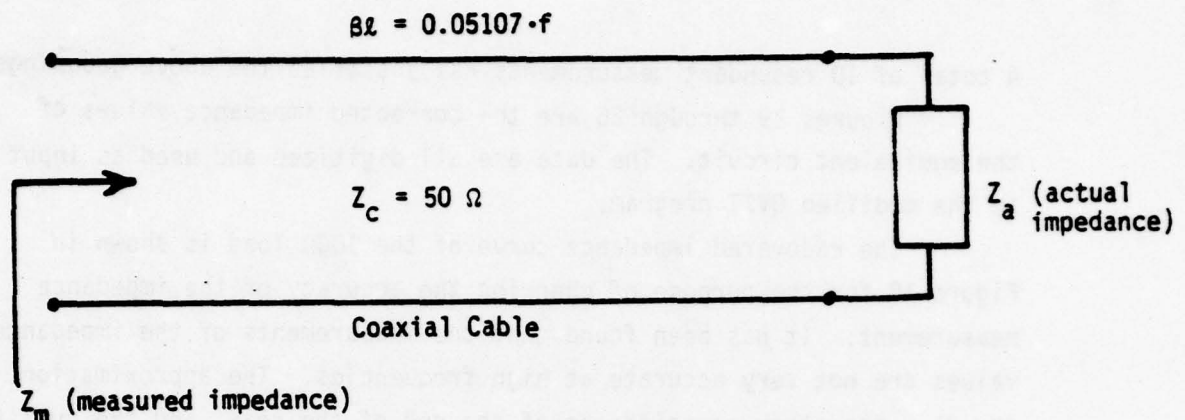


Figure 16. Impedance measurement using a coaxial cable.

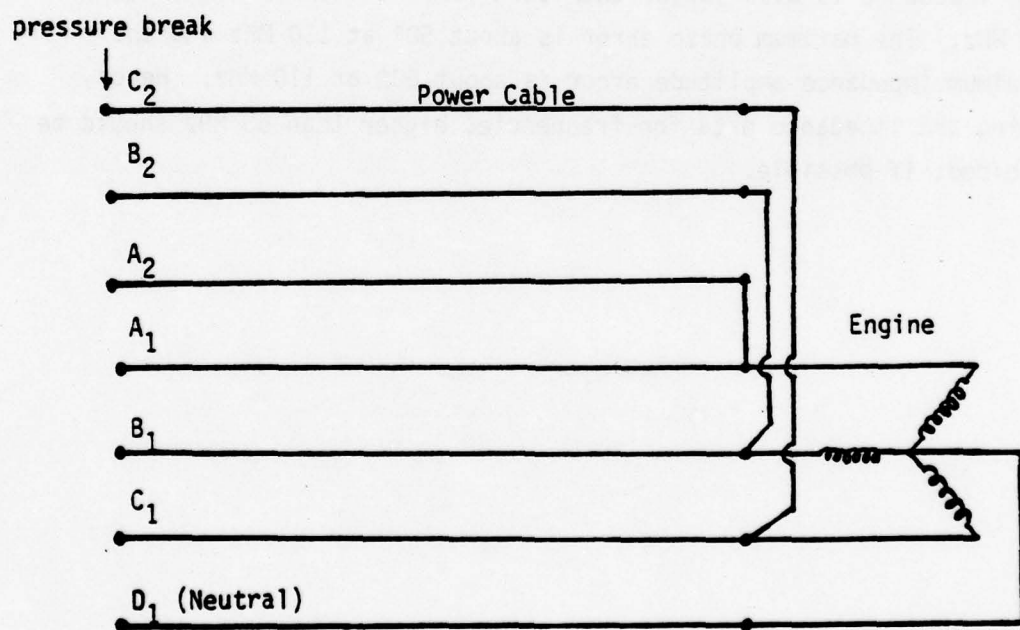


Figure 17. Power cable geometry outside the pressure break.

A total of 10 redundant measurements has justified the above groupings.

Figures 19 through 26 are the corrected impedance values of the equivalent circuit. The data are all digitized and used as input to the modified QV7T program.

The recovered impedance curve of the 100Ω load is shown in Figure 18 for the purpose of checking the accuracy of the impedance measurement. It has been found that the measurements of the impedance values are not very accurate at high frequencies. The approximation on βL , the stray capacitances of the end of the coax, and the quality of the resistor may be some of the reasons for the discrepancies. At frequencies above 65 MHz, the phase of the impedance becomes negative while for a pure resistor it should remain zero. The amplitude of the impedance is also larger than 100Ω for frequencies higher than 65 MHz. The maximum phase error is about 50° at 110 MHz and the maximum impedance amplitude error is about 50Ω at 110 MHz. Hence, using the impedance data for frequencies higher than 65 MHz should be avoided, if possible.

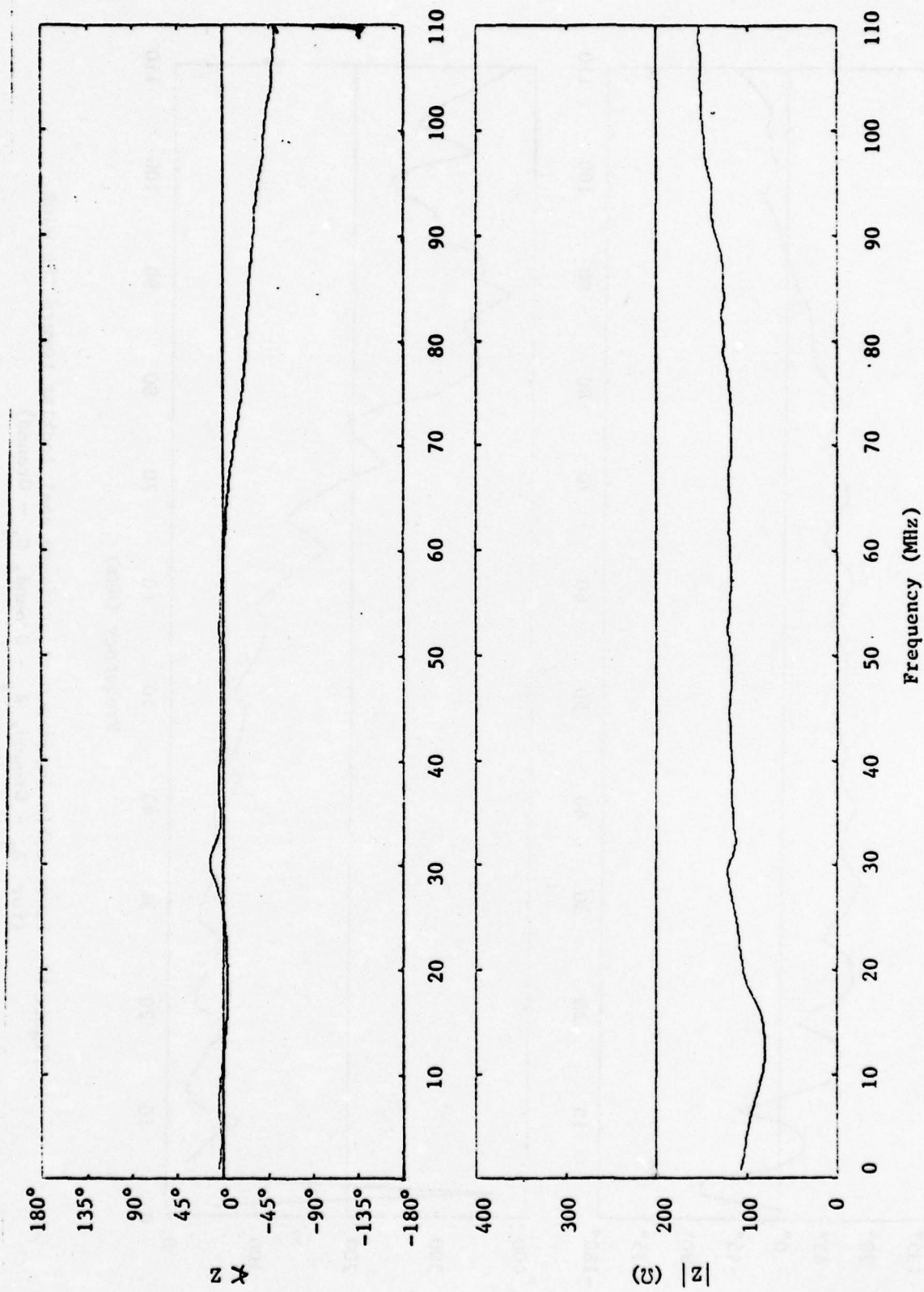


Figure 18. Measured 100Ω load at the end of the coax

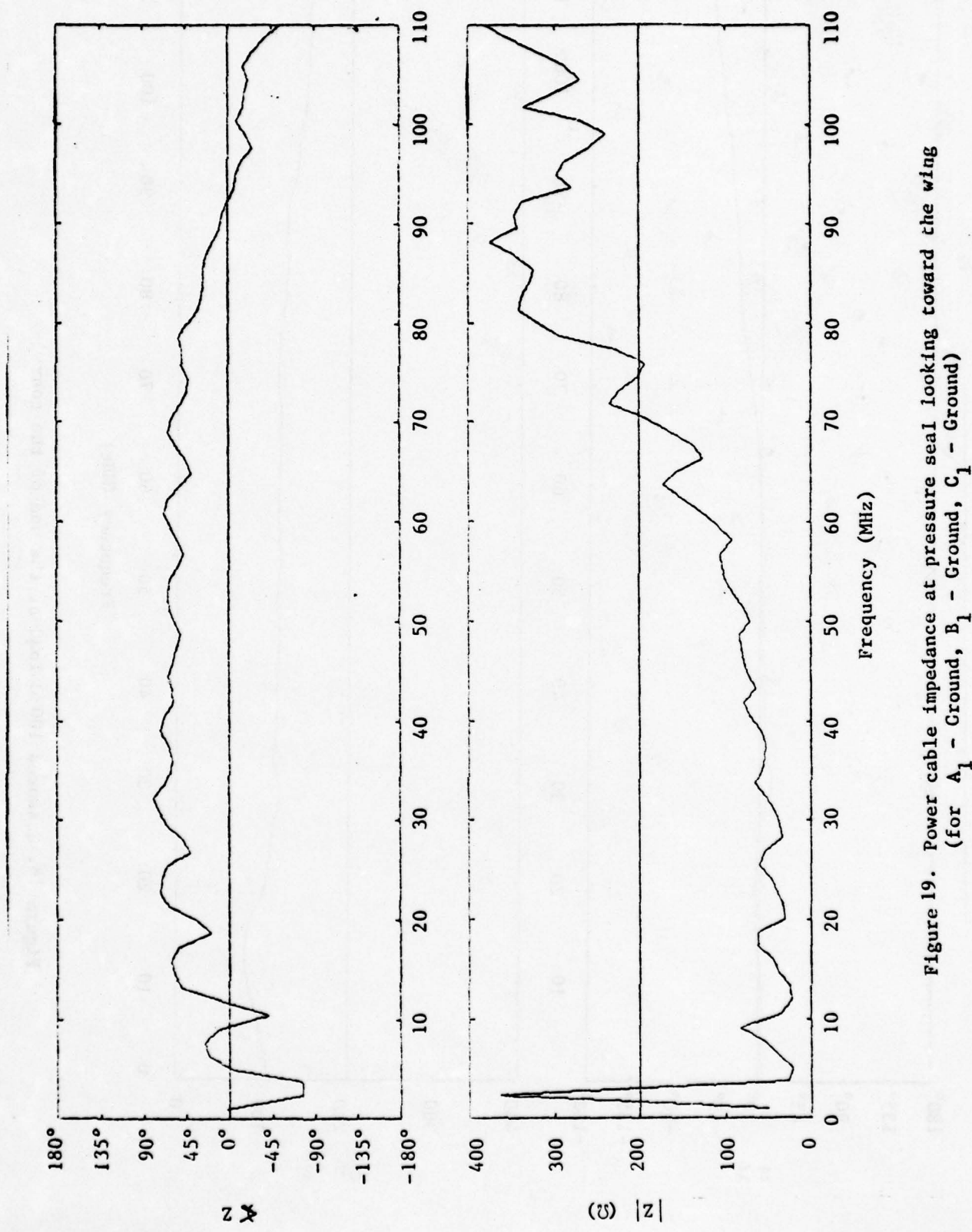


Figure 19. Power cable impedance at pressure seal looking toward the wing
(for A₁ - Ground, B₁ - Ground, C₁ - Ground)

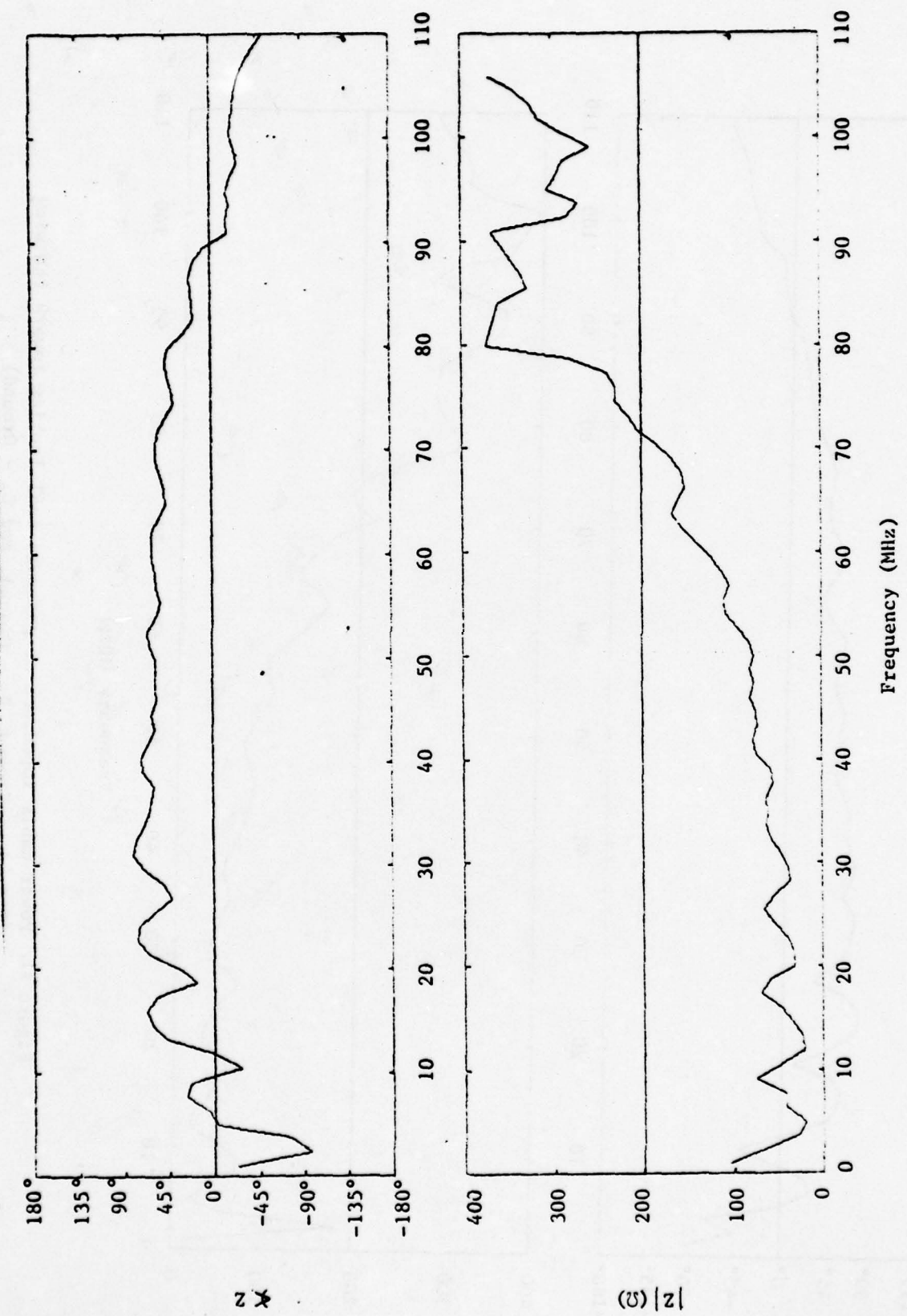


Figure 20. Power cable impedance at pressure seal looking toward the wing (for D_1 - ground)

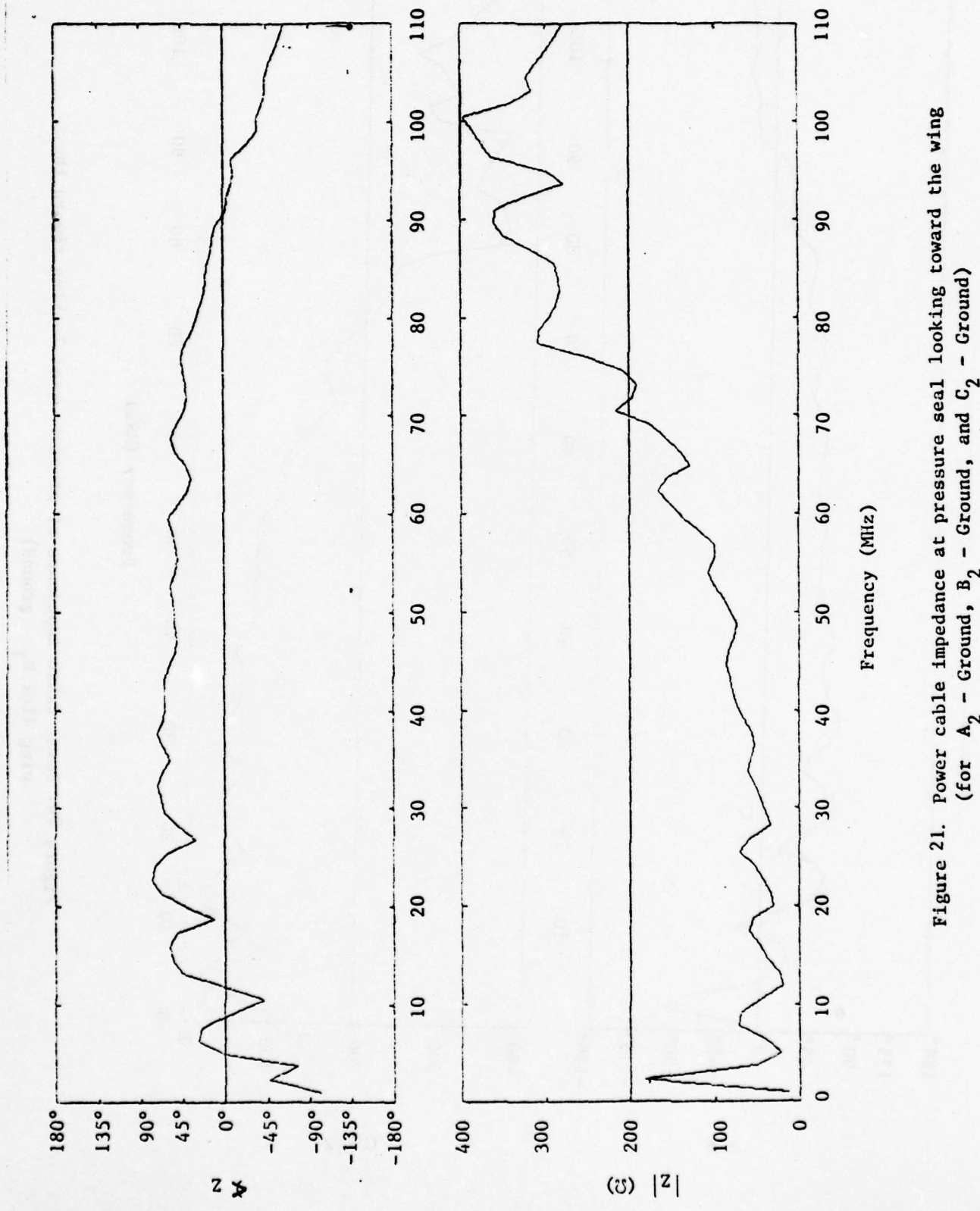


Figure 21. Power cable impedance at pressure seal looking toward the wing
(for A_2 - Ground, B_2 - Ground, and C_2 - Ground)

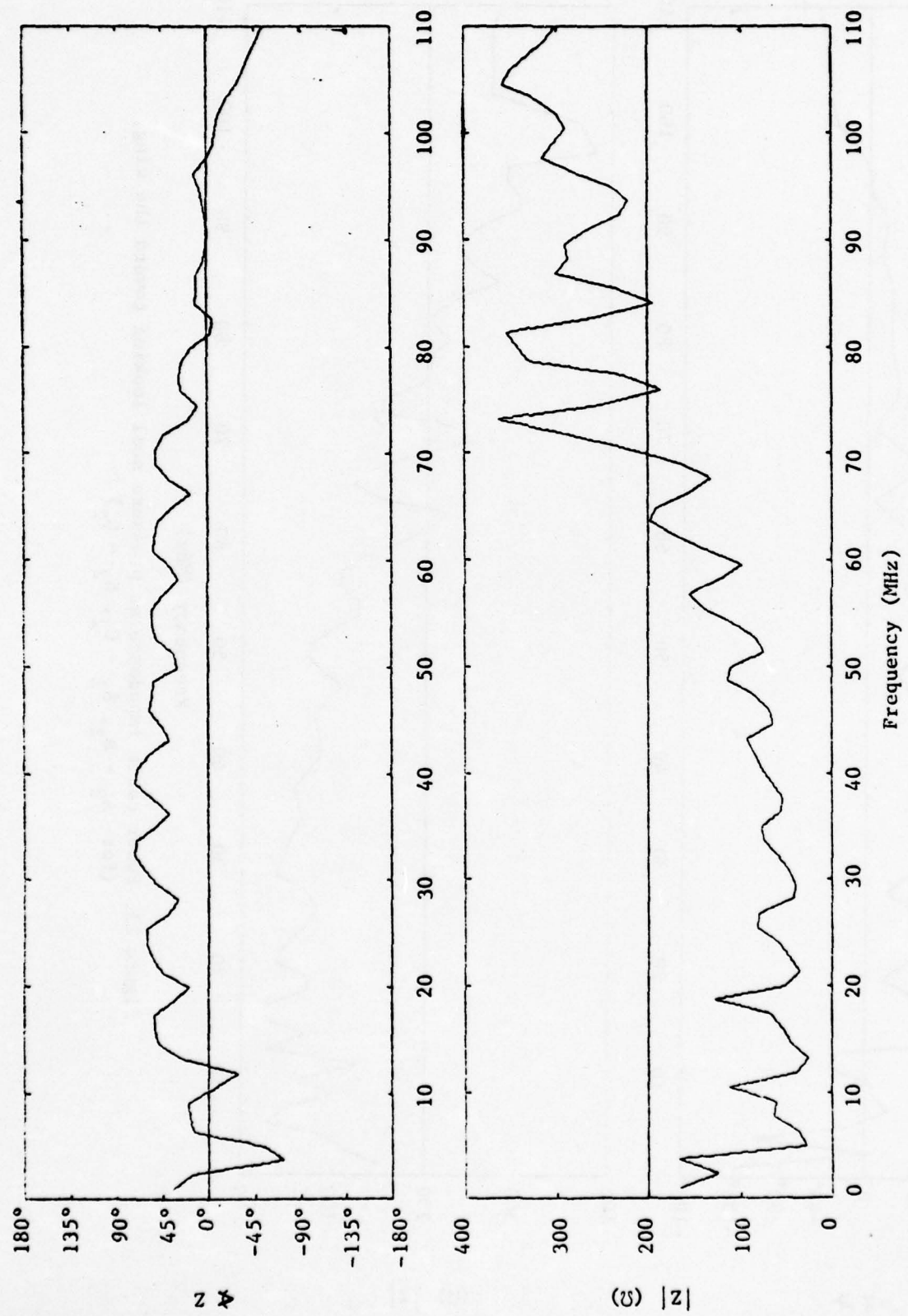


Figure 22. Power cable impedance at pressure seal looking toward the wing
(for $A_1 - B_1$, $A_1 - C_1$, $B_1 - C_1$)

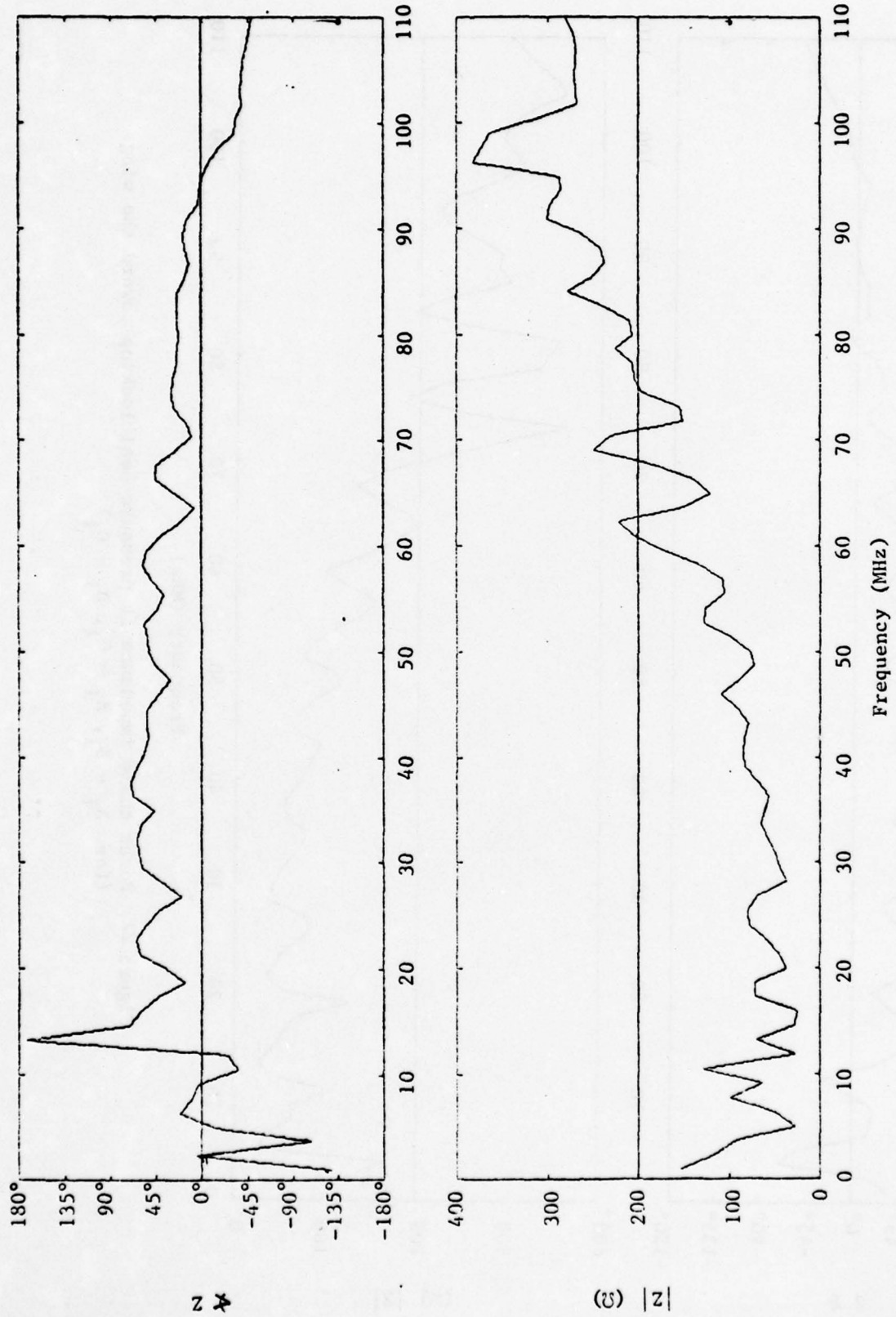


Figure 23. Power cable impedance at pressure seal looking toward the wing
(for $A_2 - B_2$, $A_2 - C_2$, $B_2 - C_2$)

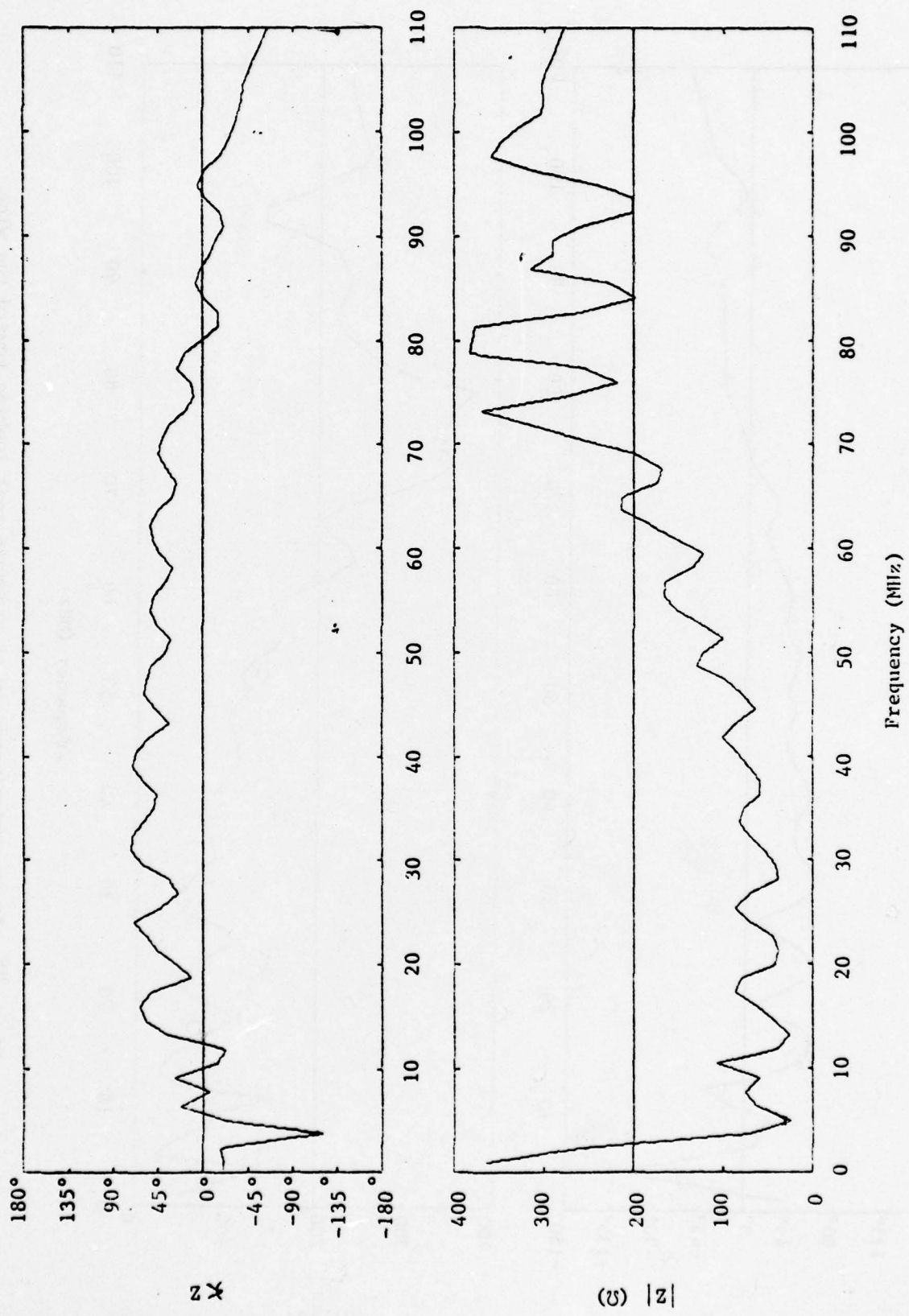


Figure 24. Power cable impedance at pressure seal looking toward the wing
(for $A_1 - D_1$, $B_1 - D_1$, and $C_1 - D_1$)

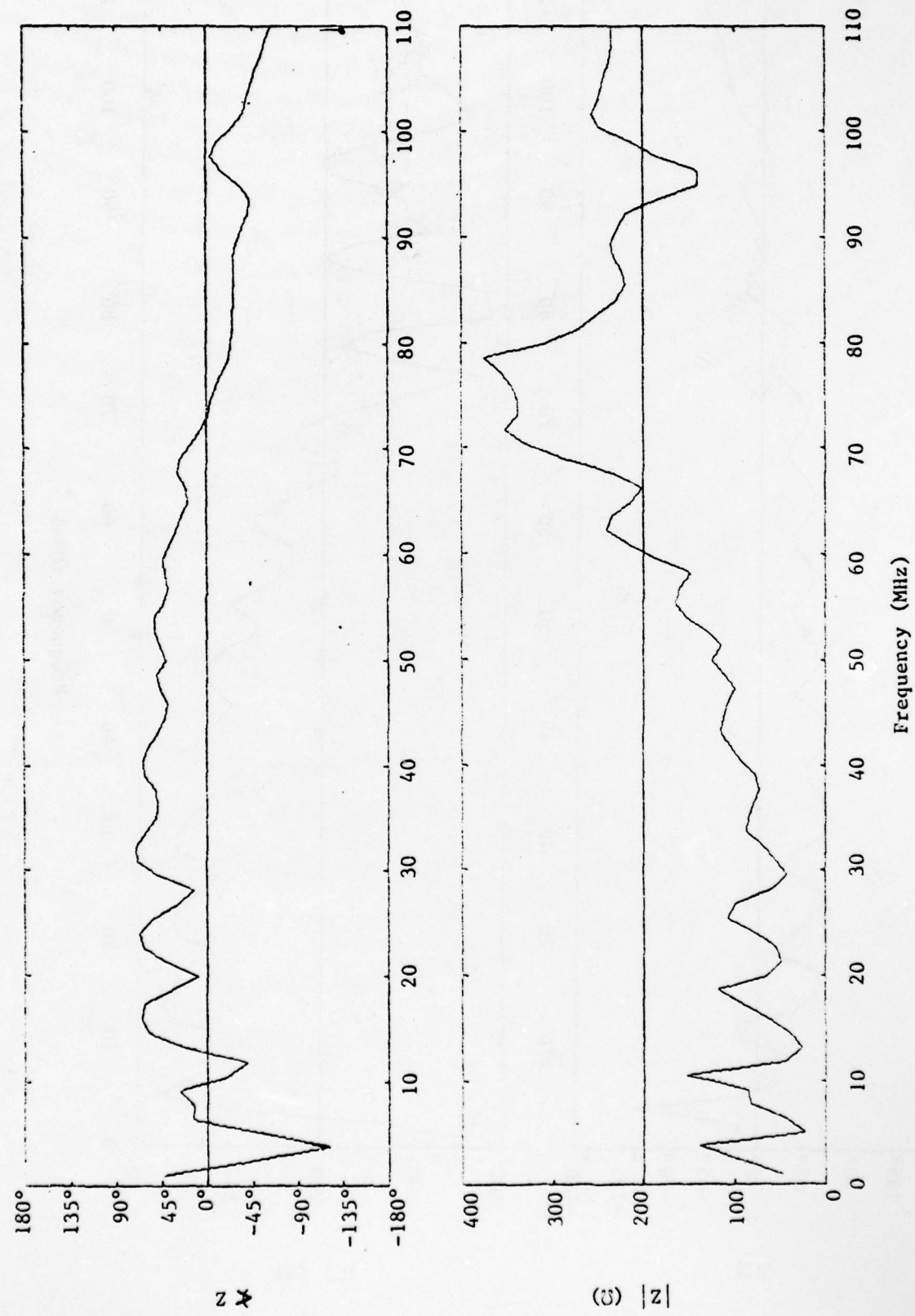


Figure 25. Power cable impedance at pressure seal looking toward the wing
(for $D_1 - A_2$, $D_1 - B_2$, $D_1 - C_2$)

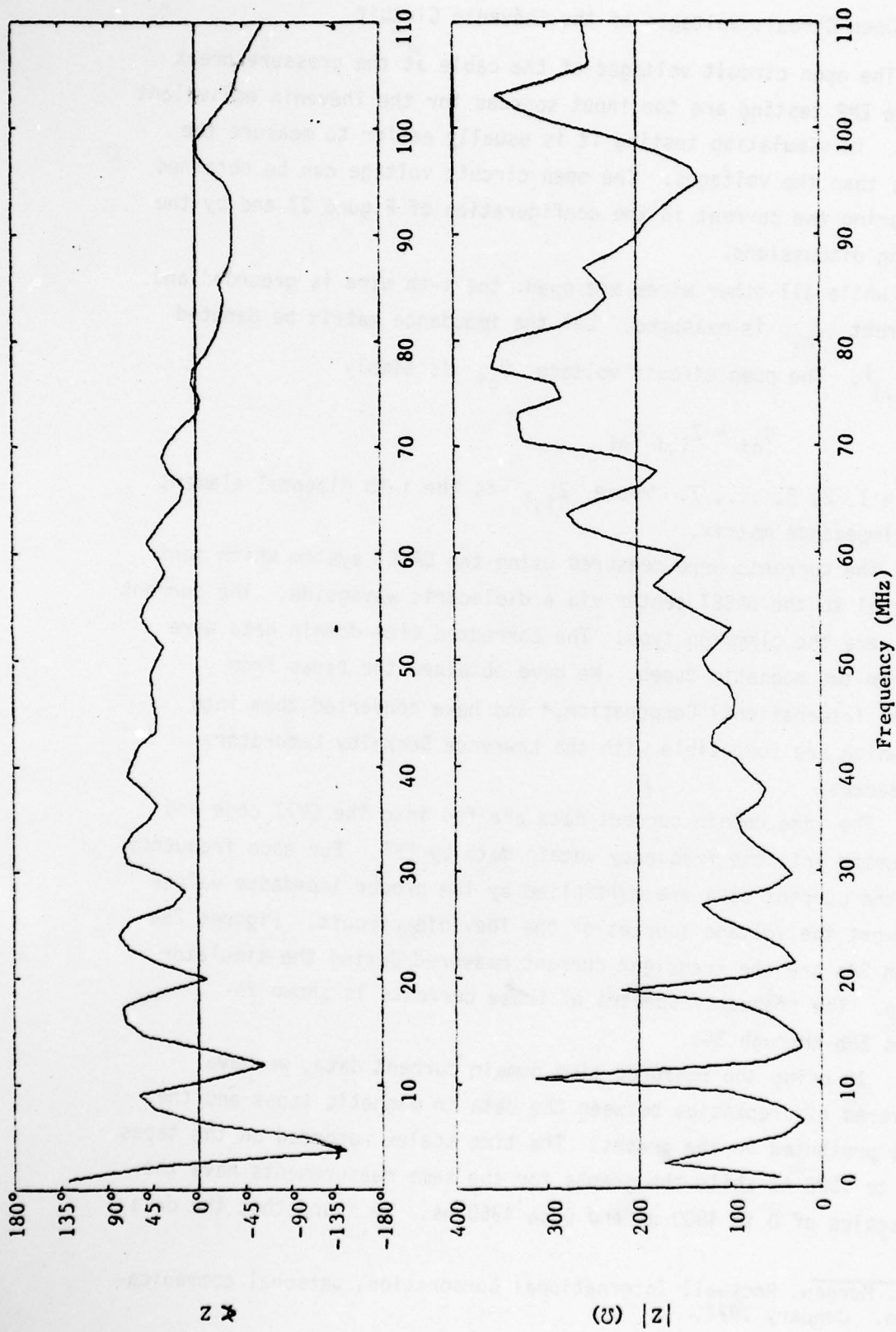


Figure 26. Power cable impedance at pressure seal looking toward the wing
 (for $A_1 - A_2$, $A_1 - B_2$, $A_1 - C_2$, $B_1 - B_2$, $B_1 - C_2$, $C_1 - A_2$,
 $C_1 - B_2$, $C_1 - C_2$)

C. The Open Circuit Voltages of the Thévenin Circuit

The open circuit voltages of the cable at the pressure break under the EMP testing are the input sources for the Thévenin equivalent circuit. In simulation testing it is usually easier to measure the currents than the voltages. The open circuit voltage can be obtained by measuring the current in the configuration of Figure 27 and by the following discussions.

While all other wires are open, the i -th wire is grounded and the current I_{mi} is measured. Let the impedance matrix be denoted by $[z_{ij}]$. The open circuit voltage V_{oi} is simply

$$V_{oi} = z_{ii} I_{mi}$$

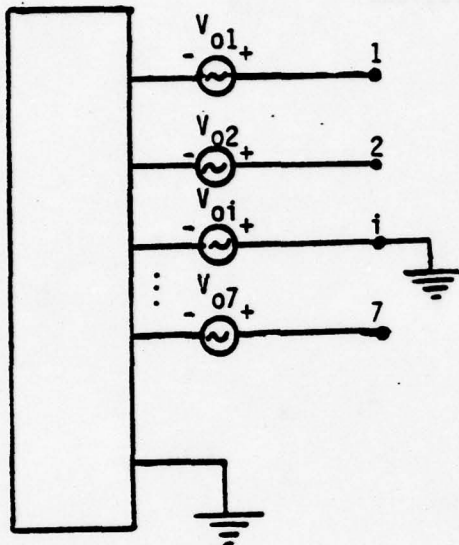
for $i = 1, 2, 3, \dots, 7$. Where z_{ii} is the i -th diagonal element of the impedance matrix.

The currents were measured using the DASET system which sent the signal to the DASET center via a dielectric waveguide. The current probes were the clamp-on type. The corrected time domain data were stored in two magnetic tapes. We have obtained the tapes from Rockwell International Corporation,* and have converted them into tapes which are compatible with the Lawrence Berkeley Laboratory tape readers.

The time domain current data are fed into the QV7T code and transformed into the frequency domain data by FFT. For each frequency point the current data are multiplied by the proper impedance values to convert the voltage sources of the Thévenin circuit. Figures 28a through 34a are the transient current measured during the simulator testing. The frequency spectra of these currents is shown in Figures 28b through 34b.

In using the measured time domain current data, we have discovered discrepancies between the data in magnetic tapes and the curves presented in the graphs. The time scales recorded on the tapes are 0 to 1000 ns while the graphs for the same measurements have the time scales of 0 to 4800 ns and 0 to 4960 ns. We found that the data

* G.E. Morgan, Rockwell International Corporation, personal communication, January 1977.



Note 1. All the wires except i are open circuited.

Note 2. Ground wire i and measure current $I_m i$.

Figure 27. Configuration for obtaining the open-circuit voltages from current measurement.

on the magnetic tapes are incorrect because their fundamental frequencies are about five times higher than that of the actual aircraft resonant frequency ($\approx 3.8\text{MHz}$). The time domain current data were obtained from the magnetic tapes by correcting the time scales.

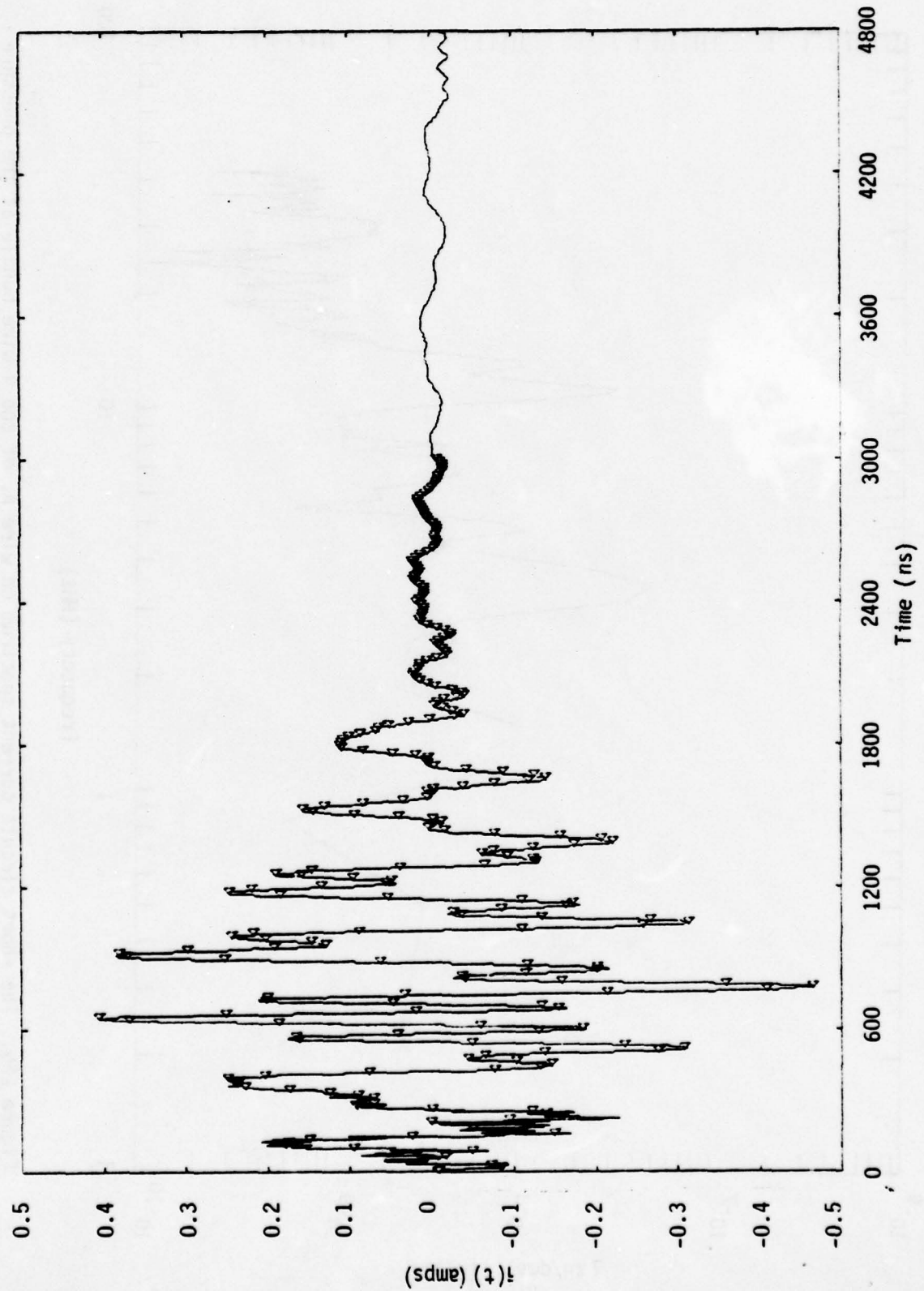


Figure 28a. The transient current measurement on wire A_1 of the 4-wire bundle at the pressure break

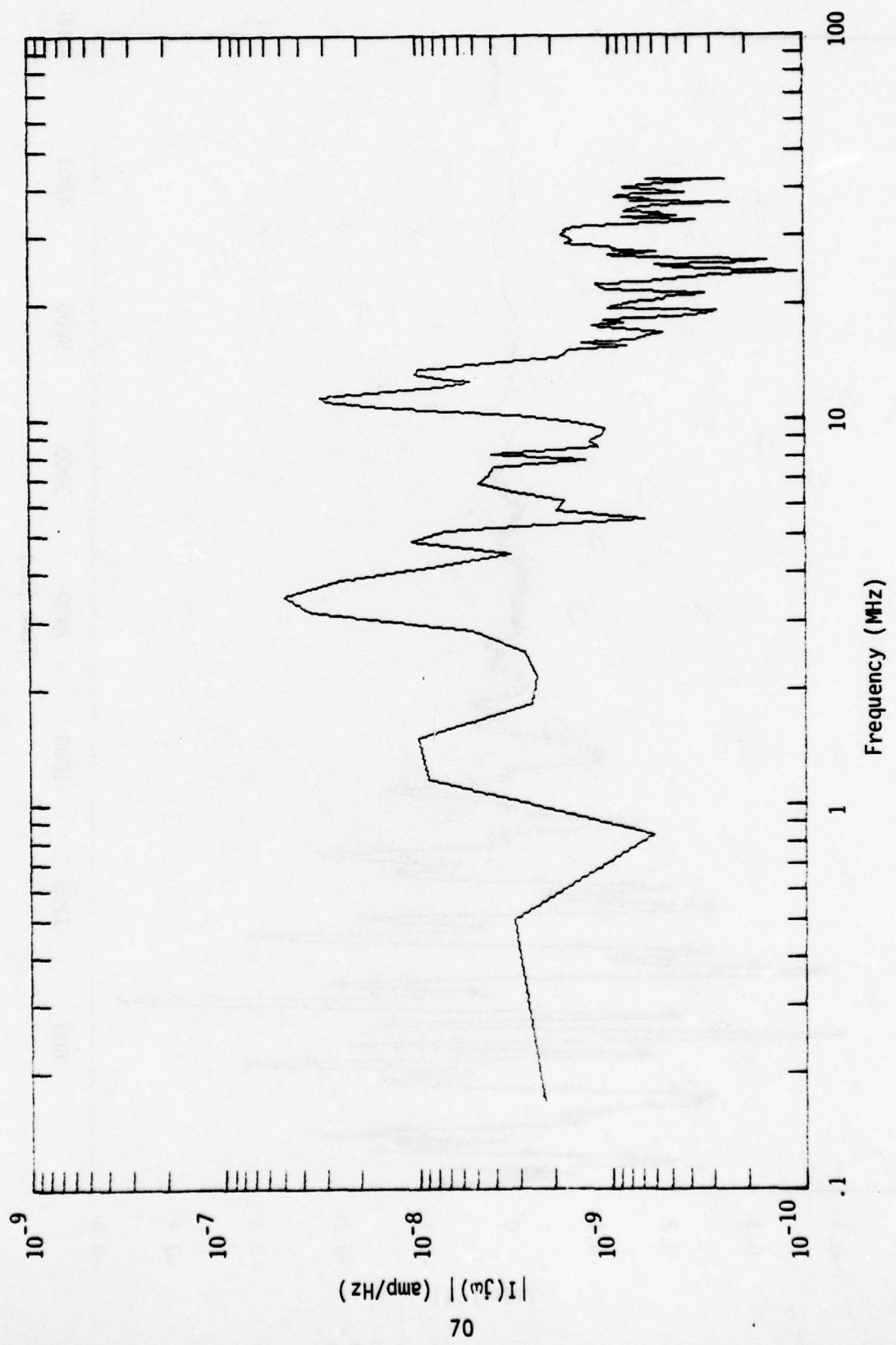


Figure 28b. The short circuit current spectrum on wire A₁ of the 4-wire bundle at the pressure break

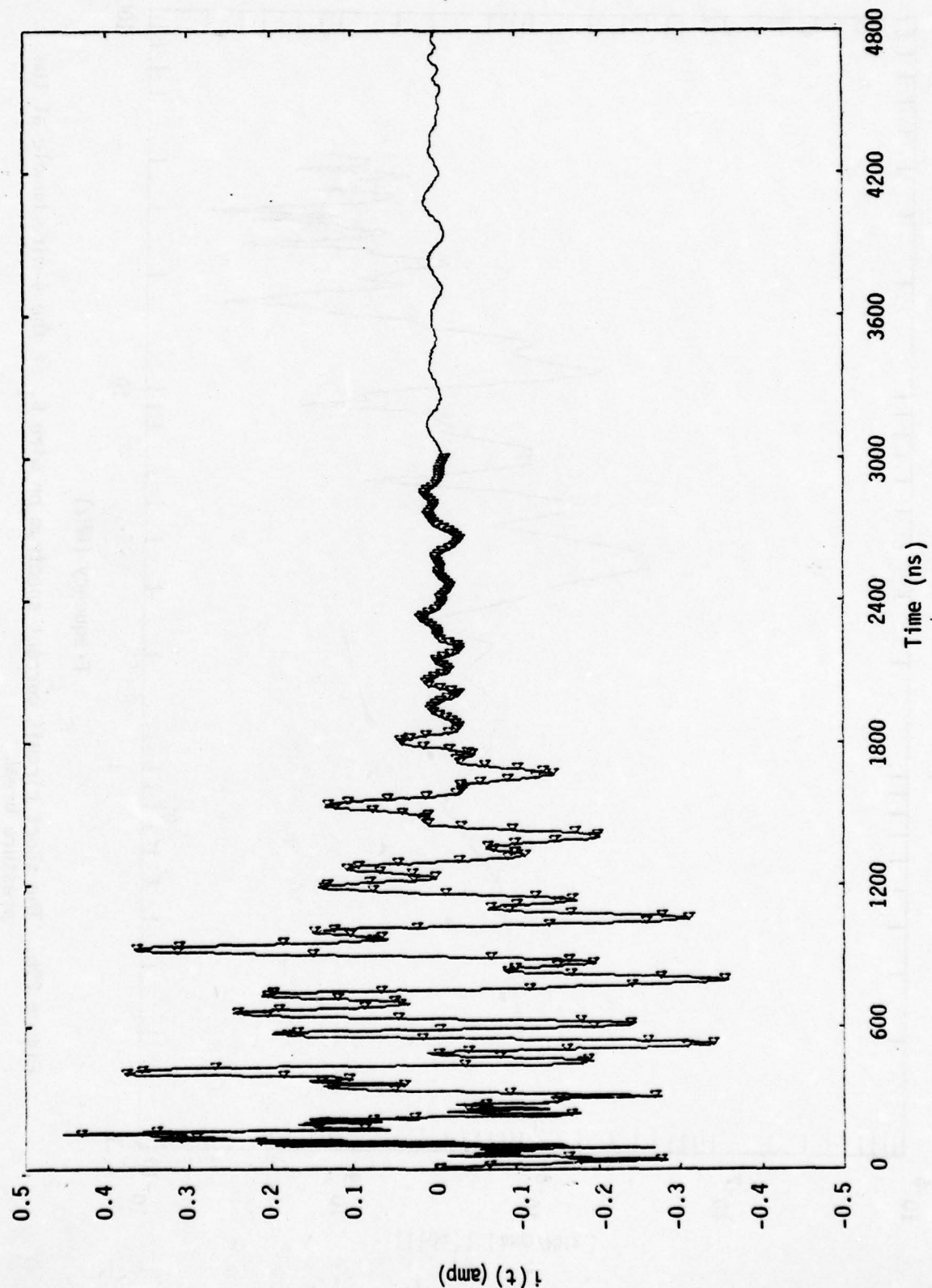


Figure 29a. The transient current measurement on wire B_1 of the 4-wire bundle at the pressure break

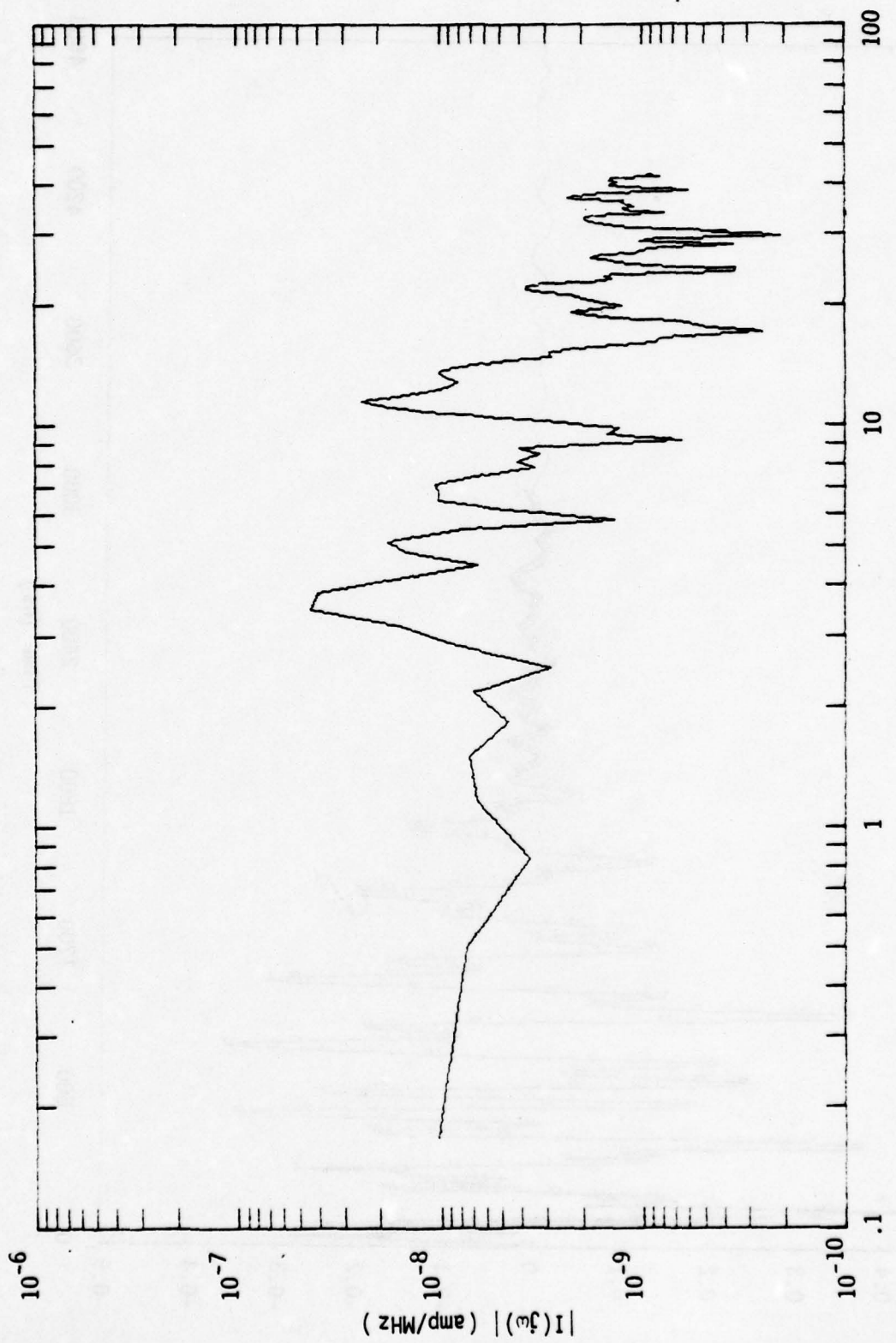


Figure 29b. The short circuit current spectrum on wire B₁ of the 4-wire bundle at the pressure break

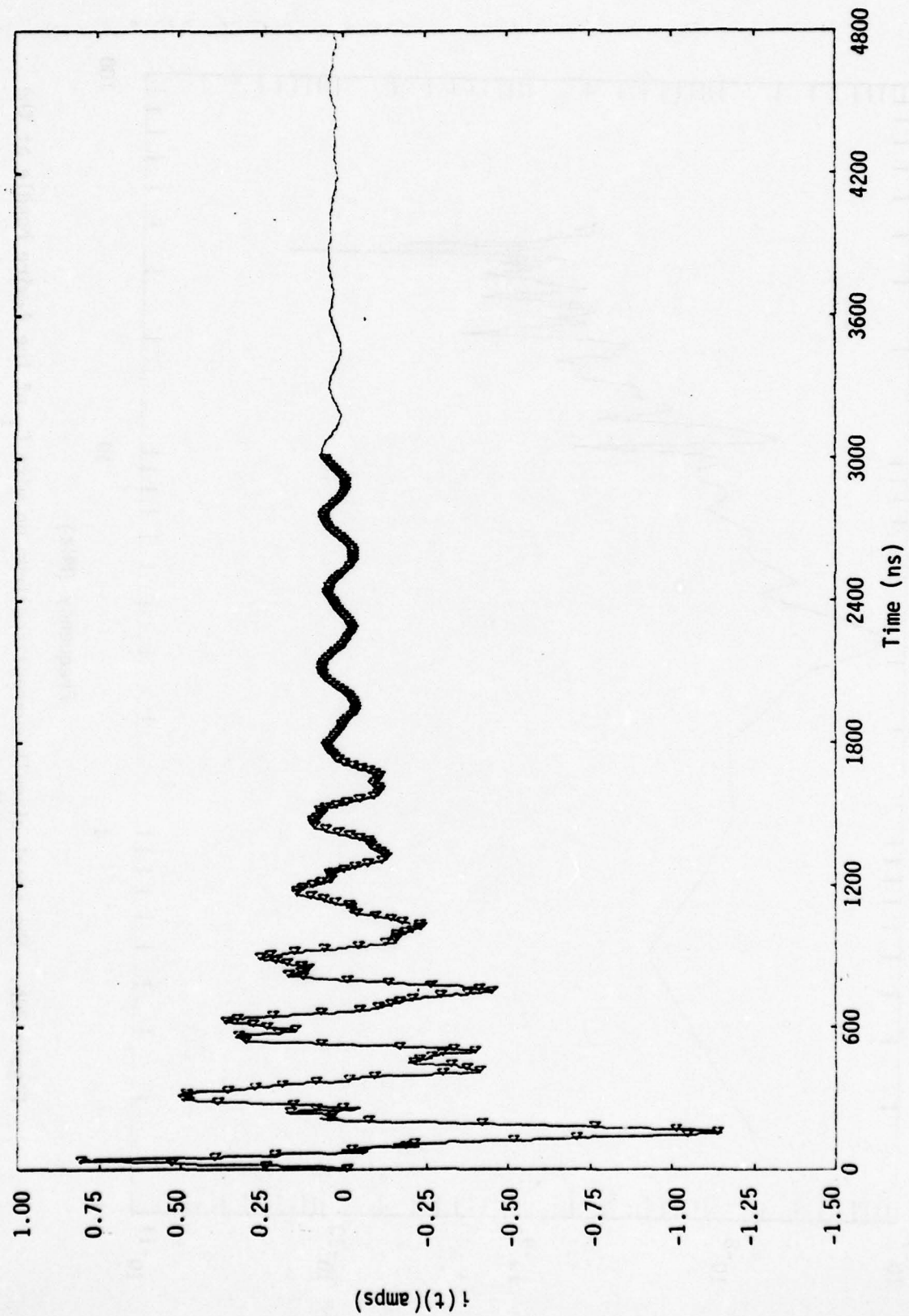


Figure 30a. The transient current measurement on wire C_1 of the 4-wire bundle at the pressure break

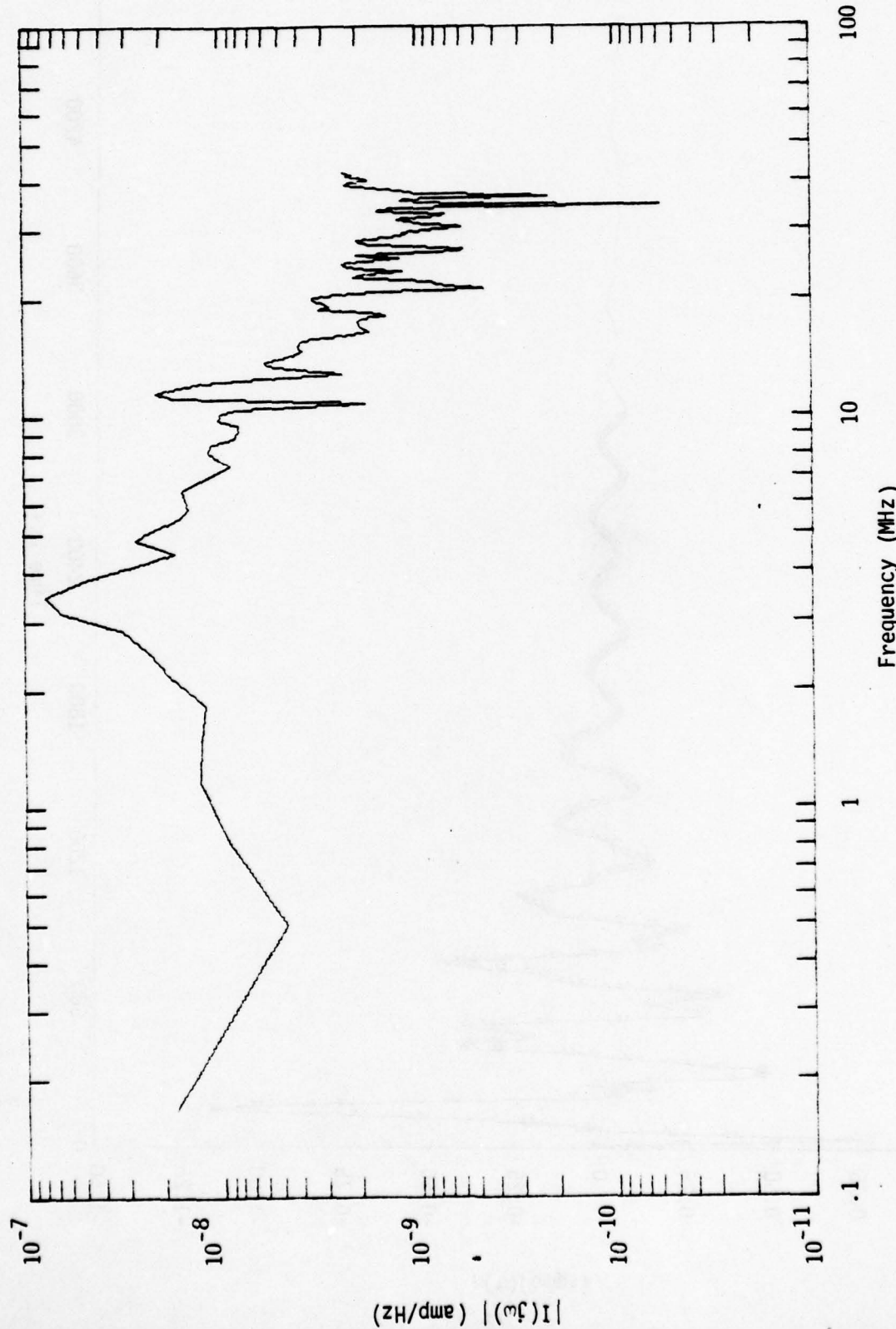


Figure 30b. The short circuit current spectrum on wire C₁ of the 4-wire bundle at the pressure break

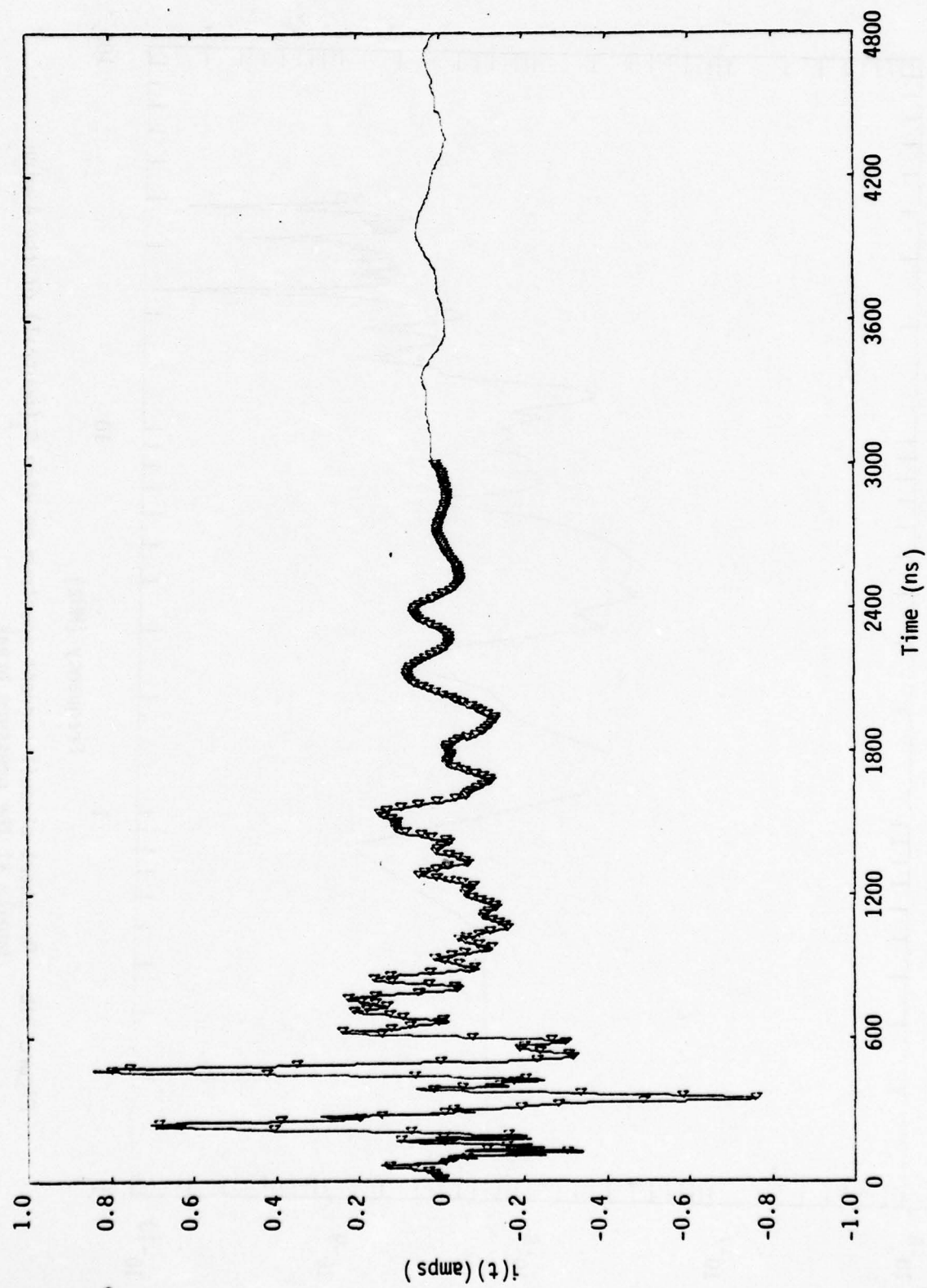


Figure 31a. The transient current measurement on wire D_1 (neutral) of the 4-wire bundle at the pressure break

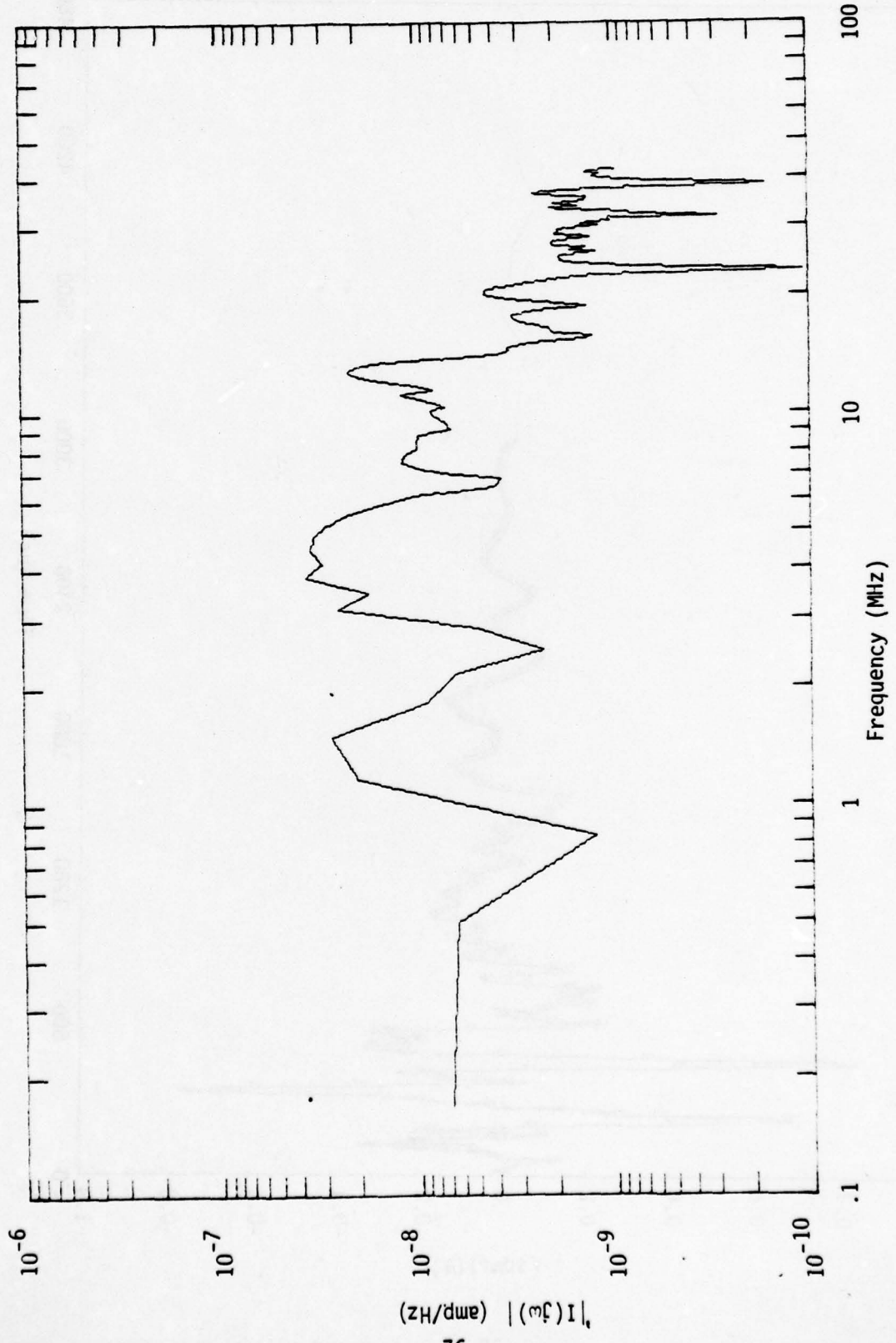


Figure 31b. The short circuit current spectrum on wire D₁ (neutral) of the 4-wire bundle at the pressure break

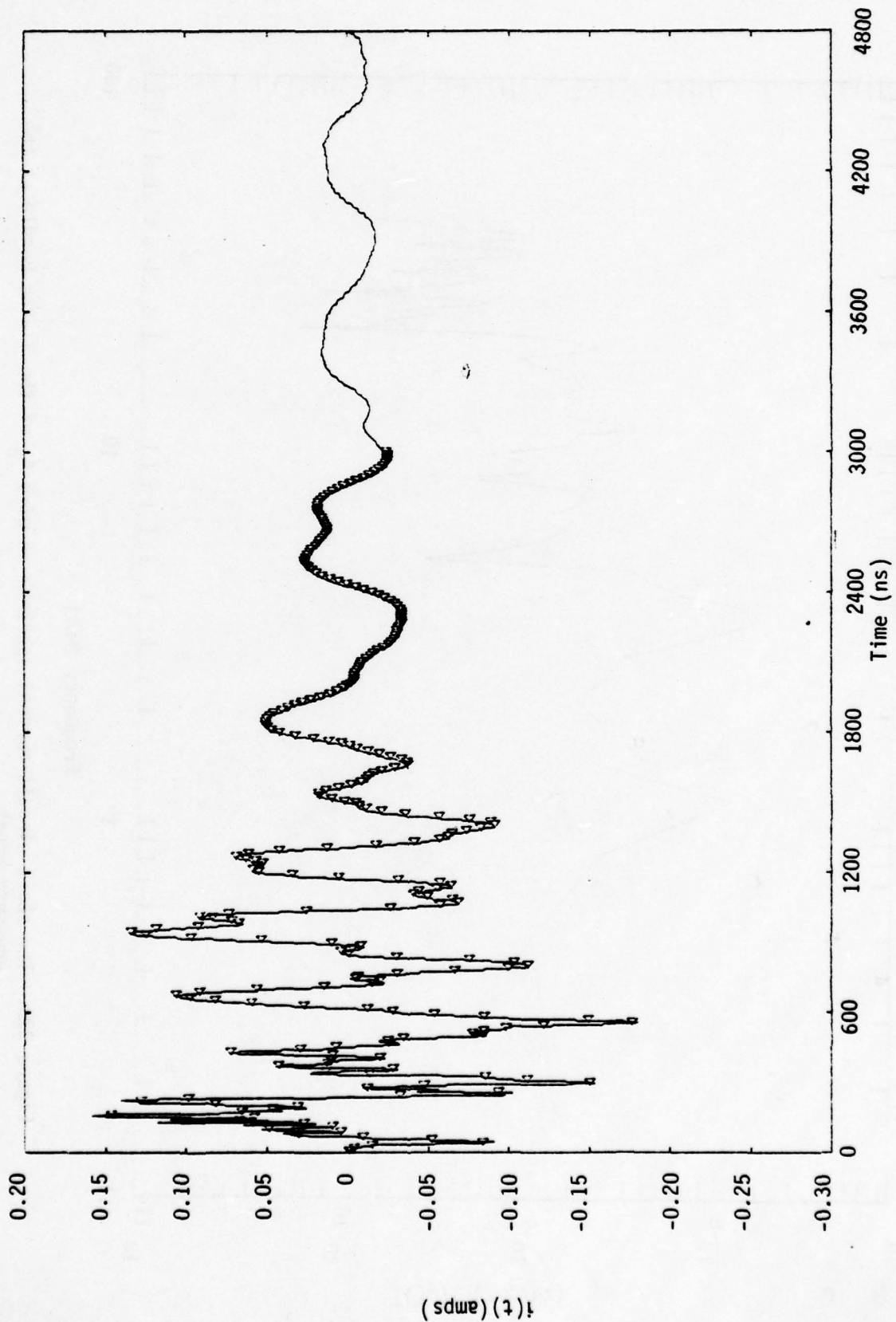


Figure 32a. The transient current measurement on wire A_2 of the 3-wire bundle at the pressure break

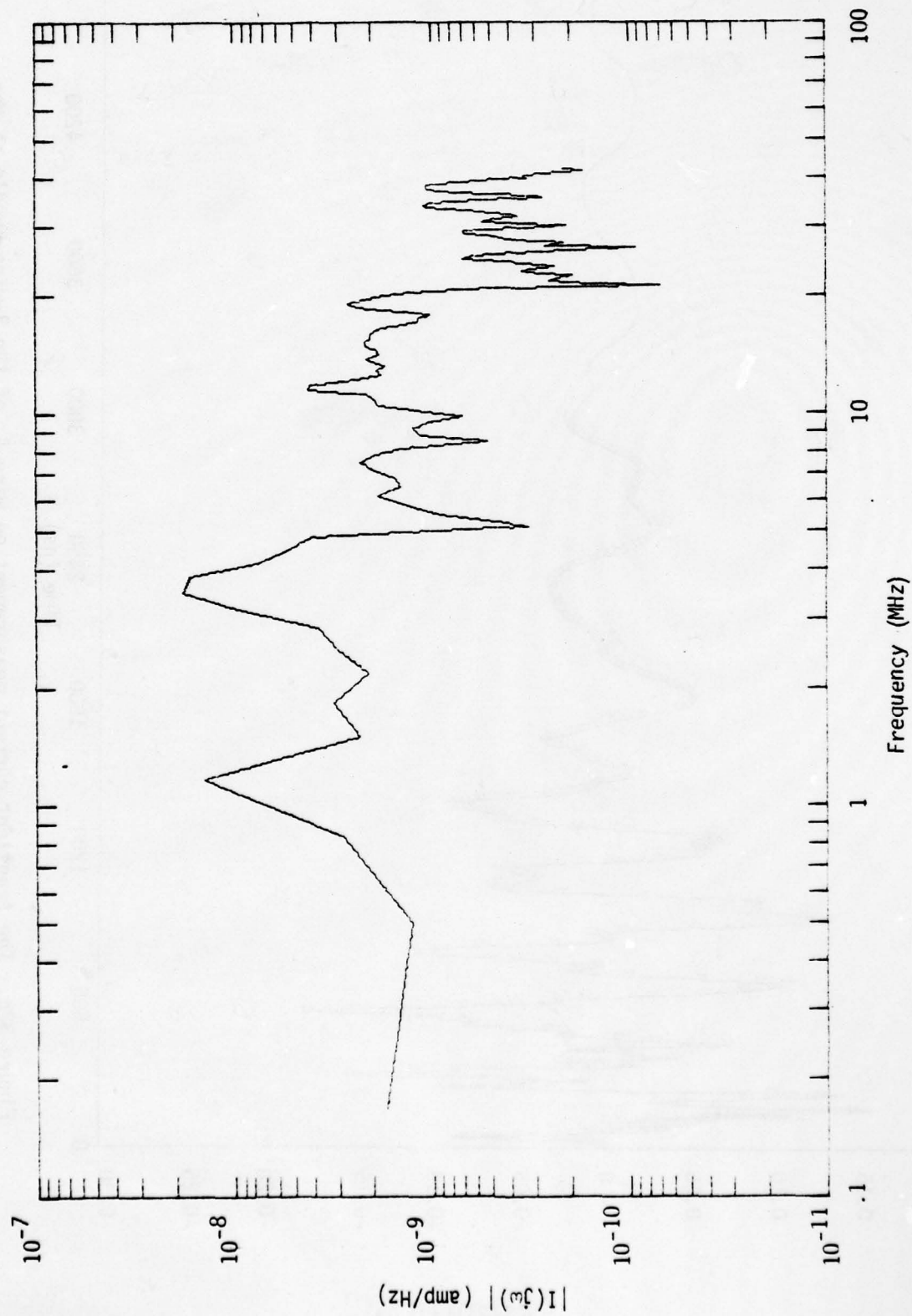


Figure 32b. The short circuit current spectrum on wire A₂ of the 3-wire bundle at the pressure break

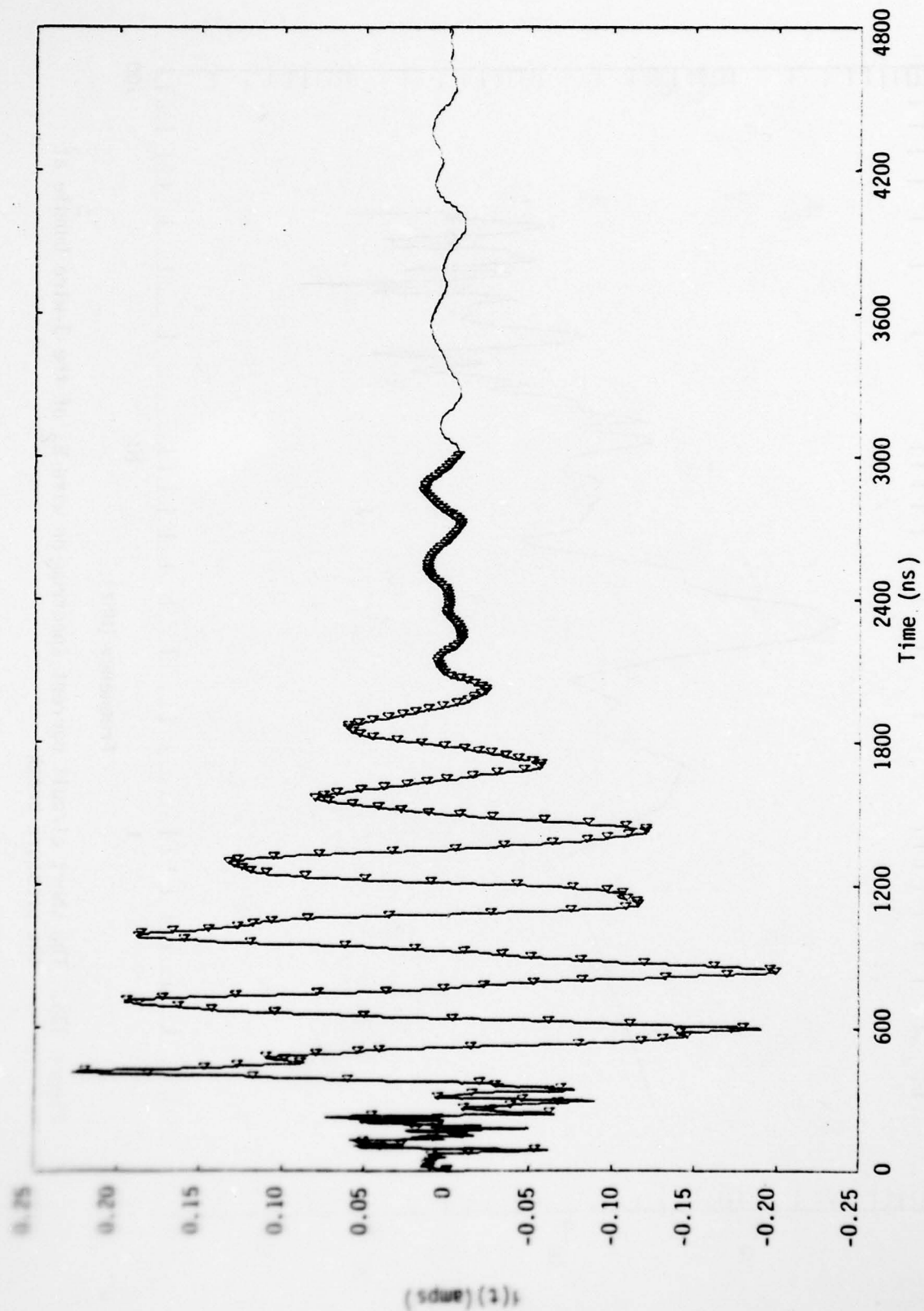


Figure 33a. The transient current measurement on wire B_2 of the 3-wire bundle at the pressure break

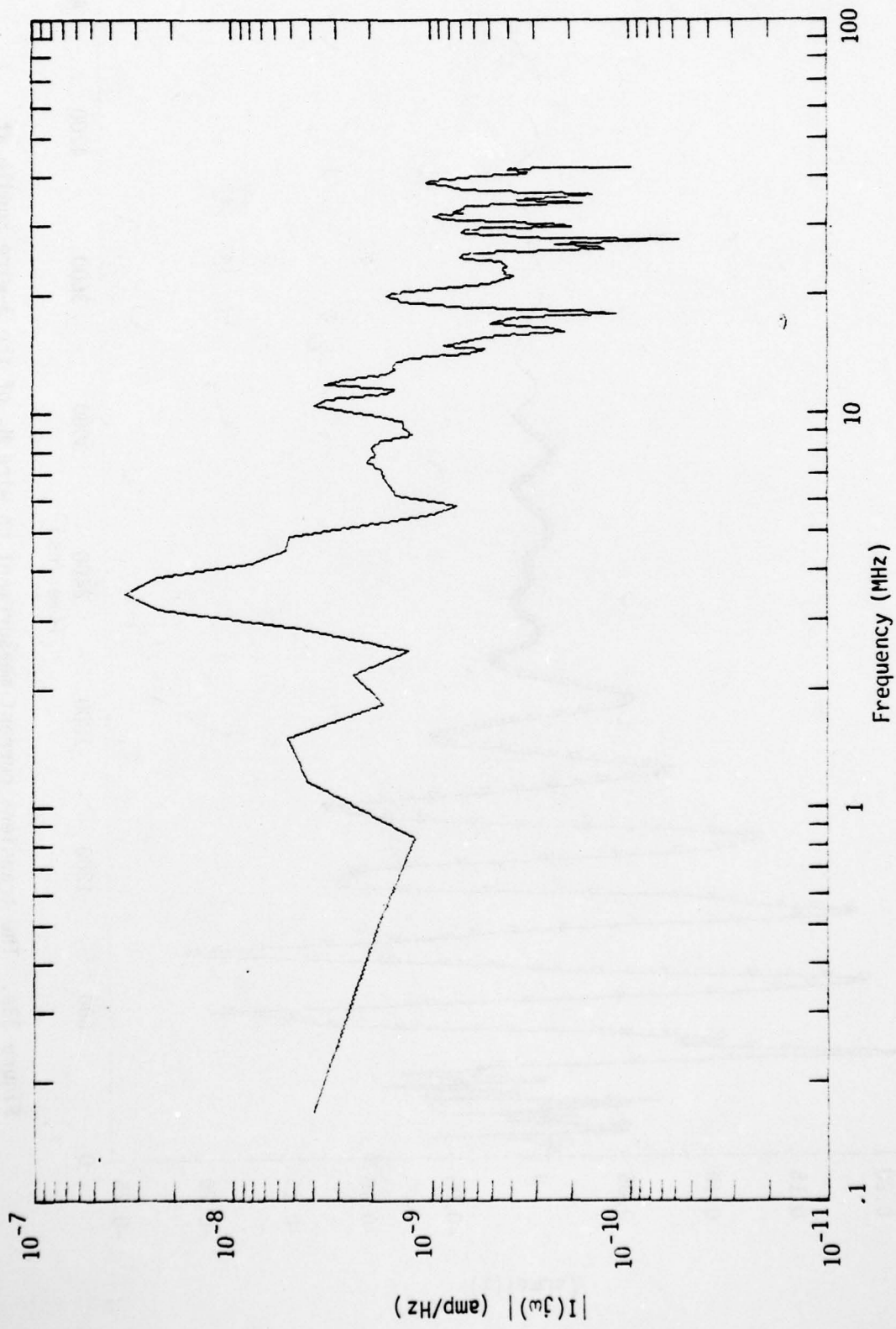


Figure 33b. The short circuit current spectrum on wire B_2 of the 3-wire bundle at the pressure break

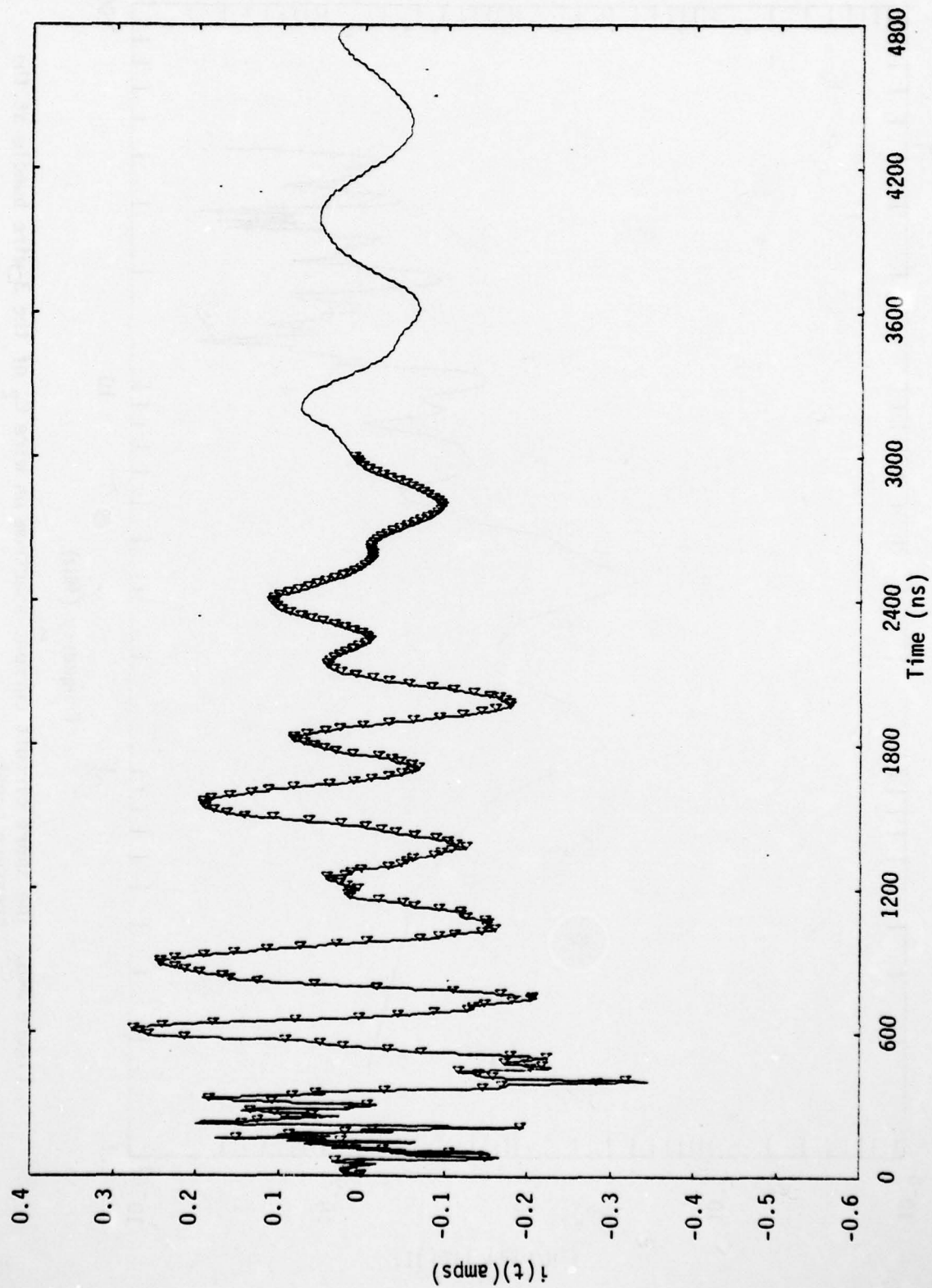


Figure 34a. The transient current measurement on wire C_2 of the 3-wire bundle at the pressure break

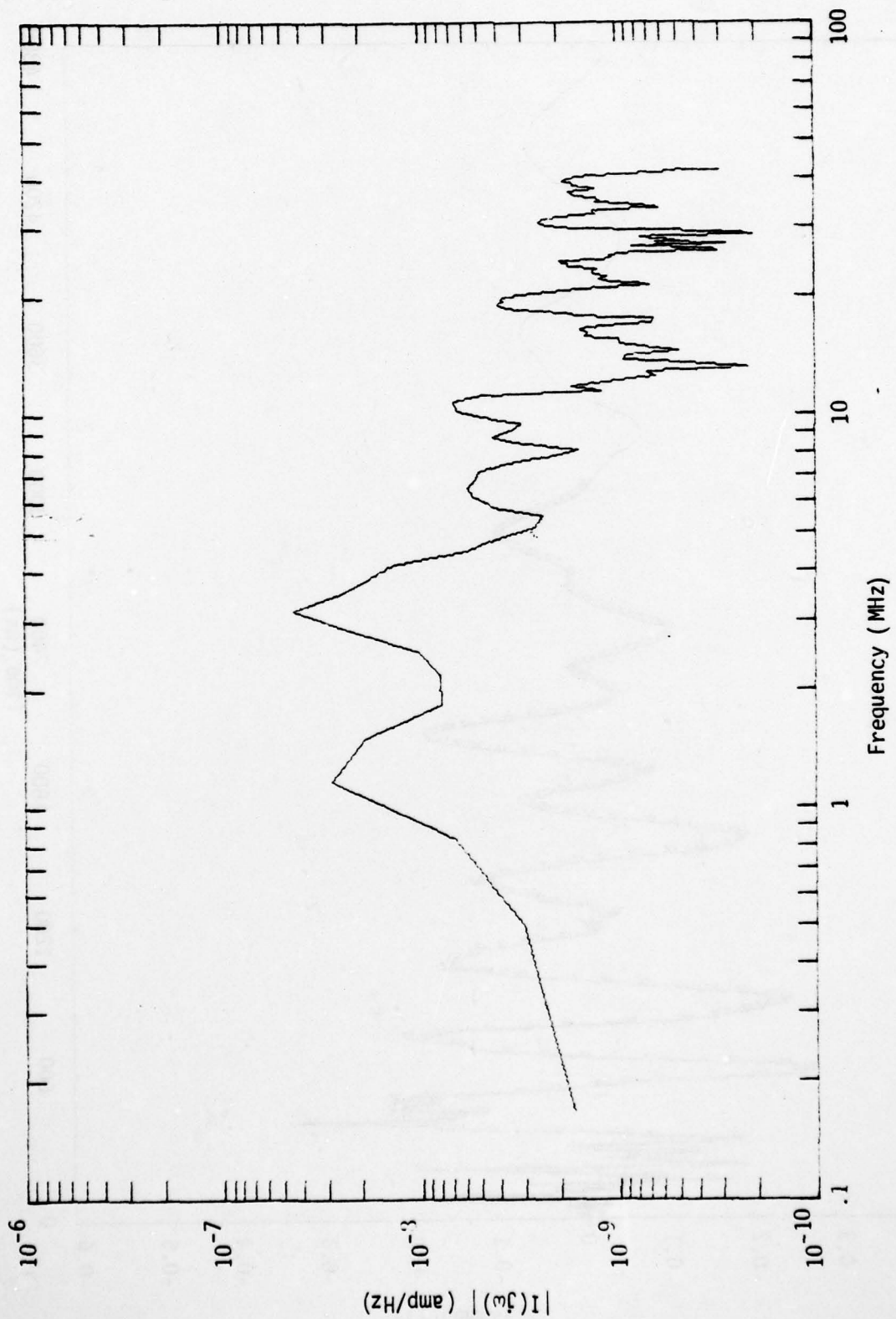


Figure 34b. The short circuit current spectrum on wire C_2 of the 3-wire bundle at the pressure break

D. The Transmission Line Parameters of the Power Cable

The seven wire branch of the power cable consists of two twisted bundles, one with four wires and the other with three wires. Since the two bundles are not packed together, we shall assume no coupling between the bundles. The cross section of the four and three wire bundles is shown in Figure 35. The four wire bundle has a high degree of symmetry against the ground plane; thus only the configuration in Figure 35a will be used in calculating the line parameters. The three wire bundle has two entirely different configurations against the ground plane as shown in Figure 35 b and c. There are many different positions of the wires when they are twisting along the path. The transitional positions are disregarded because the average values of the per-unit-length capacitance and inductance matrices will be used.

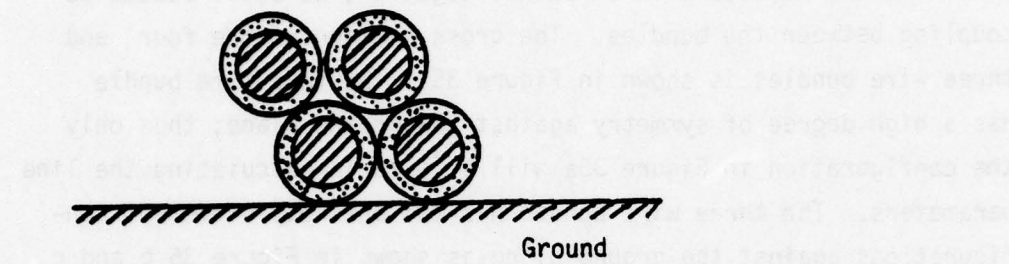
The radius of the conductors of each individual wire is 3.5 mm and the radius of the insulator is 5.6 mm. The relative dielectric constant is assumed to be 2.

A separate computer code using the multi-series expansion method [Ref.6] was used to obtain the per-unit-length capacitance matrix of each wire configuration.

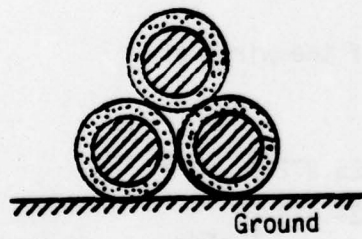
The per-unit-length capacitance matrix of the wires of Figure 35a was found to be

$$[C] = \begin{bmatrix} 78.508 & -26.905 & -19.563 & -25.872 \\ -26.905 & 64.210 & -23.936 & -24.471 \\ -19.563 & -23.936 & 124.120 & -18.583 \\ -25.872 & -24.471 & -18.583 & 110.680 \end{bmatrix} \text{ pF/m}$$

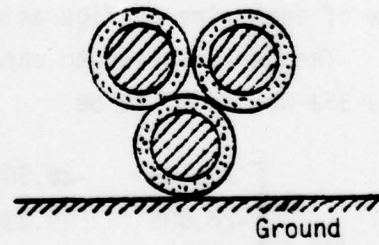
The elements of the matrix are averaged when the wires are twisted. The new per-unit-length capacitance matrix of the twisted four wire bundle becomes



(a) 4-wire bundle



(b) 3-wire bundle



(c) 3-wire bundle
when twisted

Figure 35. The cross section of the power cable;

 dielectric medium with a relative
dielectric constant ϵ_r .

$$[C] = \begin{bmatrix} 94.380 & -23.222 & -23.222 & -23.222 \\ -23.222 & 94.380 & -23.222 & -23.222 \\ -23.222 & -23.222 & 94.380 & -23.222 \\ -23.222 & -23.222 & -23.222 & 94.380 \end{bmatrix} \text{ pF/m}$$

The per-unit-length capacitance matrix of the wires of Figure 35b is

$$[C_1] = \begin{bmatrix} 110.67 & -18.611 & -25.990 \\ -18.611 & 110.67 & -25.990 \\ -25.990 & -25.990 & 62.383 \end{bmatrix} \text{ pF/m}$$

and that for Figure 35c is

$$[C_2] = \begin{bmatrix} 64.206 & -27.008 & -23.941 \\ -27.008 & 64.206 & -23.941 \\ -23.941 & -23.941 & 115.48 \end{bmatrix} \text{ pF/m}$$

The elements of the matrices $[C_1]$ and $[C_2]$ are averaged to obtain the new per-unit-length capacitance matrix of the twisted three wire bundle as follows

$$[C] = \begin{bmatrix} 87.936 & -24.247 & -24.247 \\ -24.247 & 87.936 & -24.247 \\ -24.247 & -24.247 & 87.936 \end{bmatrix} \text{ pF/m}$$

The inductance of the transmission lines for the quasi-TEM modes are usually independent of the dielectric constants which insulate the wires. Hence we can assume $\epsilon_r = 1$ and obtain the capacitance matrices as described above for this new ϵ_r . The per-unit-length inductance matrix can be obtained from the per-unit-length capacitance matrix ($\epsilon_r = 1$) by using the following equation

$$[L] = \frac{1}{c^2} [C_0]^{-1}, \text{ where } c \text{ is the speed of light.}$$

The resulting per-unit-length inductance matrix for the twisted four wire bundle is

$$[L] = \begin{bmatrix} 0.267706 & 0.099478 & 0.088478 & 0.088478 \\ 0.088478 & 0.267706 & 0.088478 & 0.088478 \\ 0.088478 & 0.088478 & 0.267706 & 0.088478 \\ 0.088478 & 0.088478 & 0.088478 & 0.267706 \end{bmatrix} \mu\text{H/m}$$

and that for the twisted three wire bundle is

$$[L] = \begin{bmatrix} 0.276717 & 0.102229 & 0.102229 \\ 0.102229 & 0.276727 & 0.102229 \\ 0.102229 & 0.102229 & 0.276717 \end{bmatrix} \mu\text{H/m}$$

The portion of the neutral wire leading to the ground from junction J_2 is a single wire and ground plane. The per-unit-length capacitance and inductance of this single wire line over a ground plane are

$$C = 80.563 \text{ pF/m}$$

$$L = 1.37918 \text{ nH/m.}$$

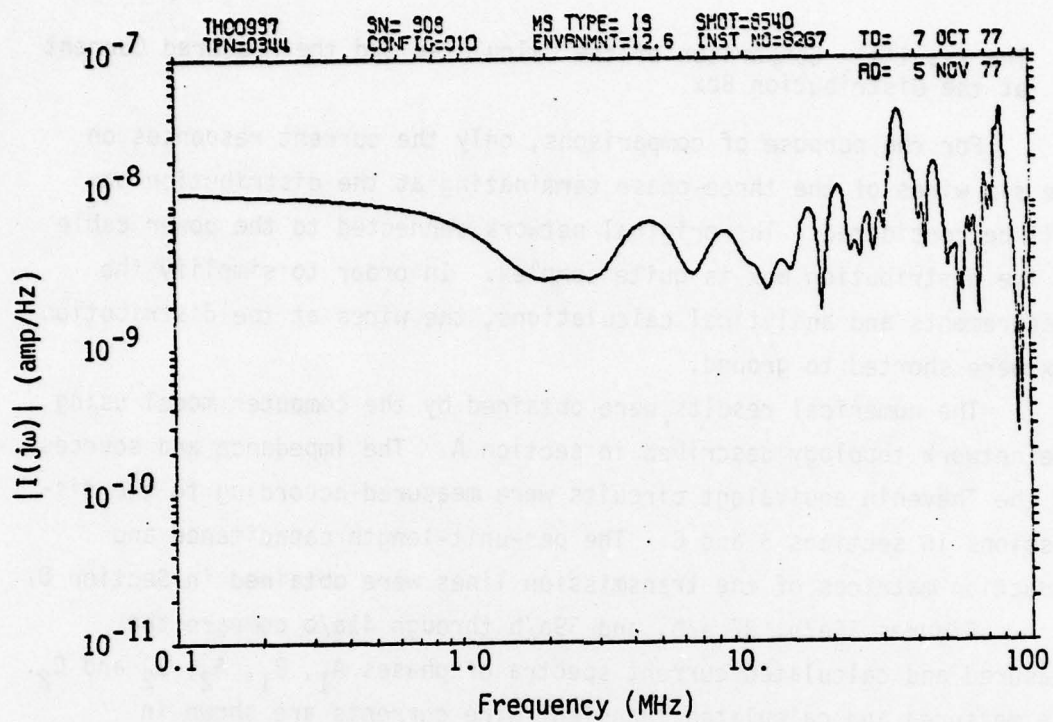
E. The Results - Comparison of the Calculated and the Measured Current at the Distribution Box

For the purpose of comparisons, only the current responses on the six wires of the three-phase terminating at the distribution box will be considered. The original network connected to the power cable at the distribution box is quite complex. In order to simplify the measurements and analytical calculations, the wires at the distribution box were shorted to ground.

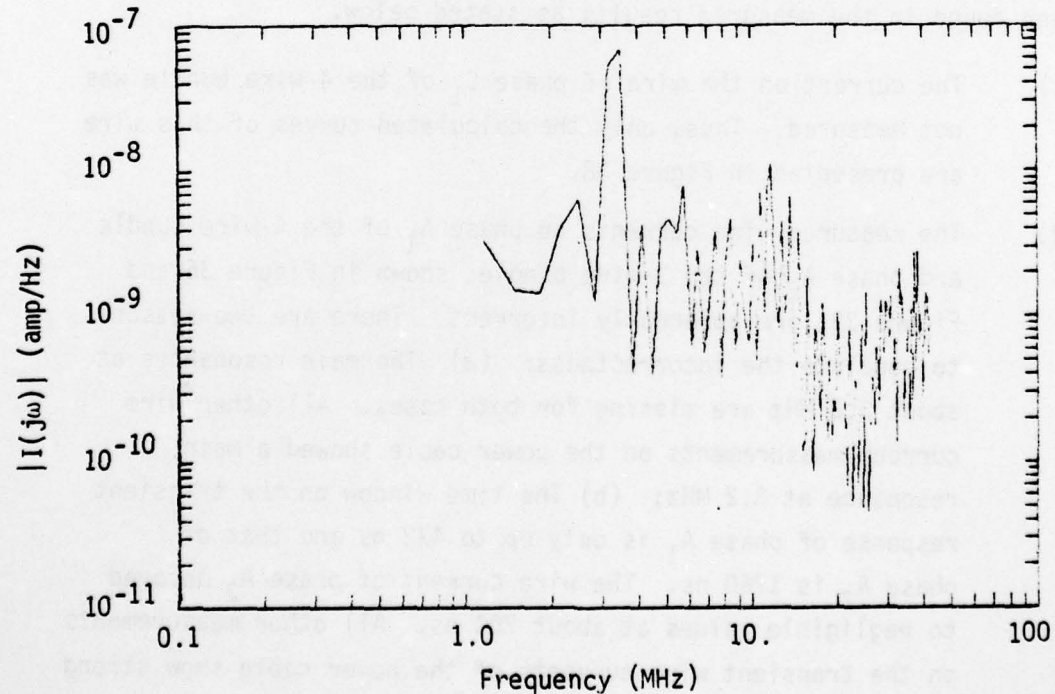
The numerical results were obtained by the computer model using the network topology described in section A. The impedance and sources of the Thévenin equivalent circuits were measured according to the discussions in sections B and C. The per-unit-length capacitance and induction matrices of the transmission lines were obtained in Section D.

Figures 36a/b, 37 a/b, and 39a/b through 41a/b compare the measured and calculated current spectra of phases A_1 , B_1 , A_2 , B_2 and C_2 . The measured and calculated transient wire currents are shown in Figures 36c/d, 37c/d, and 39c/d through 41 c/d. Some inadequacies have been found in the measured results as stated below.

- (1) The current on the wire of phase C_1 of the 4-wire bundle was not measured. Thus, only the calculated curves of this wire are presented in Figure 38.
- (2) The measured wire currents on phase A_1 of the 4-wire bundle and phase A_2 of the 3-wire bundle, shown in Figure 36 and Figure 39, are apparently incorrect. There are two reasons to conclude the incorrectness: (a) The main resonances at about 3.2 MHz are missing for both cases. All other wire current measurements on the power cable showed a main resonance at 3.2 MHz; (b) The time window on the transient response of phase A_1 is only up to 432 ns and that of phase A_2 is 1760 ns. The wire current of phase A_2 decayed to negligible values at about 700 ns. All other measurements on the transient wire currents of the power cable show strong signals even after 1500 ns.

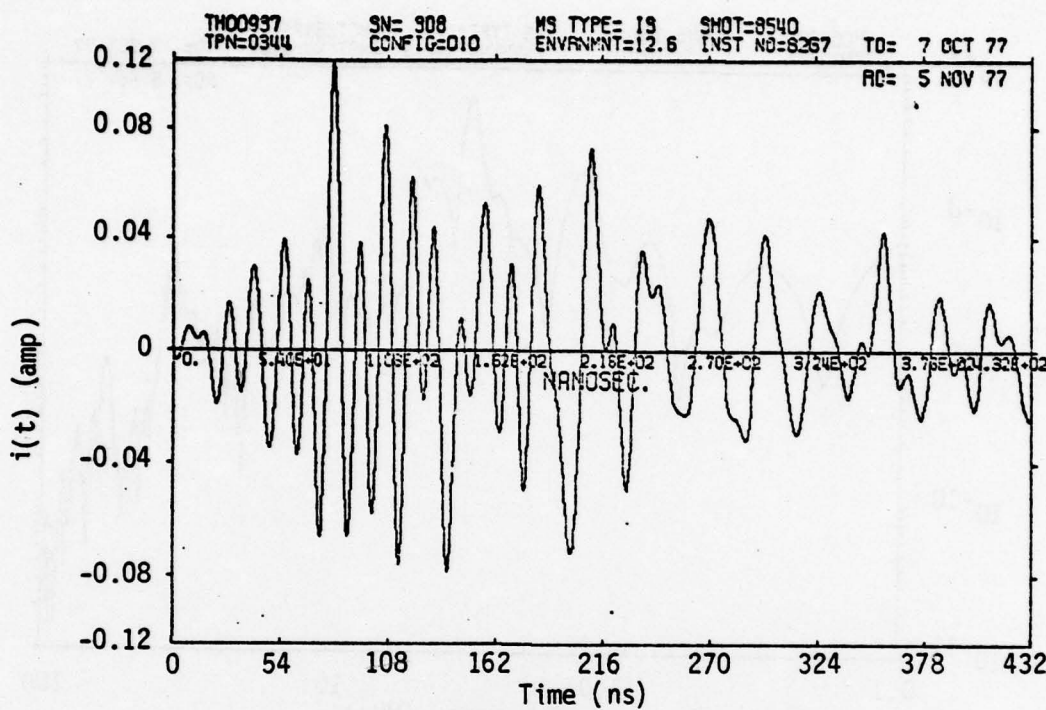


(a) Measured current spectrum (data incorrect)

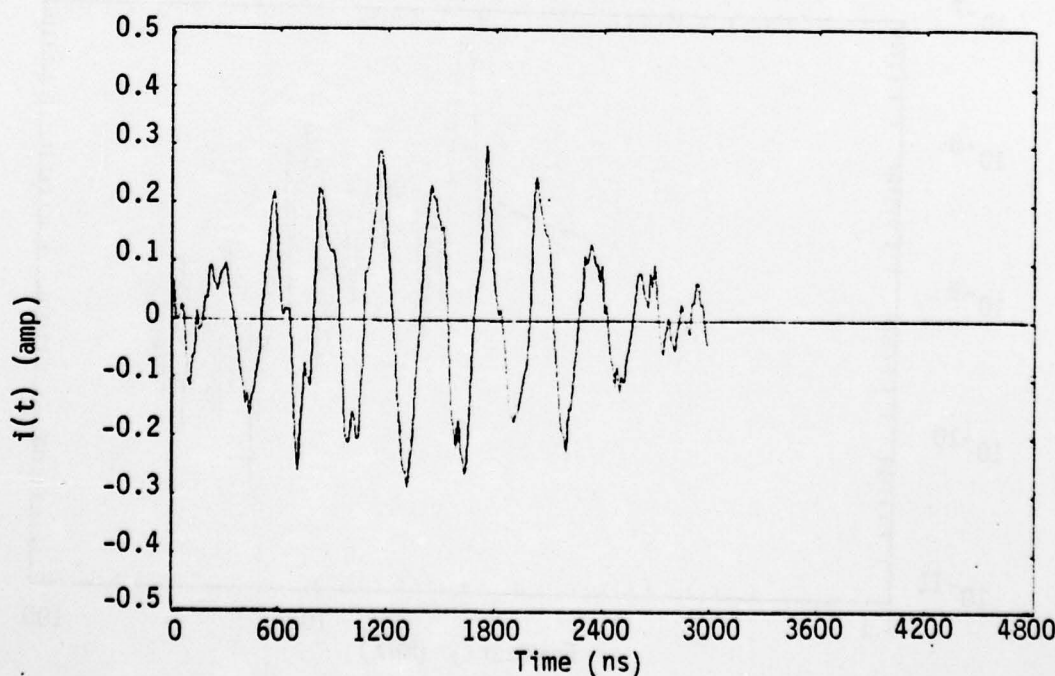


(b) Calculated current spectrum

Figure 26a,b. Comparison of the wire current spectrum on phase A₁ of the 4-wire bundle at the distribution box

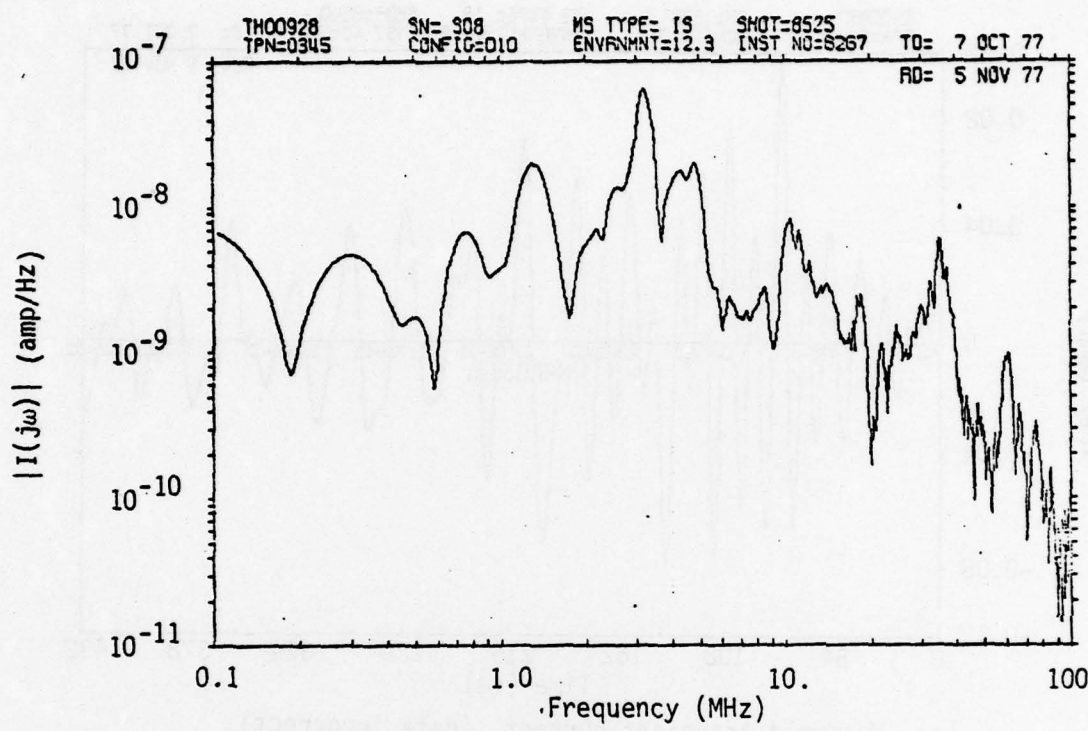


(c) Measured transient current (data incorrect)

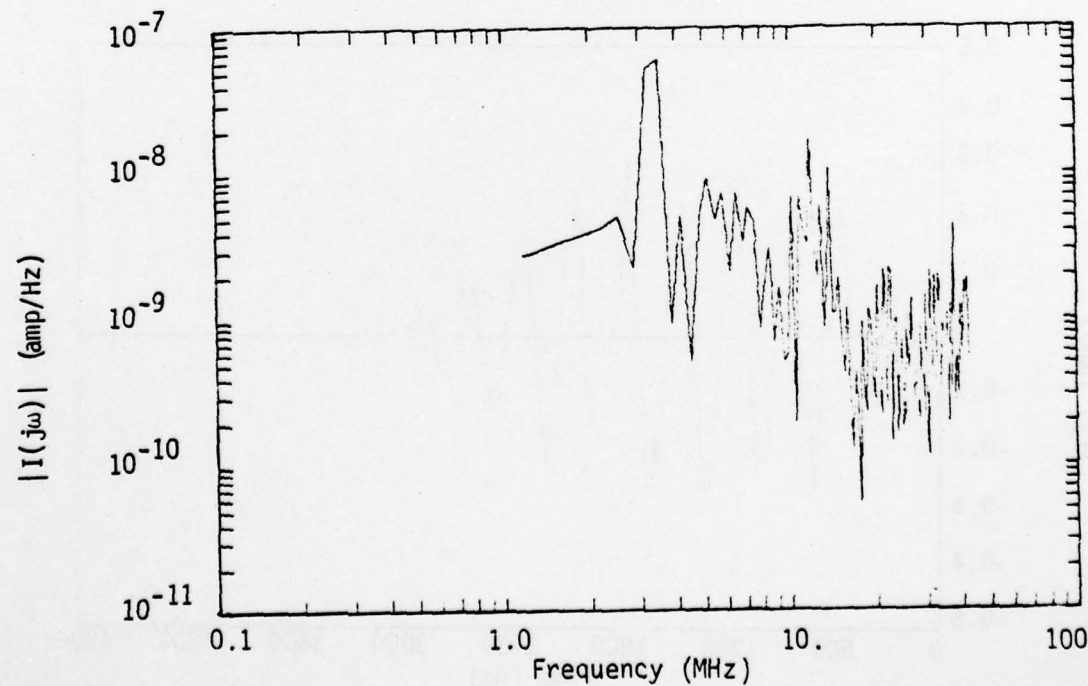


(d) Calculated transient current

Figure 36c,d. Comparison of transient wire current on phase A₁ of the 4-wire bundle at the distribution box

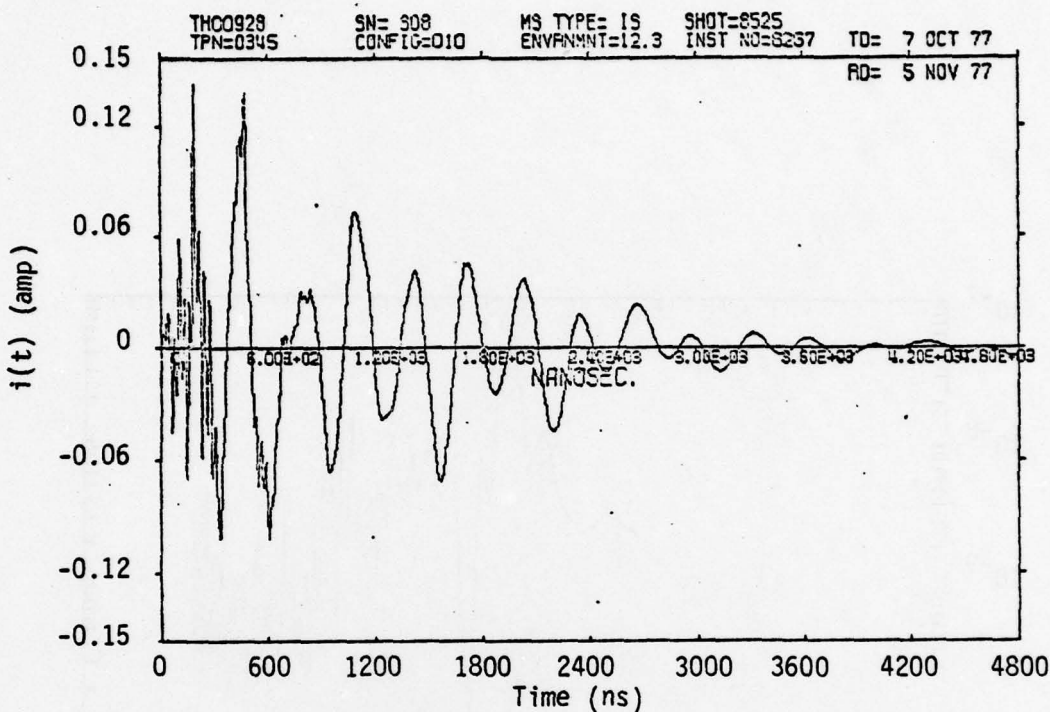


(a) Measured current spectrum

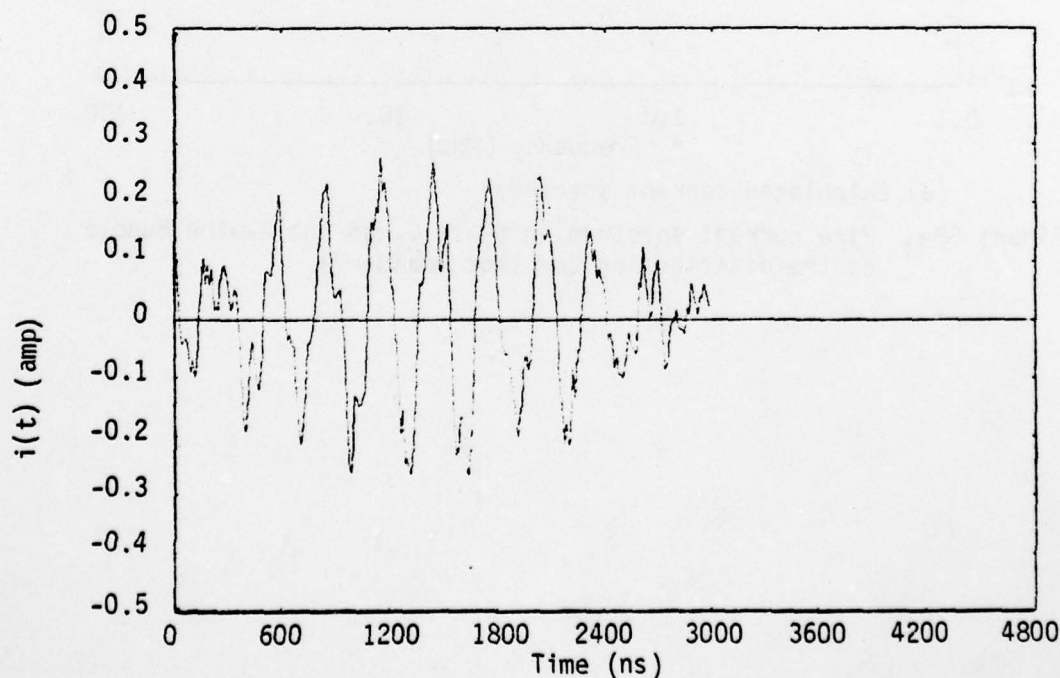


(b) Calculated current spectrum

Figure 37a,b. Comparison of the wire current spectrum on phase B_1 of the 4-wire bundle at the distribution box

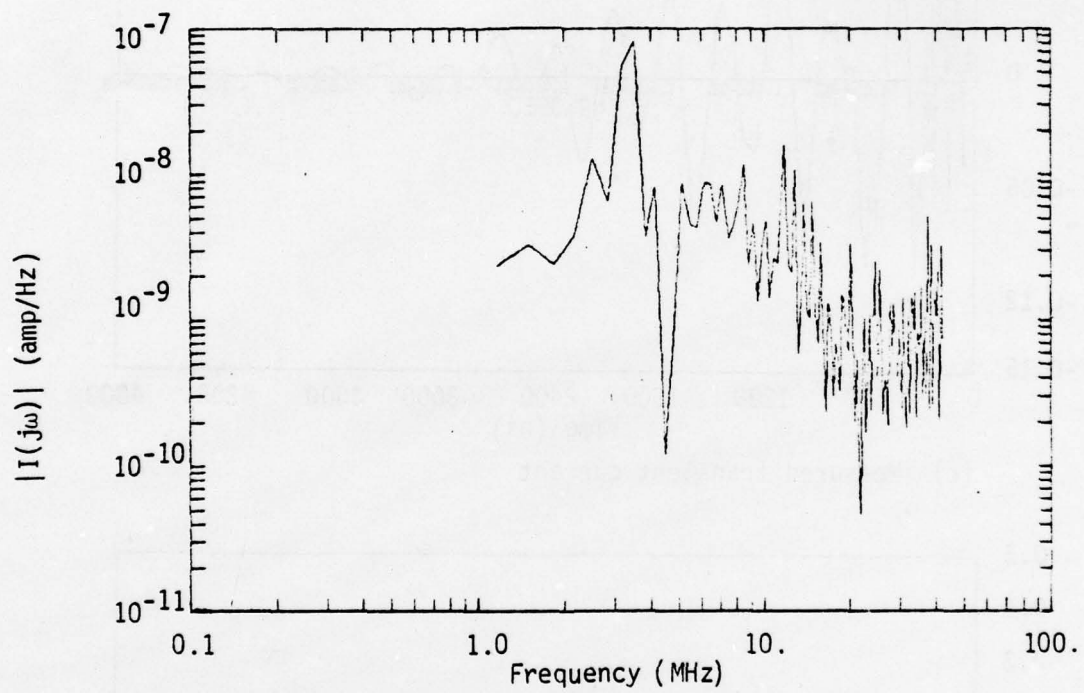


(c) Measured transient current



(d) Calculated transient current

Figure 37c,d. Comparison of transient wire current on phase B₁ of the 4-wire bundle at the distribution box



(a) Calculated current spectrum

Figure 38a. Wire current spectrum on phase C₁ of the 4-wire bundle
at the distribution box (Not measured)

AD-A074 950

SCIENCE APPLICATIONS INC BERKELEY CALIF
TRANSIENT ANALYSIS OF MULTICONDUCTOR TRANSMISSION LINE NETWORKS--ETC(U)
FEB 79 S K CHANG, F M TESCHE, D V GIRI

F29601-78-C-0002

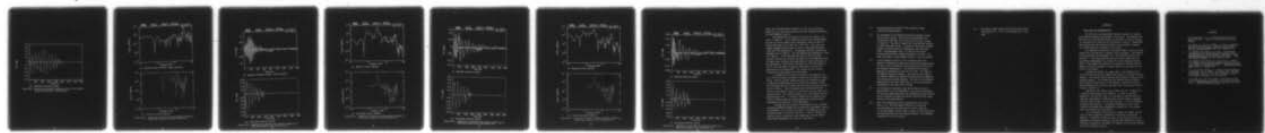
F/G 20/14

AFWL-TR-78-152

NL

UNCLASSIFIED

2 OF 2
ADA
074950

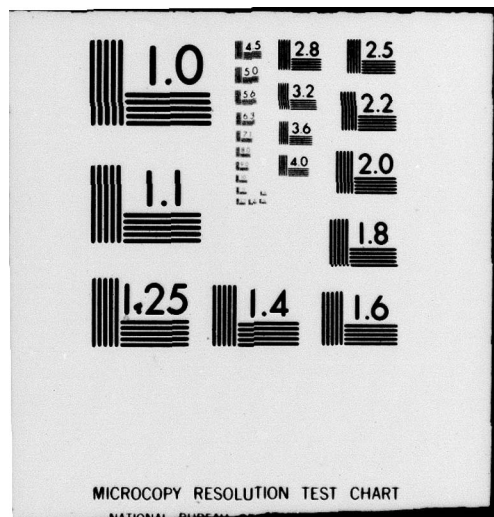


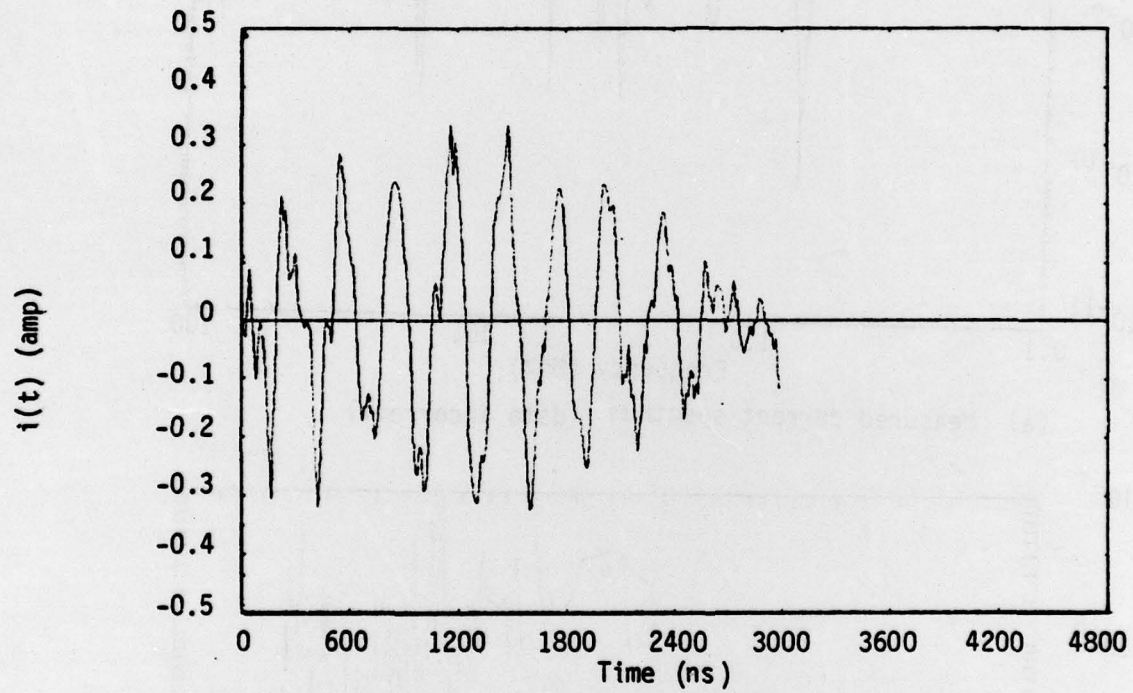
END

DATE
FILED

10-79

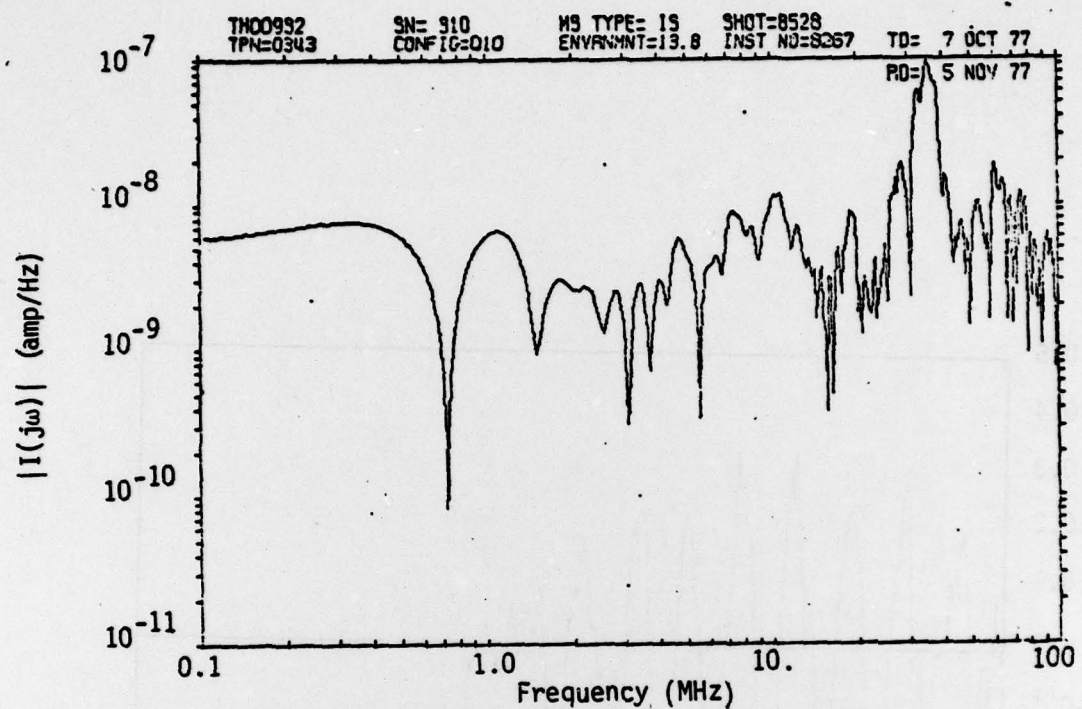
DDC



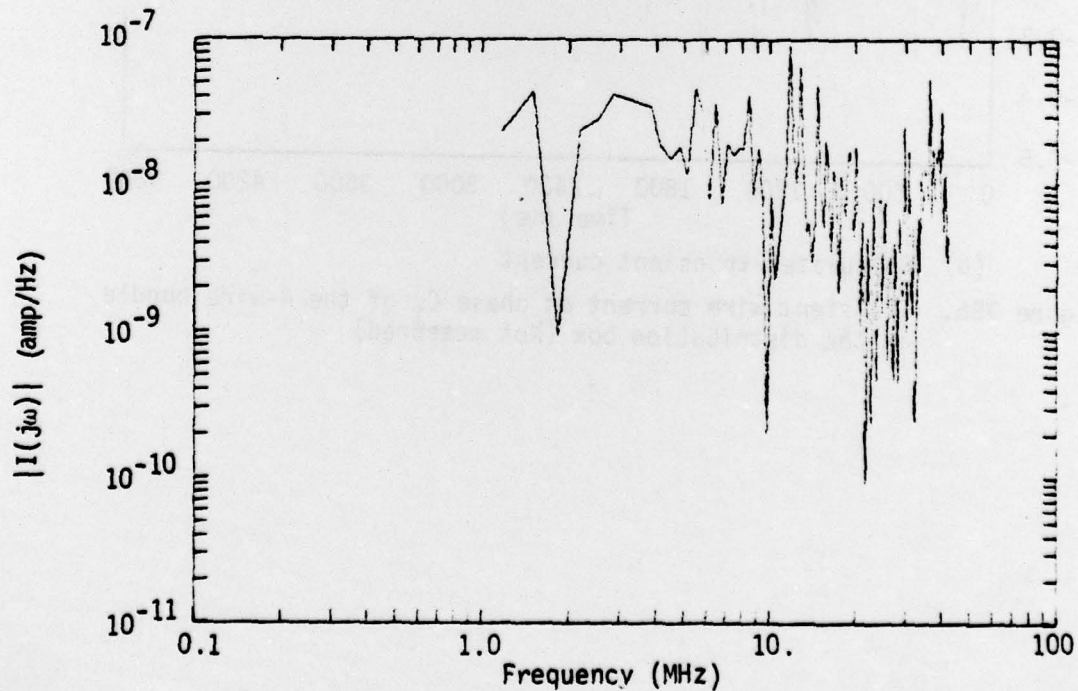


(b) Calculated transient current

Figure 38b. Transient wire current on phase C₁ of the 4-wire bundle
at the distribution box (Not measured)

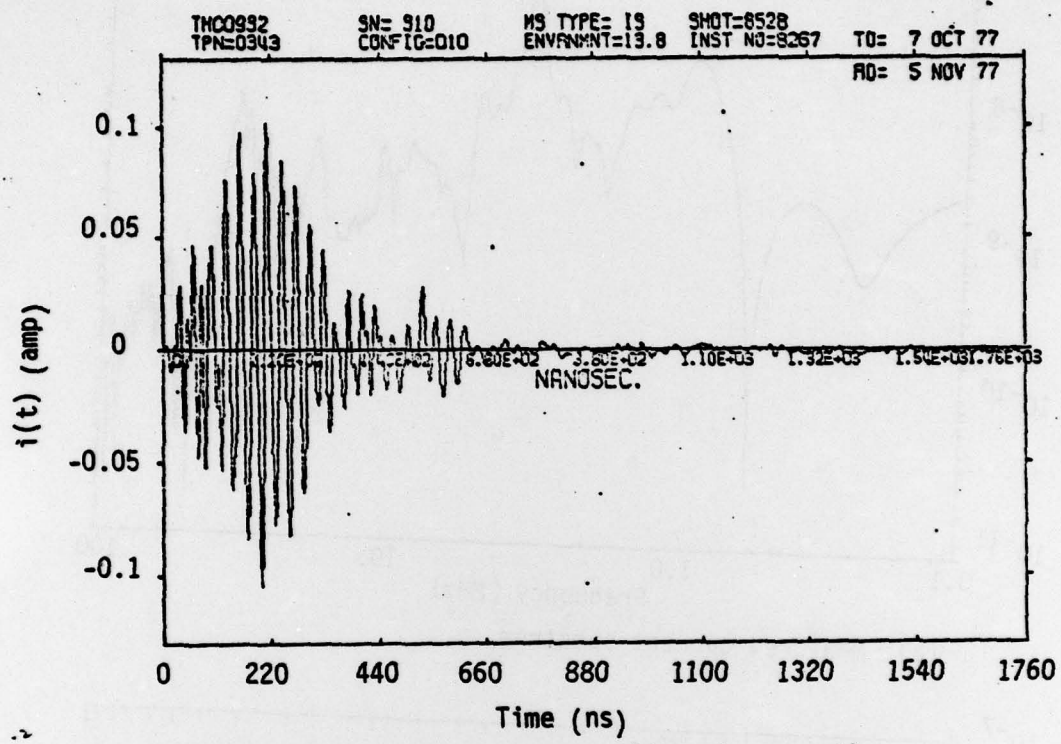


(a) Measured current spectrum (data incorrect)

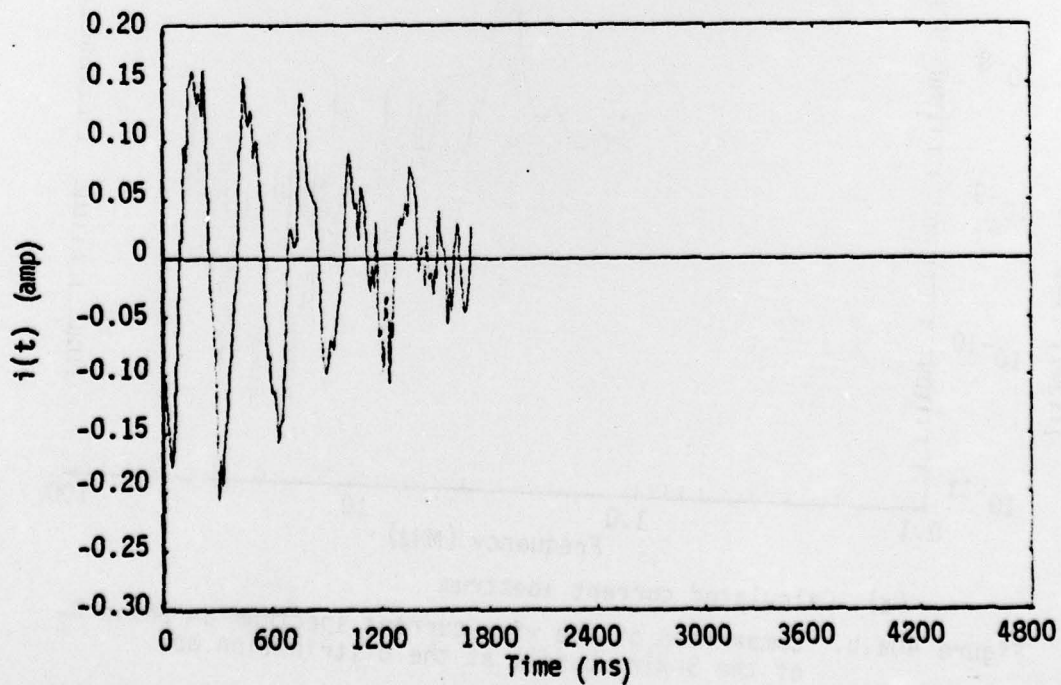


(b) Calculated current spectrum

Figure 39a,b. Comparison of the wire current spectrum on phase A₂ of the 3-wire bundle at the distribution box

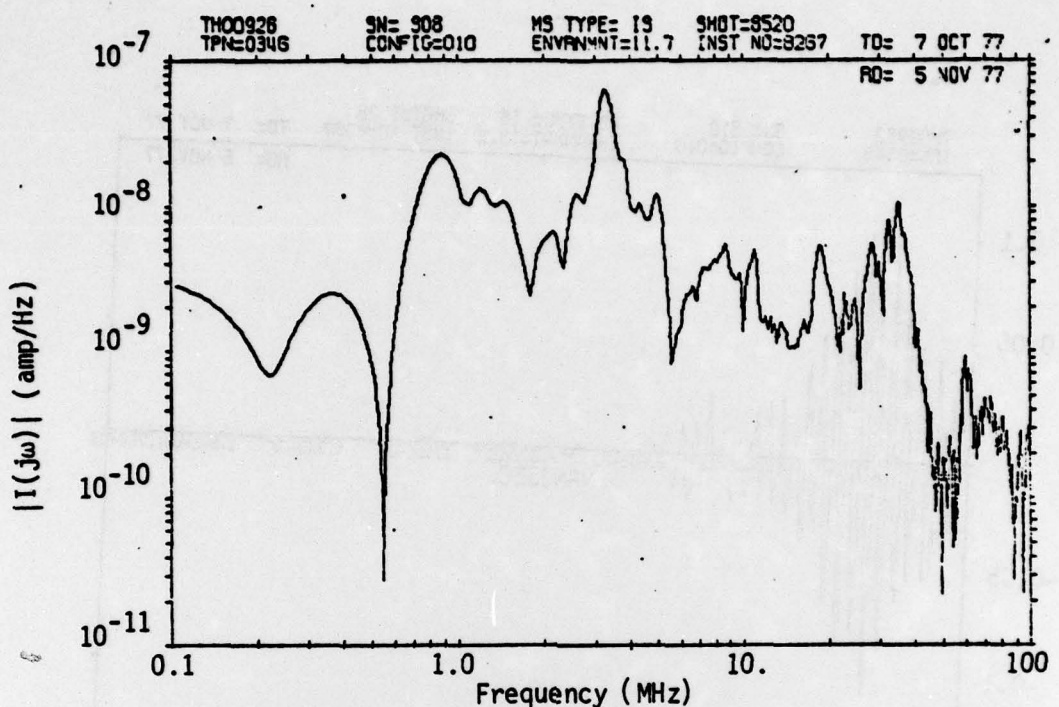


(c) Measured transient current (data incorrect)

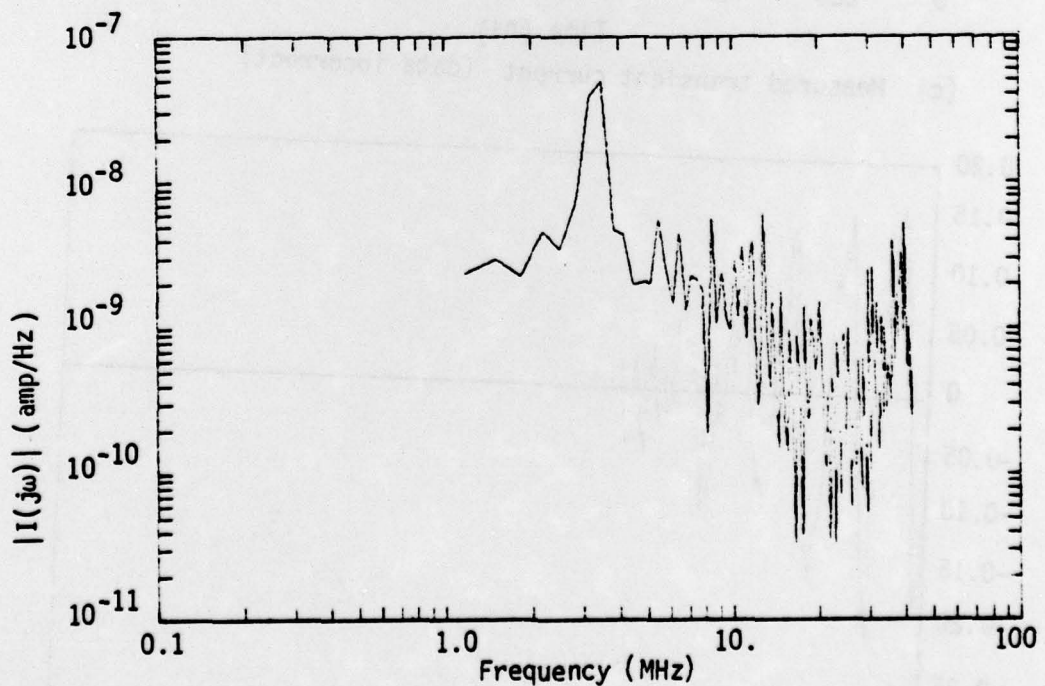


(d) Calculated transient current

Figure 39c,d. Comparison of transient wire current on phase A₂ of the 3-wire bundle at the distribution box

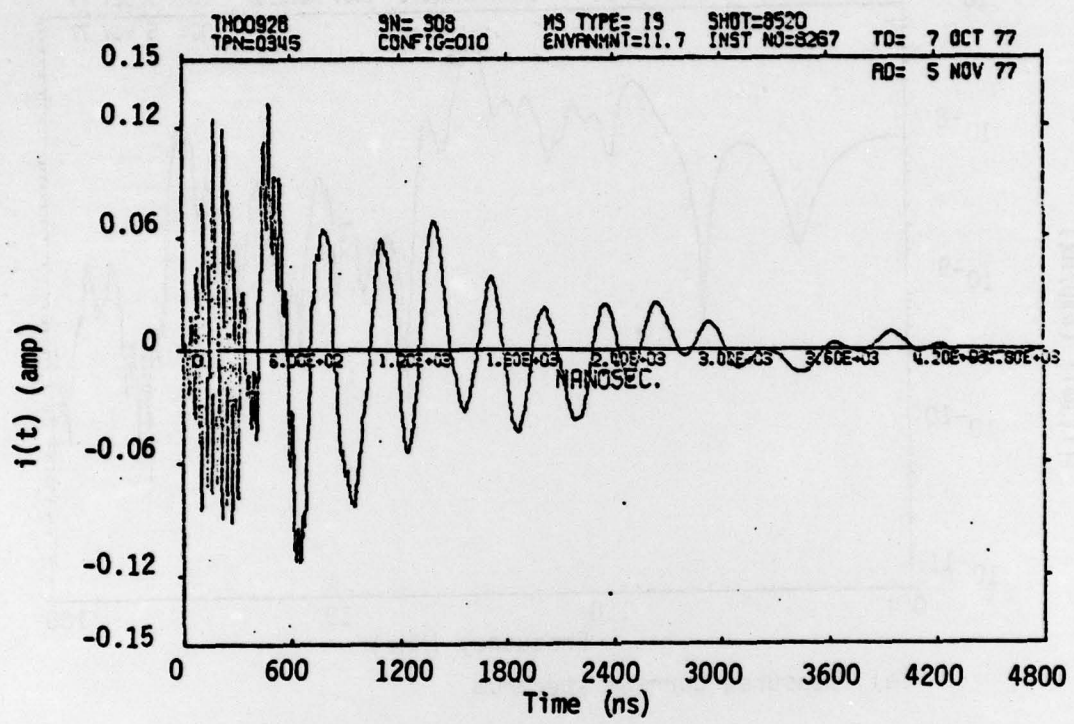


(a) Measured current spectrum

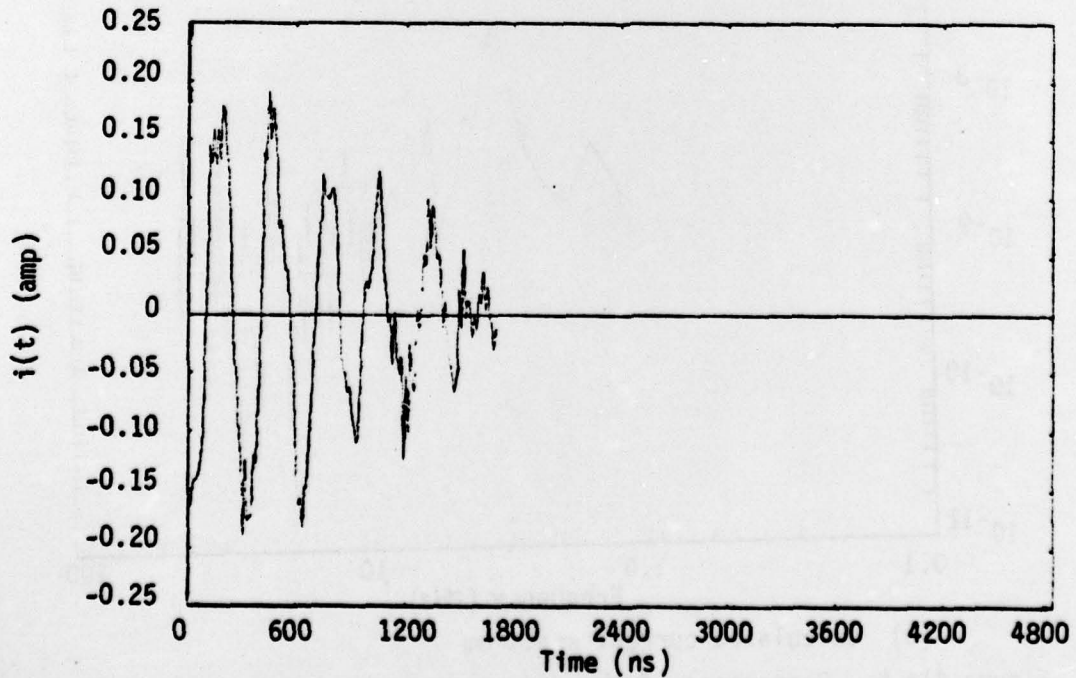


(a) Calculated current spectrum

Figure 40a,b. Comparison of the wire current spectrum on phase B₂ of the 3-wire bundle at the distribution box

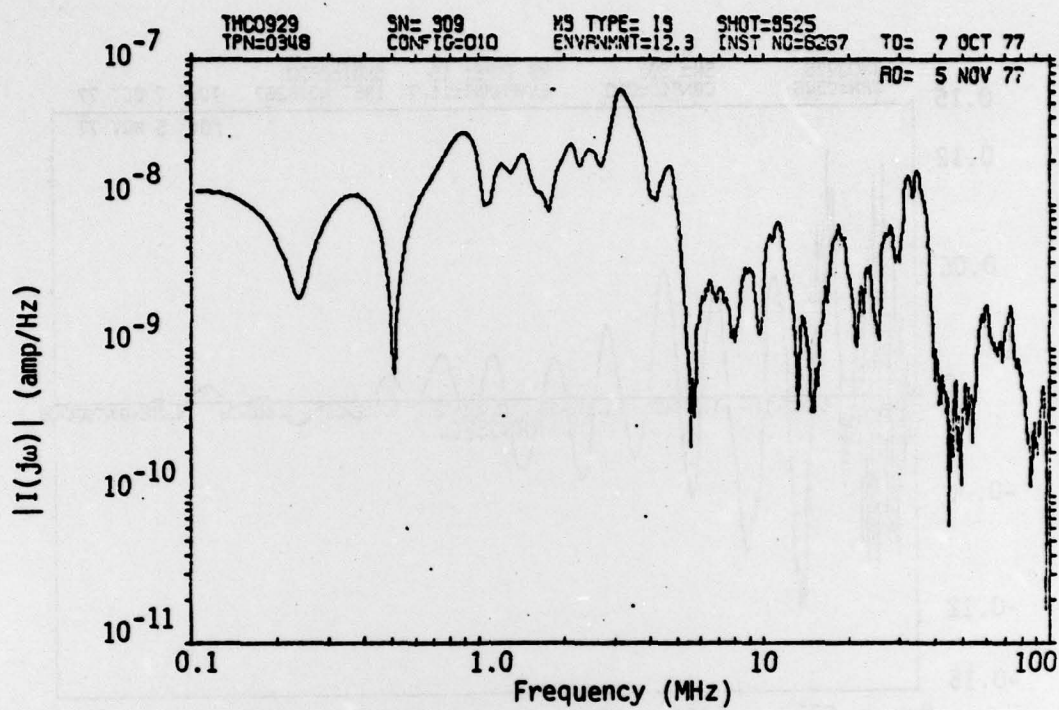


(c) Measured transient current

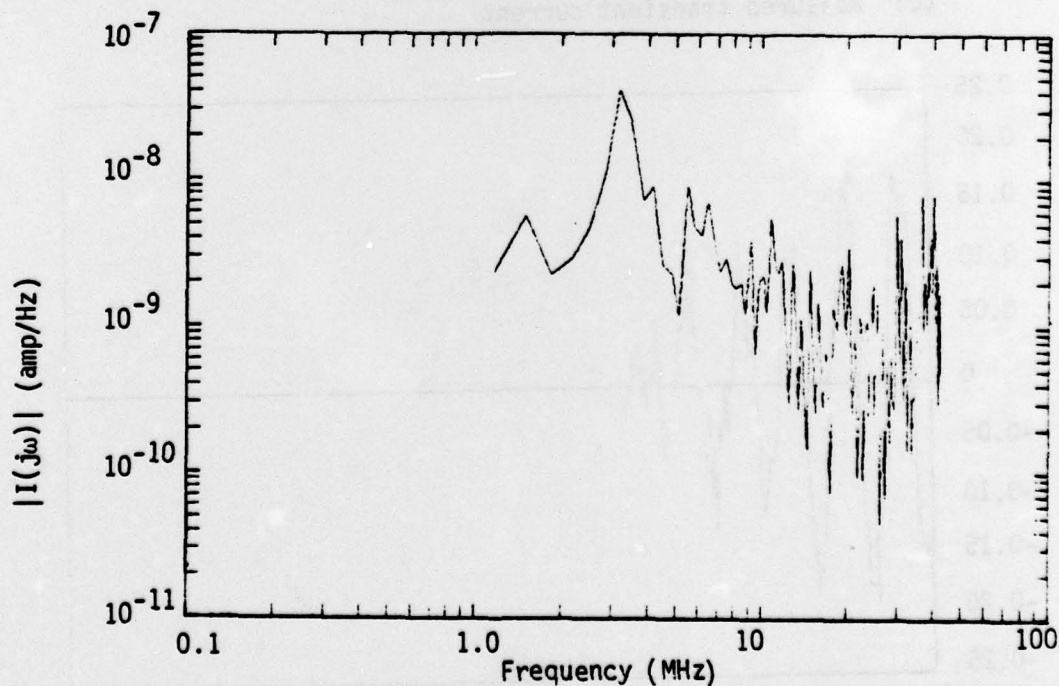


(d) Calculated transient current

Figure 40c,d. Comparison of transient wire current on phase B₂ of the 3-wire bundle at the distribution box

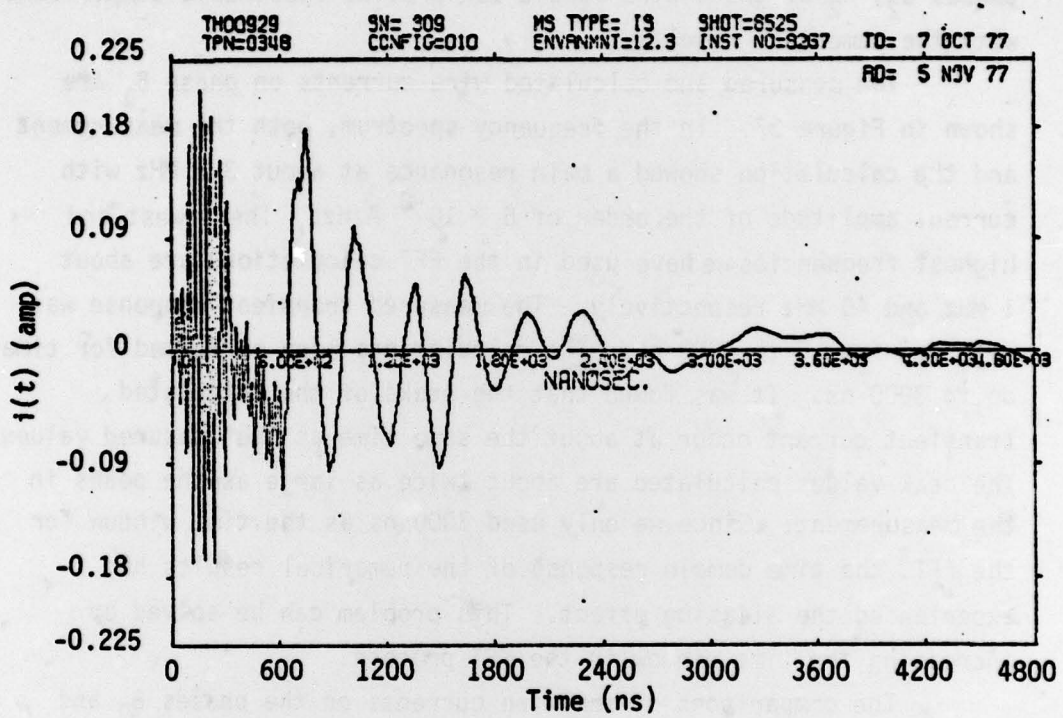


(a) Measured current spectrum

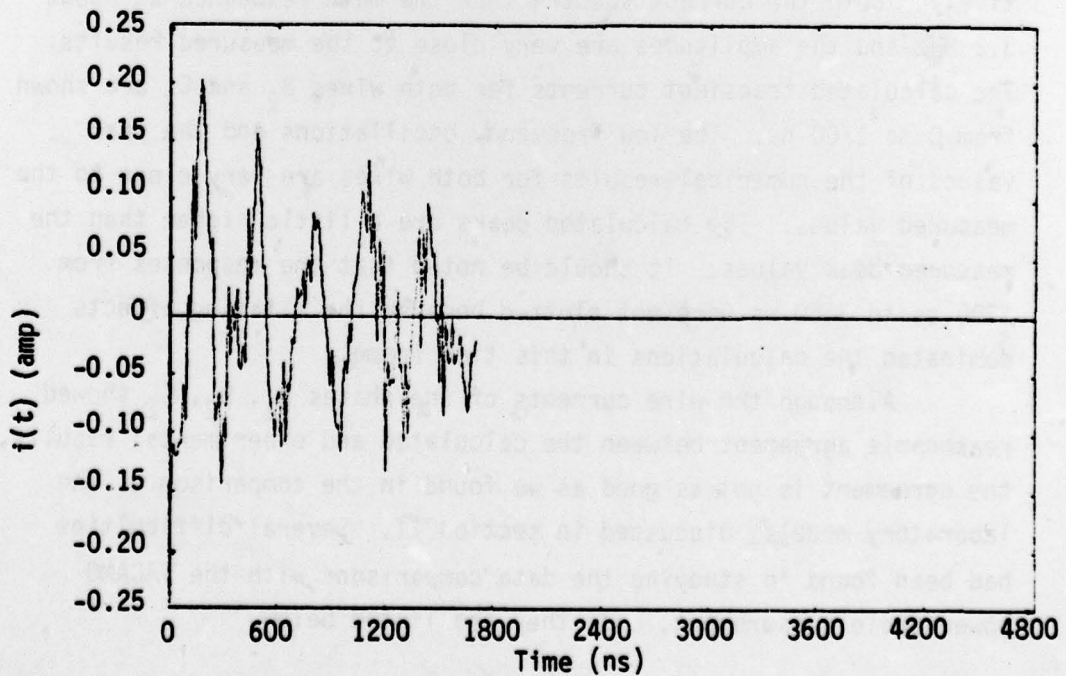


(b) Calculated current spectrum

Figure 41a,b. Comparison of the wire current spectrum on phase C₂ of the 3-wire bundle at the distribution box



(c) Measured transient current



(d) Calculated transient current

Figure 41c,d. Comparison of transient wire current on phase C₂ of the 3-wire bundle at the distribution box

Hence, only the measurement on phase B_1 of the 4-wire bundle and phases B_2 , C_2 of the 3-wire bundle can provide reasonable comparisons with the numerical results.

The measured and calculated wire currents on phase B_1 are shown in Figure 37. In the frequency spectrum, both the measurement and the calculation showed a main resonance at about 3.2 MHz with current amplitude of the order of 6×10^{-8} A/Hz. The lowest and highest frequencies we have used in the FFT calculations are about 1 MHz and 40 MHz respectively. The measured transient response was recorded from 0 to 4800 ns. The calculations were performed for times up to 3000 ns. It was found that the peaks of the calculated transient current occur at about the same time as the measured values. The peak values calculated are about twice as large as the peaks in the measurement. Since we only used 3000 ns as the time window for the FFT, the time domain response of the numerical results had experienced the aliasing effect. This problem can be solved by increasing the time window in the FFT process.

The comparisons of the wire currents on the phases B_2 and C_2 of the 3-wire bundle are shown in Figure 40 and Figure 41, respectively. Both the current spectra show the main resonance at about 3.2 MHz and the amplitudes are very close to the measured results. The calculated transient currents for both wires B_2 and C_2 are shown from 0 to 1700 ns. The low frequency oscillations and the peak values of the numerical results for both wires are very close to the measured values. The calculated peaks are a little higher than the measured peak values. It should be noted that the responses from 1700 ns to 3000 ns were not plotted because the aliasing effects dominated the calculations in this time frame.

Although the wire currents of the phases B_1 , B_2 , C_2 showed reasonable agreement between the calculated and experimental results, the agreement is not as good as we found in the comparison of the laboratory models, discussed in section II. Several difficulties had been found in studying the data comparisons with the TACAMO power cable measurement, and they are listed below.

- (1) The pulse-to-pulse variation of the simulation causes inconsistent measured data.
- (2) The measurement of the Thévenin equivalent impedance network was not very accurate. The error of the measurement was illustrated by the 100Ω load at the end of the coax as shown in Figure 18. The error is especially large when the frequency is higher than about 65 MHz. In addition, the network analyzer displays nonlinear effects at frequencies lower than about 4 MHz. The measurement from 1 to 4 MHz may not be very accurate while the main resonant frequency is 3.2 MHz. This might contribute a certain amount of error in the calculations.
- (3) It was proposed originally to use the Norton equivalent network to represent the power cable outside the pressure break. The short circuit currents must be measured when all the wires are grounded simultaneously. The currents were mistakenly measured by grounding only one wire at a time. This leads to the Thévenin equivalent network. The open circuit voltage of the Thévenin network was obtained by multiplying the impedances with the measured current spectrum. The errors in the measured impedances can also cause some errors in the driving waveform represented by the open circuit voltage.
- (4) The transmission line model using the twisted wires over a ground plane is only an estimation of the actual configuration. The per-unit-length capacitance and inductance matrices obtained from the twisted wire model may deviate from the actual values because of the approximations.
- (5) Most of the measured transient currents decay very slowly within 3 μ s. This may cause difficulties in adjusting the time window and the time steps in the FFT algorithm. If the time window is taken larger to cover all the oscillations, the time resolutions will be affected because of the DIMENSION limitations in the FFT routines.

- (6) There may be other sources exciting the cable inside the pressure hull. This is not accounted for in the model.

SECTION IV

CONCLUSIONS AND RECOMMENDATIONS

The analytical and experimental transient responses of example multiconductor networks were studied in this report. The computer code QV7T which utilizes the BLT equation, was modified and used in performing the numerical calculations for the analytical results. Measurements were furnished for both laboratory models of multiconductor networks and the EMP simulation of cables on an aircraft.

The laboratory transmission line network models involved a 3-wire transmission line section, a T-network, and an H-network. Two different driving waveforms were considered, i.e., the pulse and the unit step functions. It was found that the analytical results agree with the experimental measurements very closely for all the laboratory network models. These comparisons enhance our confidence in the QV7T code for computing transient responses of certain types of multiconductor transmission line networks.

The measured response of a power cable in the TACAMO aircraft during simulator testing was compared with analysis of the EMP transient response. The computer results show the same resonance frequency as the measured response. It was found that the computer analysis tends to over-estimate the peak values of the response. Several difficulties were encountered while analyzing the power cable and they have been discussed, in Section III.

Admittedly, the studies of this report are still incomplete for a complete understanding of the networks. In order to have more comparisons with the QV7T code, it is advisable to perform additional laboratory measurements on networks which include frequency dependent loads and which include loops in their topology. It is also suggested to measure some canonical multiconductor transmission lines in the simulator environment and to measure the transmission line responses under distributed source excitations.

For an extension of the analytical studies, we suggest the SEM study of simple laboratory transmission line models using the BLT equation. In addition it would be useful to use the Prony analysis of experimentally measured responses to recover SEM frequencies of simple laboratory transmission line models and compare with the values obtained from the BLT equation analysis.

REFERENCES

1. F.M. Tesche and T.K. Liu, "Code Description and User's Manual for QV7T," June 1977; can be obtained from the authors.
2. C.E. Baum, T.K. Liu, F.M. Tesche, S.K. Chang, "Numerical Results for Multiconductor Transmission-Line Networks," AFWL EMP Interaction Notes, Note 322, September 1977.
3. A.K. Agrawal, H.M. Fowles, L.D. Scott, "Experimental Characterization of Multiconductor Transmission Lines in Inhomogeneous Media Using Time Domain Techniques," AFWL EMP Interaction Notes, Note 332, February 1978.
4. A.K. Agrawal, H.M. Fowles, L.D. Scott, and L.T. Simpson, "Time Domain Analysis of Multiconductor Transmission Lines with Branches in Inhomogeneous Media," AFWL EMP Interaction Notes, Note 333, February 1978.
5. T.K. Liu and F.M. Tesche, "Test Results on Multiconductor Transmission Lines on TEMPAT/AFWL Add-On Test," published as SAI Report 102-78-17, July 1978, submitted to the Air Force Weapons Laboratory, Kirtland AFB, NM.
6. S.K. Chang, T.K. Liu, F.M. Tesche, "Calculation of the per-unit-length-Capacitance Matrix for Shielded Insulated Wires," AFWL EMP Interaction Notes, Note 319, April 1977.